High-Sensitivity Searches for Radio Pulsars

Thesis by
Paul Shelton Ray

In Partial Fulfillment of the Requirements
for the Degree of
Doctor of Philosophy

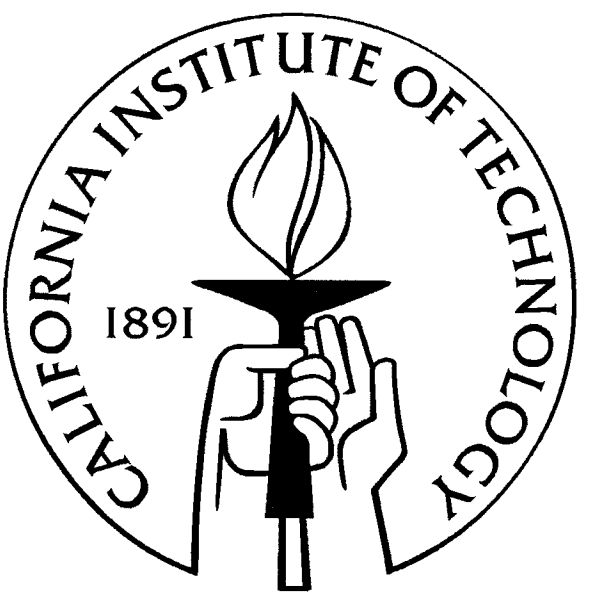

California Institute of Technology
Pasadena, California

1995

(Submitted January 11, 1995)

Acknowledgements

First of all, I would like to express my deepest gratitude to my advisor, Tom Prince, for his continued support and guidance during the completion of this work. His enthusiasm for science and ability to tackle an astounding variety of projects will remain an inspiration for years to come.

There are many other people who I need to acknowledge for assistance of one kind or another—hopefully I haven't forgotten too many...

Steve Thorsett for working closely on the large surveys, being involved in the discovery of my first pulsar, and being an invaluable source of information on the mysteries of TEMPO and the tricks of the pulsar timing trade.

Stuart Anderson for forging the path into the parallel processing of pulsar data.

Peter Gorham for all of his work on the supernova remnant search and his always impressive tan.

Alex Wolszczan for showing me where to find good coffee, good snorkeling, and Ron del Barrilito on the island of Puerto Rico, and teaching me how to use the Arecibo telescope.

Deepto Chakrabarty, Fiona Harrison, Biff Heindl, and Romeel Davé for way too many lunches in the basement of the Athenaeum, good friendships, and single-malts when we needed to unwind.

I would also like to acknowledge Will Deich for supplying the PSRPACK suite of software that made a great deal of the data reduction possible and for putting up with my many questions and bug reports.

I am also indebted to Fernando Camilo and David Nice for allowing me to use their telescope time for followup observations of several of the new pulsars.

Of course, the path that led me to Caltech was initiated by my parents and step-parents, who engendered my love of science at an early age.

This work could not have been completed without the accompanyment of Madonna, Hole, Green Day, Offspring, R.E.M., Nirvana, and many others.

This thesis is dedicated to my wife, Susan Wetzel Ray without whose support, both emotional and financial, graduate school would have been a much more painful experience.

Abstract

Radio pulsars are rapidly spinning, highly magnetized neutron stars which emit beams of radio waves and are observed to pulse when the beam crosses the Earth. They represent the end-point in the evolution of massive stars, and are excellent laboratories for the study of the bulk properties of matter at nuclear densities and beyond. Millisecond pulsars are old pulsars reborn through accretion of matter from a companion star, spinning so fast that the surface velocities approach the speed of light.

We describe several high-sensitivity searches for radio pulsars, both for very recently born pulsars in supernova remnants and for ancient millisecond pulsars born early in the history of the Galaxy.

We have conducted a survey of 18 supernova remnants for young pulsars using the 305-m radio telescope in Arecibo, Puerto Rico at 430 MHz and 1400 MHz. No pulsars were discovered in this survey which was sensitive to pulsars as faint as 0.2 mJy. The selection effects making pulsars difficult to find in supernova remnants, including high background temperatures of the remnants and high birth velocities of pulsars, are discussed. We conclude that deeper and more extensive surveys are required to constrain the pulsar population in supernova remnants.

We have also performed several very large area surveys with excellent sensitivity to pulsars as fast as 1 millisecond, also employing the Arecibo 305-m dish. These surveys will help place limits on the population of low-luminosity pulsars in the Galaxy. A total of 12 non-recycled pulsars were discovered with periods ranging from 96 ms to 2.06 seconds.

The primary motivation for these surveys was the discovery of new millisecond pulsars. One 5.9 ms pulsar was discovered and initial timing observations show that it is in a binary system with orbital period 56.2 d and semi-major axis 20.1 lt-s. The implied companion mass is at least 0.2 solar masses. This pulsar, as well as a number of others discovered in recent surveys, are providing excellent laboratories for studies of the formation and evolution of millisecond pulsars, as well as measurements of general relativistic parameters, constraints on the cosmological background of gravitational waves, a pulsar based time standard and dynamical-optical frame ties.

Contents

List of Figures

List of Tables

Chapter 1

The Study of Pulsars

1.1 Introduction

Pulsars were a serendipitous discovery, first observed by graduate student Jocelyn Bell in 1967, the year of this author's birth. The description of a radio pulsar reveals some of the reasons they are so interesting. They are about the size of a small city ($\sim$ 10 miles across), but have a mass almost one and a half times that of the Sun. They have a magnetic field as large as 10^{12} times that of the Earth. Without a doubt, these are very exotic conditions! Conditions like these test the limits of physical theories and of experimental techniques. Pulsars have been used to provide the most stringent tests of general relativity and to push the limits of the best atomic time standards on Earth. They are also being used to hunt for ripples in spacetime left over from the Big Bang. Their precisely-timed, pulsed signals make them extremely useful tools for studying the interstellar medium in the Galaxy. They have been used to probe the gravitational potential and mass-to-light ratio of globular clusters.

I entered the field of pulsar research seeking an interesting application of high-performance supercomputing. However, my research soon became motivated by the physics of these fascinating objects. Modern searches for pulsars produce large data sets and require a great deal of computation to search. High-performance computing has opened a new window on the Universe and will allow rapid growth of our observational capabilities in the coming years.

This thesis describes several large surveys for new radio pulsars: a directed search for very young pulsars towards the supernova remnants in which they are formed and other

undirected surveys designed to be sensitive to the oldest and fastest known pulsars, the millisecond pulsars.

1.2 A Brief Sketch of Pulsar Formation, Evolution, and Properties

The term *radio pulsar* refers to celestial objects distinguished observationally by their periodic radio pulsations. Since shortly after their discovery, the association of these signals with rotating neutron stars has been widely accepted. In this thesis I will discuss searches for, and observations of, rotation-powered pulsars, using radio telescopes. (The term "pulsar" is also used for accretion-powered X-ray pulsars, which will not be discussed here except to mention their possible evolutionary connection to the rotation-powered pulsars.)

Far from being a complete review, this chapter summarizes some of the basic observational facts and models used to interpret radio pulsars. I refer the reader to several longer works on the subject. Manchester and Taylor (1977) give an excellent and comprehensive, though dated, introduction to pulsars. Lyne and Smith (1990) provide a more recent introductory level text which includes millisecond and globular cluster pulsars as well as X-ray binaries. Michel (1991) reviews the status of pulsar observations and introduces various theoretical aspects of neutron star magnetospheres.

1.2.1 The *P-B* Diagram

One device which has proven useful for classifying pulsars and providing a framework within which to discuss their evolution is the P-B diagram (Figure 1.1). The P-B diagram is a scatter plot of pulsars according to their pulse period (P) and their estimated magnetic field strength (B). The surface dipole magnetic field strength of a pulsar is estimated from a measurement of the intrinsic pulse period derivative ($\dot{P}$) using the energy loss rate of a magnetic dipole rotating in a vacuum:

$$B = 3.2 \times 10^{19} (P\dot{P})^{1/2} \,\text{gauss}. \tag{1.1}$$

The estimate of B should only be taken as a representative value of the field, because the actual surface magnetic field may have contributions from higher multipoles, and the

vacuum approximation certainly does not hold in radio pulsar magnetospheres. In addition, the measurement of $\dot{P}$ can be complicated by the orbital motion of the Earth, the orbital motion of the pulsar, and in some cases by kinematic contributions such as changing Doppler shift due to the pulsar's velocity transverse to the line of sight. Usually, $\dot{P}$ can be measured in less than one year of timing observations.

Near a pulsar's surface, the magnetic field co-rotates with the neutron star. There is a critical surface, called the *light cylinder*, where particles co-rotating with the field would have to move at the speed of light. This cannot occur, and near this surface a transition from a co-rotating field to traveling electromagnetic and plasma waves takes place. The energy and angular momentum lost to this radiation and plasma comes from the rotational energy of the pulsar, and the pulsar spins down. The youngest pulsar known, the Crab pulsar, has a period of only 33 ms, while some pulsars have periods of up to 5 seconds. The median pulsar period is about 0.6 seconds. In several models, the spin evolution of a pulsar can be parameterized as

$$\dot{\Omega} = -k\Omega^n, \tag{1.2}$$

where $\Omega(= 2\pi/P)$ is the spin angular frequency, k is a constant of proportionality, and n is referred to as the *braking index.* The braking index is determined by measuring $\ddot{\Omega}$, since $n = \Omega\ddot{\Omega}/\dot{\Omega}^2$. The braking index has been measured for a few young pulsars, and is in the range 2–3. The interpretation of these measurements, however, are often made difficult by glitches (sudden changes in P and $\dot{P}$ due to a sudden change in the neutron star's moment of inertia, or the crust-core coupling) and timing noise (random, low-level irregularities in the spin-down behavior). The expected value for pure magnetic dipole radiation is $n = 3$. Assuming constant k and n, the true age (t) of a pulsar is related to the initial spin period and the braking index by

$$t = \frac{P}{(n-1)\dot{P}}\left[1 - \left(\frac{P_0}{P}\right)^{n-1}\right]. \tag{1.3}$$

The characteristic age ($\tau_c = P/2\dot{P}$) is the time it would have taken for a pulsar born with $P_0 \ll P$ to evolve to its current period according to the $n = 3$ spin-down law. The two solid lines on Figure 1.1 indicate lines of constant characteristic age. (The line at 10^{10} yr is sometimes called the *Hubble line,* since a pulsar born at a short period cannot evolve to the right of that line within a Hubble time.)

The lower dashed line is the so-called *death line,* to the right of which the electric potential of the rotating, magnetized neutron star is thought not to be sufficient to generate

electron-positron pairs in the magnetosphere, which presumably causes the pulsar to stop emitting radio waves. This is semi-empirically parameterized as

$$\log B = 1.6 \log P + 11.4, \tag{1.4}$$

where B is the surface dipolar magnetic field strength in gauss and P is the pulsar period in seconds (Chen and Ruderman 1993). The upper dashed line is the *spin-up line,* which represents the equilibrium period a pulsar will be spun up to by mass accretion at the Eddington rate. This is shown by Ghosh and Lamb (1992) to be

$$P_{\rm eq} \approx 1.3 \left(\frac{B}{10^{12}\,{\rm G}}\right)^{6/7} \left(\frac{\dot{M}}{\dot{M}_{\rm Edd}}\right)^{-3/7} {\rm s}, \tag{1.5}$$

where $\dot{M}$ is the mass accretion rate and $\dot{M}_{\rm Edd}$ is the Eddington rate ($\dot{M}_{\rm Edd} \sim 1.5 \times 10^{-8}\,M_\odot\,{\rm yr}^{-1}$). At rates higher than $\dot{M}_{\rm Edd}$, radiation pressure overcomes gravitational attraction, placing an upper limit on the accretion rate.

There are several notable features of this diagram that have led to the conventional theory of pulsar evolution.

- The pulsars in supernova remnants are clustered near the $\tau_c = 10^4\,{\rm yr}$ line, implying that they are very young.
- There are two clear groups in the diagram. The *young pulsars* are clustered in the upper right quadrant of the diagram ($P \gtrsim 30\,{\rm ms}$, $B \gtrsim 10^{11}\,{\rm G}$), and the *recycled pulsars* (see §1.2.4) are clustered in the lower left quadrant ($P \lesssim 30\,{\rm ms}$ and $B \lesssim 10^{10}\,{\rm G}$).
- The binary fraction is vastly larger among the recycled pulsars than the young pulsars.

1.2.2 The Young Pulsars

Before 1974, the only known pulsars were young pulsars. Observationally, their pulse periods range from 33 ms to just over 5 s. Their inferred surface magnetic field strengths are $\sim 10^{11} - 10^{13}\,{\rm G}$.

Young pulsars are believed to be formed in supernova explosions. A main-sequence star is supported from collapsing under its own weight by internal energy generated by nuclear fusion. Stars spend most of their lifetime burning hydrogen into helium. When a massive star ($\gtrsim 4\,M_\odot$) exhausts its supply of hydrogen in the core, it begins to burn heavier

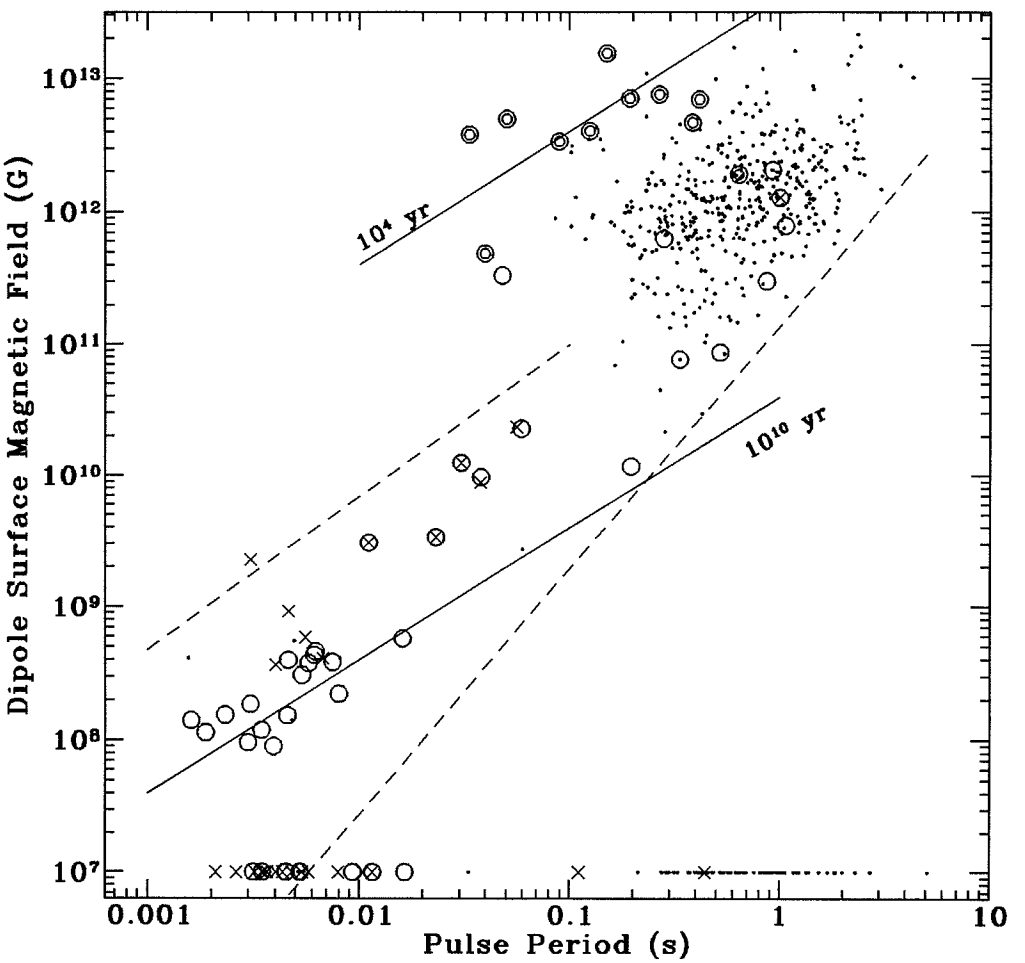

Figure 1.1: The P-B diagram. Pulsars with no measurement of $\dot{P}$ are shown at the bottom of the figure. Isolated pulsars in the Galactic disk are plotted as a dot. Pulsars in binary systems are plotted as an open circle (○). Isolated pulsars in globular clusters are plotted as a cross (×), and binary pulsars in globular clusters are plotted as a circumscribed cross (⊗). Finally, double circles represent pulsars which are associated with supernova remnants (◎). The period derivatives for the millisecond pulsars have been corrected to their intrinsic values by subtracting the $\dot{P}$ induced by the Shklovskii effect (Camilo, Thorsett, and Kulkarni 1994).

elements such as helium and carbon. Each time the core of the star depletes one element it contracts and heats up until it can burn the next heavier element. But once iron is reached energy can no longer be released by nuclear fusion. With no source of internal energy, the core is supported only by electron degeneracy pressure, and more and more mass is

dumped onto it from the burning of heavy elements in higher layers of the star. Eventually the core reaches the Chandrasekhar mass ($\sim 1.4\ M_\odot$) where electron degeneracy pressure is no longer powerful enough to prevent gravitational collapse. At this point it collapses from a 10^4 km degenerate core to a 10 km neutron star supported by the much stronger neutron degeneracy pressure. This releases a tremendous amount of gravitational potential energy in the form of neutrinos and blows the outer part of the star off in an immense explosion, called a *supernova*. Left behind, deep in this expanding, cooling envelope, is a rapidly rotating, very strongly magnetized neutron star. For a very massive star ($\gtrsim 10\,M_\odot$), the collapse may not be halted at the neutron star stage, and it may collapse to form a black hole. Black holes do not become radio pulsars because they cannot support a magnetic field. A slight asymmetry in this supernova explosion may give the neutron star a large velocity "kick" of 200–1000 km/s or more (Dewey and Cordes 1987; Bailes 1989).

Once the envelope expands and dissipates, the neutron star may become visible as a radio pulsar. The radio pulses are created by the rapidly-rotating dipole field of the neutron star which generates huge electric potential differences in the region near the neutron star surface and pulls charged particles off the surface creating a plasma-filled magnetosphere (Goldreich and Julian 1969). Also, at the polar cap, electron-positron pairs will be created. These particles, moving in the magnetic field, can generate synchrotron and curvature radiation resulting in the broad-band low-frequency radio emission that is observed from pulsars. This radiation is not emitted isotropically, but is directed along the magnetic dipole axis. In most neutron stars, the magnetic dipole is apparently not aligned with the rotation axis, and thus the radio beam from the pulsar sweeps like a lighthouse beam across the sky. As observed from Earth, the pulsar appears to blink on when the beam is directed at the Earth, and is off the rest of the time. For most pulsars the duty cycle (ratio of pulse width to pulse period) is only a few percent. All but a few of these rotation-powered pulsars are observed only at radio wavelengths and show a steep ($S_\nu \propto \nu^\alpha$, $-2 \lesssim \alpha \lesssim -4$) power-law spectrum from about 100 MHz to several GHz. A few of the youngest, or nearest, pulsars are observed to pulse in optical, X-ray, and gamma-rays, as well.

1.2.3 Binary Systems

About 40 pulsars show a periodic modulation of their pulse period that is due to Doppler shifts as the pulsar orbits a companion. According to Newtonian mechanics, the

projected velocity of the pulsar along the line of sight is

$$\mathbf{v_1} \cdot \mathbf{n} = \frac{2\pi a_1 \sin i}{P_b\sqrt{1-e^2}} [\cos(\omega + \phi) + e\cos\omega] \tag{1.6}$$

(Shapiro and Teukolsky 1983), where $\mathbf{v_1}$ is the pulsar velocity, $\mathbf{n}$ is the unit vector in the direction of the pulsar from Earth, P_b is the orbital period, a_1 is the semi-major axis of the pulsar's orbit, i is the orbital inclination with respect to the plane of the sky, e is the orbital eccentricity, ω is the longitude of periastron, and ϕ is the true anomaly. Observed orbital periods range from $\sim$ 108 minutes to several years. The two observed quantities P_b and $a_1 \sin i$ are related to the masses of the orbiting bodies, and Newton's gravitational constant (G), through the mass function

$$f(m_1, m_2, i) = \frac{(m_2 \sin i)^3}{(m_1 + m_2)^2} = \frac{4\pi^2 (a_1 \sin i)^3}{P_b^2 G}. \tag{1.7}$$

The individual masses and orbital inclination cannot be determined from the orbit of one of the bodies by purely Newtonian effects. Additional relativistic effects on the orbital motion allow the masses to be determined in some systems (see §1.5). In systems without these effects measured, a fiducial mass of the companion can be determined from the mass function by assuming a pulsar mass of $1.4\,M_\odot$ and an inclination of 60° (the median value for randomly oriented orbits).

1.2.4 Recycled Pulsars

The recycled pulsars populate the low-field ($B = 10^8 - 10^{11}$ G) and short period (1.5 ms – 40 ms) portion of the P-B diagram. Their spin-down rates are tiny ($10^{-21} - 10^{-18}$) compared to that of the young pulsars, and they therefore live far longer ($\gtrsim 10^8$ yr). They are referred to as recycled because the standard model for their formation is spin-up of a slow pulsar through accretion of matter from a companion star. The recycled pulsars are divided into two categories based on their characteristics and their inferred evolutionary path.

High-mass Binary Pulsars

The high-mass binary pulsars (HMBPs) were the first type of recycled pulsar discovered. PSR B1913+16[1] ("The Binary Pulsar") was discovered by Hulse and Taylor

[1] As recommended by the International Astronomical Union, pulsars are named in two possible ways; according to their equatorial coordinates at the epoch B1950.0, and more recently, the J2000.0 epoch. Some

TABLE 1.1

Known high-mass binary pulsars (HMBPs).

PSR	P (ms)	$\dot{P}$ (10^{-18})	τ_c (10^6 yr)	P_b (d)	$a_1 \sin i/c$ (s)	e	f_1 ($M_\odot$)	m_2 ($M_\odot$)
J0045-7319	926.27	4465.	3.3	51.169	174.235	0.808	2.17	5.33
B1259-63	47.76	2280.	0.3	1236.81	1296.00	0.870	1.53	4.19
B1534+12	37.90	2.43	240.	0.421	3.730	0.274	0.31	1.34†
B1820-11	279.82	1378.	3.	357.762	200.672	0.795	0.068	0.80
B1913+16	59.03	8.63	110.	0.323	2.342	0.617	0.13	1.39†
B2127+11C	30.53	5.0	97.	0.335	2.518	0.681	0.15	1.37†
B2303+46	1066.37	569.3	30.	12.340	32.688	0.658	0.25	1.46

m_2 is determined by assuming $m_1 = 1.4\,M_\odot$ and $i = 60°$ except for the values marked with a dagger (†) which were determined by relativistic effects.

(1974) and earned them the Nobel Prize in Physics.

HMBPs consist of an active pulsar in a highly eccentric orbit about high-mass star ($\gtrsim M_\odot$). To date, there are only about six such systems known in the Galactic disk, and one other in a globular cluster (see Table 1.1). In no case have pulsations been observed from the companion, which for at at least four of them is probably a neutron star.

In the Galactic disk, these systems begin as two high-mass stars. The more massive member evolves more quickly and goes supernova, leaving a neutron star remnant, but not disrupting the binary system. Two of the HMBPs appear to be in this intermediate state, where a radio pulsar orbits a massive main-sequence star (PSR B1259-63 and PSR J0045-7319).

As the stellar companion evolves, it will begin to dump matter onto the neutron star, transferring angular momentum to the neutron star and possibly spinning it up to tens of millisecond periods. This state is identified with the high mass X-ray binaries (Bhattacharya and van den Heuvel 1991). There are many examples of X-ray pulsars with B or Be stellar companions, where the X-ray pulsations are powered by accretion of matter

pulsars will therefore be referred to as PSR 1937+21 or PSR B1937+21 (where PSR denotes the source type pulsar and the coordinates are 19^h37^m right ascension and $+21°$ declination). Pulsars that were named in the older coordinate system will continue to be referred to by their familiar names. All new pulsars reported here will be referred to with their new names, e.g. PSR J2043+2740. This pulsar is at 20^h43^m right ascension and $+27°40'$ declination in the J2000.0 coordinate system. The extra precision on the declination is optional and will only be included when the pulsar position is known well enough.

onto the neutron star. Finally, the second star will go supernova, and if the mass loss is small enough, or the velocity kick is in the right direction, the system might not unbind. In this case, two neutron stars in a highly eccentric orbit remain. One will be a newly formed young pulsar, and the other will be the newly recycled pulsar. The young pulsar may spin-down below the death line in a few million years, while the characteristic ages of some of the known HMBPs are $1 - 2 \times 10^8$ years. This difference in lifetimes, as well as beaming effects may explain why pulsations from the neutron star companion have not been detected. There is one isolated pulsar (PSR J2235+1506) which has a period of 59 ms and a magnetic field of $\sim 3 \times 10^9$ G which was likely spun up by a high mass companion, but then became unbound in the second supernova explosion. These pulsars have moderate magnetic fields of $\gtrsim 10^{10}$ G and periods that range from 30 ms to over 1 second. These pulsars are not spun up to millisecond periods because their accretion stage lasts only $\sim 10^6$ yr since it is driven by the rapid evolution of a high-mass star. Also, their magnetic fields are higher than the LMBPs described below and thus the equilibrium spin period is higher (see Eqn. 1.5). In the globular cluster system, the formation of double neutron star systems is quite different. The HMBP PSR B2127+11C was probably formed through a stellar exchange collision in the dense core of the globular cluster M15 (Prince *et al.* 1991).

Some of the HMBP systems consist of two neutron stars orbiting each other at up to 0.1% of the speed of light, and one is a superbly accurate clock. This makes these systems ideal laboratories for the study of the theory of gravitation in far more extreme conditions than are available in the Solar system. The pulsar PSR B1913+16 displays experimental evidence for the emission of gravitational waves. Measurements of relativistic effects in the timing of PSR B1913+16 combined with those of PSR B1534+12 are providing stringent tests of Einstein's theory of general relativity in strong-field conditions and have ruled out large classes of competing theories of gravity (see §1.5).

Since these binary systems lose energy due to the emission of gravitational waves, they slowly spiral in towards an eventual coalescence in $\sim 10^8$ yr. These coalescence events are the most predictable sources of powerful gravitational waves that may be detectable by the Laser Interferometer Gravitational-wave Observatory (LIGO) (Abramovici *et al.* 1992).

Low-mass Binary Pulsars

More numerous than the HMBPs are the low-mass binary pulsars (LMBPs) of which there are about 30 known systems. These are typified by much shorter pulse periods (1.5–16 ms) and very nearly circular orbits with light companions ($\lesssim 0.5\,M_\odot$, as determined from the mass function, Eqn. 1.7). These pulsars have very low spin-down rates, implying low magnetic fields ($\lesssim 5 \times 10^8$ G). Several of these systems have characteristic ages older than the disk of the Galaxy ($\sim 10^{10}$ yr), probably implying that they were born with periods near their current values (Camilo, Thorsett, and Kulkarni 1994, and Eqn. 1.3). Essentially all of these systems formed are still pulsing today.

Current evolutionary theories identify the LMBPs as the end product of the low-mass X-ray binaries (LMXBs). The LMXBs are formed from binary systems consisting of a massive star and a low-mass companion. When the massive star evolves and goes supernova, it leaves behind a neutron star with a low mass companion. These systems live for a long time before stellar evolution, tidal coupling, or gravitational radiation drive them close enough for the normal star to transfer matter through an accretion disk onto the neutron star. During this stage, the system may be a bright X-ray source as the accreted matter deposits energy onto the neutron star surface. The neutron star is spun up to periods around 1 millisecond and is re-born as a recycled pulsar. The low-mass companion eventually collapses to a white dwarf. The long duration of the accretion stage tends to circularize the orbit, and these systems usually have eccentricities less than 10^{-4}.

A few isolated millisecond pulsars have been found (including the first millisecond pulsar). These are usually grouped with the LMBPs because they are believed to have formed in a similar manner. It is believed that these pulsars have evaporated their companion with a powerful pulsar wind—a process that may be in progress in the eclipsing binary pulsar PSR B1957+21 (Fruchter *et al.* 1990; Kluźniak *et al.* 1989).

There is a competing theory for the formation of LMBPs, called accretion-induced collapse (AIC). In this model a system consisting of a low-mass main sequence star and a white dwarf evolves until mass transfer onto the white dwarf begins. If the initial white dwarf mass is sufficiently close to $1.4\,M_\odot$, it may accrete enough matter to surpass the Chandrasekhar limit and collapse to a neutron star. This scenario has been used to explain Type Ia supernovae (Branch 1990), but may also be a quieter event that produces a millisecond pulsar.

1.3 Pulsar Detection and Sensitivity

Because pulsar signals are quite faint (many of them have fluxes of 1 mJy or less[2]), pulsar searching is typically done with large single-dish radio telescopes. Normal radio source detection is done by chopping the telescope on-source, then off-source and measuring a difference in received power. Conveniently, the pulsar signal is intrinsically modulated and one can search for periodic increases in radio intensity without having to move the telescope. Pulsar data collection systems are described in Chapter 2.

Detailed formulae for pulsar search sensitivities are given in Chapters 3 and 4. Briefly, the energy carried by the pulsar emission is collected by the large radio antenna and focused on a receiver. The incident electric field is converted to a voltage and amplified by the receiver electronics. This voltage is squared to determine the instantaneous power. These powers are averaged and recorded by various types of backend electronics (Chapter 2). When this time series is analyzed, the pulsar signal adds coherently, while the sky and system noise add incoherently, so the signal-to-noise ratio (S/N) detected from a pulsar increases as the square root of the integration time. Similarly, the S/N goes as the square root of the receiver bandwidth (B).

$$S/N \sim \left[\frac{G\left(N_p B t\right)^{1/2}}{T_{\rm sys}}\right] \times \left(\frac{P - w_{\rm eff}}{w_{\rm eff}}\right)^{1/2} \times S, \tag{1.8}$$

where $T_{\rm sys}$ is the total system temperature, G is the telescope gain, N_p is the number of received polarizations, t is the observation time, $w_{\rm eff}$ is the effective width of the pulse after folding in instrumental effects and dispersion, and P is the pulsar period, and S is the pulsar flux.

1.4 Previous Searches and Motivation for Additional Large-Area Searches

The 305-m radio telescope at Arecibo, Puerto Rico can observe a strip of sky from declinations $-1°39'$ to $+38°21'$ — over 13,000 square degrees. However, before 1990 virtually all of the untargeted pulsar searching from Arecibo was confined to a narrow strip of less than 10° around the Galactic plane, and towards the Galactic center (see Table 1.2 for a summary of published field pulsar surveys). This observing strategy maximizes the

[2] 1 Jansky = 1 Jy = $10^{-26}\,\mathrm{W\,m^{-2}\,Hz^{-1}}$

number of pulsars discovered, since pulsars are clustered towards the Galactic plane. As a consequence, the pulsar distribution is well-measured near the plane, but substantially less constrained at high Galactic latitudes. Complete surveys of high latitudes, while they discover fewer pulsars per square degree, are important because discovery of low-luminosity (nearby) pulsars is equally likely at high latitudes, and measuring the low-luminosity cutoff of the pulsar luminosity function is important for determination of the total pulsar population and birth rate. In addition, observations of high-latitude pulsars can help map the interstellar electron distribution in our local region.

The early surveys also had sample times much too long to be sensitive to millisecond pulsars, which provide interesting astrophysical laboratories for binary orbital evolution, time-keeping metrology, discovery of planetary systems, high-precision astrometry, and many other applications. The observed population of millisecond pulsars has a characteristic distance from the Galactic plane of $\gtrsim 600\,\mathrm{pc}$ (Phinney and Kulkarni 1994), which is consistent with that of the low-mass X-ray binary systems that are commonly assumed to be their progenitors. The actual scale height of the millisecond pulsar distribution is probably even larger because of their large ages ($\sim 10^9\,\mathrm{yr}$), but selection effects of surveys limit the sample to nearby pulsars. Most millisecond pulsars have been found at distances of less than 3 kpc, so their distribution on the sky is expected to be fairly isotropic (see Figure 1.2). The fact that the first four millisecond pulsars were found in the Galactic plane is simply an observational selection effect (Srinivasan and Bhattacharya 1989). Thus, the known population of millisecond pulsars may be greatly increased by sensitive high latitude surveys. All but two millisecond pulsars known in the Galactic disk (PSR J2322+2057 and PSR B1937+21) are in binary systems. For surveys requiring long integration times, this acts as a strong selection effect against short-period binary pulsars because the Doppler-shifted signal does not remain coherent across the observation. However, the Arecibo instrument can detect pulsars as faint as $\sim 1\,\mathrm{mJy}$ in a drift scan that integrates $\sim 32\,\mathrm{s}$ (see sensitivity discussion in §4.4)—a time shorter than the time scale for orbital acceleration to degrade the coherence of the signal. Surveys at smaller telescopes require longer integrations, imposing a large selection effect against short-period binary systems which is not present in the large-area surveys described here.

Hulse and Taylor (1974) surveyed 24 square degrees towards the Galactic anticenter, but the Nyquist limit of their search was 33.4 ms. Young pulsars found in the direction of the Galactic anticenter could be of great interest. The sky is much less crowded in the

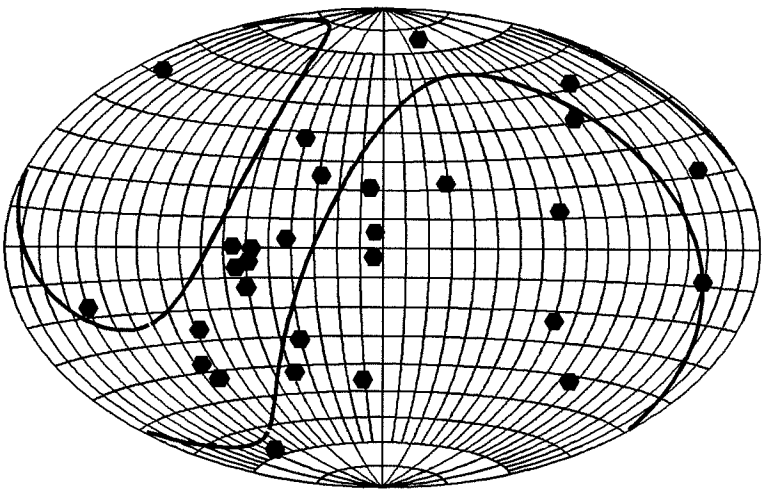

Figure 1.2: A map of all known millisecond pulsars ($P \lesssim 16$ ms) that are not in globular clusters, in Galactic coordinates. The Galactic center direction ($l = 0$, $b = 0$) is in the middle of the plot. The region of sky accessible to Arecibo is outlined in heavy lines. Only a weak concentration towards the plane is evident, and the bunching where Arecibo crosses the Galactic plane may be, in part, a selection effect.

anticenter direction than in other regions of the Galactic plane, and hence a young pulsar could be convincingly associated with the molecular cloud from which its parent massive star collapsed. In addition, timable millisecond pulsars at many separate locations are needed to become part of a millisecond pulsar timing array, which has the potential to discover cosmological gravitational waves with periods from days to years. For these reasons, we undertook a survey for fast pulsars in the Galactic anticenter.

Then, during 1990 February, while the Arecibo telescope azimuth drive was unusable, A. Wolszczan used the telescope in drift mode to survey ~ 150 square degrees of sky at high Galactic latitude (Wolszczan 1991). Two interesting pulsars (PSR B1257+12, a millisecond pulsar with a planetary system, and PSR B1534+12, a relativistic binary system) were discovered in this survey. Spurred by this success, several groups began an effort to survey the entire Arecibo sky for millisecond pulsars. This is continuing during the current upgrade of the Arecibo telescope. The three surveys noted with an "I" in Table 1.2 are incomplete and currently ongoing. They are the Parkes all southern sky survey, the Jodrell Bank northern sky survey, and the Arecibo ($0^\circ < \delta < 39^\circ$) survey. A good review of the current status of millisecond pulsar surveys is given by Camilo (1994b).

TABLE 1.2

Published field pulsar surveys, based on Table 2.1 by Nice (1992).

Survey	ν (MHz)	t_s (ms)	$S_{\min}$ (mJy)	Area (deg^2)	$N_{\rm PSR}$	Notes	Ref.
UMass-Arecibo	430	16.7	1	24	0	A	[1]
UMass-Arecibo	430	16.7	1	140	40	G	[1]
UMass-NRAO	400	16.7	10	12500	17	N	[2]
Molonglo I	408				31	M	[3]
Molonglo II	408	10.0	15	27000	155	S	[4]
Molonglo III	843	0.5	8	200	1	GS	[5]
Princeton-NRAO I	390	16.7	2	6000	34	N	[18]
Princeton-NRAO II	390	2.2	3	3725	20	N	[6]
Princeton-Arecibo I	430	0.4	2	289	5	G	[6]
Jodrell Bank A	408	40.0	10	3000	31	GN	[7]
Jodrell Bank B	1400	2.0	1	200	40	GN	[8]
Jodrell Bank C	1400	0.3	40	1500	0	GN	[9]
Jodrell Bank C	928	0.3	74	—	—	GN	[9]
Jodrell Bank C	610	0.4	97	—	—	GN	[9]
Parkes	1500	0.3	2.5	800	46	GS	[10]
Parkes	1500	1.2	1.0	—	—	GS	[10]
Princeton-Arecibo II	430	0.5	2	235	25	GN	[11]
Princeton-Arecibo III	430	0.25	0.7	170	4	N	[11]
Princeton-Arecibo IV	430	0.25	0.7	292	7	N	[12]
Penn. State-NRL	430	0.25	0.7	828	17	N	[13]
Parkes Southern	436	0.3	4	21000	75	SI	[14]
Jodrell Bank Northern	410	0.3	5	~ 8000	> 1	NI	[14]
Caltech-Arecibo I	430	0.25	0.7	515	0	AN	[15]
Caltech-Arecibo II	430	0.18	0.7	360	4	N	[16]
Caltech-Arecibo III	430	0.25	0.7	600	12	NI	[17]

Notes: G—Galactic plane; A—Galactic anti-center region; S—Southern sky; N—Northern sky; I—In progress; M—much of southern sky covered with a variety of hardware setups.

References: [1] Hulse and Taylor (1974), Hulse and Taylor (1975); [2] Damashek, Taylor, and Hulse (1978); [3] Large and Vaughan (1971); [4] Manchester *et al.* (1978); [5] D'Amico *et al.* (1988); [6] Stokes *et al.* (1986); [7] Davies, Lyne, and Seiradakis (1977); [8] Clifton *et al.* (1992); [9] Biggs and Lyne (1992); [10] Johnston *et al.* (1992); [11] Nice (1992) and Fruchter (1989); [12] Camilo, Nice, and Taylor (1993); [13] Foster, Wolszczan, and Cadwell (1994); [14] Manchester (1994); [15] Chapter 4; [16] Chapter 5 and Thorsett *et al.* (1993); [17] Chapter 5; [18] Dewey *et al.* (1985).

The Young Pulsar Population

The observed population of pulsars (shown in Figure 1.3) is heavily biased by high-luminosity and nearby pulsars, and not representative of the Galactic population of pulsars as a whole. There have been many statistical studies (Lyne, Manchester, and Taylor 1985; Lorimer *et al.* 1993, for example) which try to infer properties of the total population of pulsars based on the observed sample. These efforts must take into account the sky coverage, flux limits, and various selection effects of the many pulsar surveys. This is often done by using Monte Carlo techniques to generate sample Galactic populations of pulsars based on a model and then comparing the number of pulsars detected in the simulated surveys to the actual observed population. This is one reason why the current ongoing searches described above will be particularly important. They cover the entire sky accessible to Arecibo with a nearly constant sensitivity of ~ 0.7 mJy, and the selection effects against short period pulsars are minimal. Taken as a whole they should allow good statistical studies of the young pulsar population. Deep, unbiased surveys such as these are needed to resolve some of the disputed points in pulsar population models, such as the pulsar birth rate, the existence of magnetic field decay or the need for a substantial fraction of pulsars to be born at long (0.5–1.0 s) periods. These surveys are somewhat limited in their dispersion measure (see §2.1) coverage because the Arecibo filter bank channels are rather wide (0.25 MHz). However, this is only relevant very close to the Galactic plane where only a tiny fraction of the time is spent. In addition, the region with $b \lesssim 5°$ has been well-covered by many of the surveys in Table 1.2.

Several characteristics of the young pulsar population are now reasonably well-established.

- The pulsar birth rate is roughly consistent with estimates of the Galactic supernova rate of $\sim 0.01\,\mathrm{yr}^{-1}$.
- The pulsar scale height is ~ 400 pc, much larger than the scale height of the massive stars that are pulsar progenitors.
- Consistent with their large scale height, pulsars have very high spatial velocities, with recent estimates of the mean velocity as high as 450 km/s (Lyne and Lorimer 1994).
- There are about 70,000 potentially observable pulsars with luminosity $> 0.3\,\mathrm{mJy\,kpc}^2$ (Lyne, Manchester, and Taylor 1985).

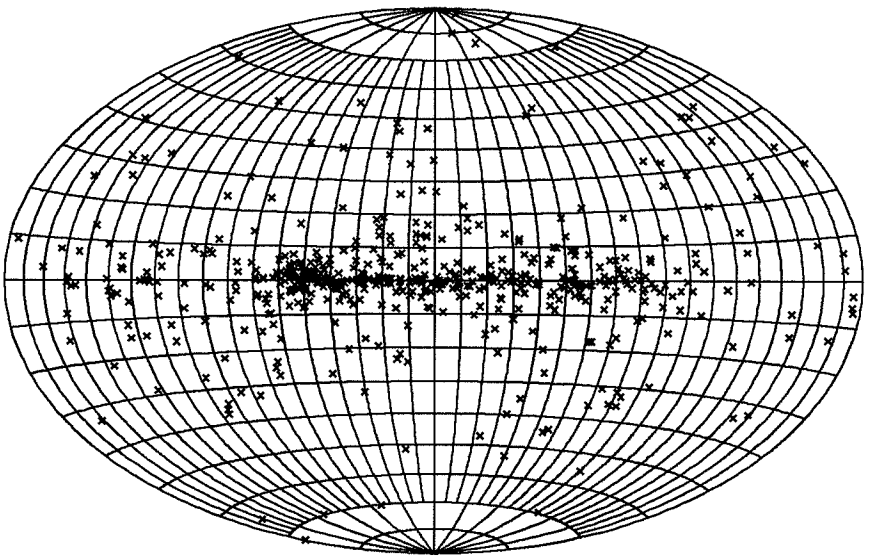

Figure 1.3: Map of known pulsar positions in Galactic coordinates.

- The pulsar luminosity function is close to a power law of slope -1 and may have a cutoff at $L \lesssim 1\,\mathrm{mJy\,kpc^2}$.

The Millisecond Pulsar Population

Since the millisecond pulsars are believed to have descended from the LMXBs, their populations should have similar characteristics. Indeed, the binary fraction among millisecond pulsars is very high ($\sim$ 75%). In addition, the scale height for millisecond pulsars ($\gtrsim 600\,\mathrm{pc}$) and their observed velocities ($\sim 75\,\mathrm{km/s}$) are commensurate with those of the LMXB population. Of course, there are significant selection effects and small-number statistics involved in the determination of these numbers. Because millisecond pulsars are very old, high-velocity systems will have moved far beyond survey limits, and because millisecond pulsars are not very luminous, systems far from the plane will be missed by many surveys. So both of these numbers have to be considered lower limits.

Working from a rather small sample of millisecond pulsars, Kulkarni and Narayan (1988) calculated the birth rate of LMBPs and compared it to the birth rate of LMXBs (of which there are $\sim$ 100 in the Galaxy). They found that the birth rate of LMXBs was a factor of 10–100 larger than that for the LMBPs. However, with the population of millisecond pulsars greatly increased by large-area surveys and an improved distance model (Taylor and Cordes 1993), Lorimer *et al.* (1995) revised the population estimate for millisecond pulsars

with luminosity greater than 2.5 mJy kpc^2 to $\sim 40,000$. This is much lower than previous estimates (Kulkarni and Narayan 1988; Johnston and Bailes 1991), and may help alleviate the apparent birth rate discrepancy between millisecond pulsars and LMXBs. In addition, Coté and Pylyser (1989) suggested several effects that may reduce the lifetime of LMXBs, thus removing some of the discrepancy.

1.5 Overview of Pulsar Timing

Once a pulsar has been discovered, measurements of linear or circular polarization, scintillation, pulse morphology, microstructure, and nulling can be performed to determine the pulsar's properties and the properties of the intervening interstellar medium. Another major source of information is *pulsar timing.* Measured pulsar periods change for a variety of reasons including a changing Doppler shift due to the motion of the Earth around the Sun, intrinsic spin-down of the pulsar itself, Doppler shift from motion of the pulsar around its companion, and acceleration of the pulsar in the gravitational potential of a globular cluster. Precise pulsar timing allows exceedingly accurate measurements of a pulsar's position, proper motion, parallax, spin-down rate, dispersion measure, binary system parameters, and even the orbits of planetary-mass bodies near the pulsar.

Pulsar timing is an iterative process whose goal is to develop a timing model which can be used to predict the pulsar's rotational phase over a large time span. The first part of pulsar timing is establishing a baseline model. This is normally done with repeated measurements of the pulsar period over several days. From these period measurements an accurate period and preliminary Keplerian parameters of the binary system (if any) are established by fitting to Equation 1.6. Then these parameters are refined through pulse time-of-arrival (TOA) analysis.

Using the preliminary timing model to predict the pulsar period for each observation, pulse profiles are generated by folding the incoming data modulo the pulse period. These profiles are cross-correlated with a high-signal-to-noise template to determine a precise arrival time of one pulse.

The fitting of a model to these TOA measurements is normally done with a powerful program called TEMPO developed at Princeton University (Taylor and Weisberg 1989). The input to TEMPO is a list of topocentric TOAs, with observation frequency and observatory codes for each. In its first stage, TEMPO uses the known position of the observatory at

the time of the observation, the configuration of the solar system based on a precise planetary ephemeris, and the model position and dispersion measure of the pulsar to transform the time and frequency of each TOA to an approximately inertial frame at the solar system barycenter at infinite frequency. Then TEMPO performs a nonlinear least-squares fit to a model of the pulsar spin and orbital parameters. The differences between the measured data points and the best-fit model are called timing *residuals*. The power of this method comes from the fact that pulses can be counted exactly over spans of many years, and deviations from a model of a small fraction of the pulse period can be measured. Thus, pulse periods are routinely measured to one part in 10^{11} and $\dot{P}$s on the order of 10^{-20} are measured for some millisecond pulsars.

Binary orbits are fitted in a theory independent way (Damour and Taylor 1992). In their parameterized post-Keplerian (PPK) formalism, a timing model is developed which consists of the five Keplerian parameters $(P_b, T_0, e_0, \omega_0, x_0)$, and 8 post-Keplerian parameters $(k, \gamma, \dot{P}_b, r, s, \delta_\theta, \dot{e}, \dot{x})$. For any particular theory of gravitation, the values of the post-Keplerian parameters are a function of the measured Keplerian parameters and the two inertial masses in the system (m_1, m_2). Thus measuring any of the post-Keplerian parameters defines an allowed line in the $m_1 - m_2$ plane. A second post-Keplerian parameter provides a measurement of m_1 and m_2. Each further parameter tests the theory of gravity by requiring that all the lines in the $m_1 - m_2$ plane meet at a point, allowing up to 6 different tests from the 8 PPK parameters. Currently, the original binary pulsar (PSR B1913+16) has yielded good measurements of three PK parameters $(\dot{\omega}, \gamma, \dot{P}_b)$. This yields one test of relativistic gravity, and shows that general relativity's prediction of orbital period decay due to emission of gravitational waves is correct. Two more strong-field tests of gravity have come from the more recently discovered pulsar PSR B1534+12. Measurements of $\dot{\omega}, \gamma, r$, and s have yielded two more confirmations of general relativity's predictions. These results have ruled out large classes of other gravitational theories which, without these binary pulsar systems, would be extremely difficult to test.

Precise pulsar timing, particularly of millisecond pulsars, has many other important applications (Taylor 1992; Phinney 1992; Kaspi 1994b). Here, I give brief descriptions of a few of them.

- Timing an array of millisecond pulsars widely distributed on the sky can test for the existence of a stochastic gravitational wave background left over from the Big Bang

(Backer and Hellings 1986). Gravitational waves with periods from months to years would manifest themselves as correlated timing residuals (Thorsett 1991).

- Neutron star masses are extremely interesting as a clue to pulsar formation and evolution. In HMBPs, masses can be measured extremely accurately by measuring $\dot{\omega}$ and γ as discussed above. LMBPs are believed to have undergone longer epochs of accretion, and thus may contain somewhat heavier neutron stars (1.5–2.0 $M_{\odot}$). These masses can be measured for systems with favorable orbital inclinations by the two Shapiro delay parameters (r, s).

- Some pulsars in globular clusters are observed to have a negative $\dot{P}$. This is due to the pulsar being accelerated in the gravitational potential of the cluster. These pulsars can be used to constrain mass-to-light ratios and mass segregation in globular clusters (Phinney 1992).

- Pulsars are important for tying together various celestial reference frames (Kaspi 1994a). Pulsar timing determines exceedingly accurate positions for pulsars in the frame of the solar system ephemerides. An accurate interferometric position measurement connects this to with the extragalactic reference frame. An optical identification of a pulsar or its companion ties in the optical reference frame.

- Timing binary pulsars can be used to constrain the rate of change of Newton's gravitational constant. A non-zero value of $\dot{G}/G$ will induce a $\dot{P}_b$ which differs from the prediction of general relativity (Damour, Gibbons, and Taylor 1988; Nordtvedt 1990).

- The pulsar PSR B1257+12 showed very unusual timing residuals when fit to the standard isolated-pulsar timing model. These were found to be due to *two* sinusoidal periodicities which were well fit with orbital models of two planetary-mass companions (Wolszczan and Frail 1992). This represents the first discovery of extra-solar system planets. Several previous claims exist in the literature, but all were eventually retracted. In the case of PSR B1257+12, the mutual gravitation of the planets, which are in a nearly 3-2 resonance, has manifested itself in detectable orbital perturbations, confirming their planetary nature.

1.6 Organization of This Dissertation

This dissertation is centered around four papers (Chapters 3 – 6) that have been or will be submitted for publication in THE ASTROPHYSICAL JOURNAL. This chapter (Chapter 1) serves to introduce the subject of pulsars, motivate the searches that were performed, and provide some of the background material that is normally assumed in the writing of a paper for publication in THE ASTROPHYSICAL JOURNAL. Chapter 2 introduces pulsar data collection and data analysis techniques which were used for this work. Chapter 3 describes a survey designed to discover very young pulsars in supernova remnants. Chapter 4 collects the results of several large-area surveys designed to discover recycled pulsars away from the Galactic plane. Chapter 5 announces the discovery of 12 pulsars in a very large survey being performed during the upgrade of the Arecibo telescope. Chapter 6 describes the preliminary findings on a 5.9 ms pulsar discovered in the upgrade survey. Appendix A reprints an IAU Circular announcing the 96 ms pulsar which is described in Chapter 5.

Chapter 2

Computational Aspects of Pulsar Searching

2.1 Basic Concepts

Dedispersion

The primary observational difficulty which pulsar data collection systems and data analysis techniques are designed to minimize is *dispersion.* Pulsar signals traveling through the partially-ionized interstellar medium suffer from a frequency-dependent delay, or dispersion. The group velocity of an electromagnetic wave traveling in a diffuse plasma is

$$v_g = c\left(1 - \frac{n_e e^2}{2\pi m_e c^2 \nu^2}\right), \tag{2.1}$$

thus the delay suffered by a pulse on its path to an Earth-based observer is

$$t = \frac{e^2}{2\pi m_e c \nu^2} \int n_e dl. \tag{2.2}$$

The integral in the above equation is the column density of free electrons along the line of sight to the pulsar, which is referred to as the dispersion measure (DM) (usually quoted in $\mathrm{pc\,cm^{-3}}$). So, the differential delay across a bandwidth $\Delta\nu_{\mathrm{MHz}}$, measured in MHz, is

$$\Delta t = \left(\frac{202}{\nu_{\mathrm{MHz}}}\right)^3 \times \Delta\nu_{\mathrm{MHz}} \times \mathrm{DM\ ms}. \tag{2.3}$$

For a pulsar signal to be detectable, the dispersive smearing across the detection bandwidth must be kept to a small fraction of the pulsar period. For this reason, radio observations of pulsars normally use filter banks or autocorrelation spectrometers (see below) to detect the pulsar in many small frequency bands. In the analysis, frequency-dependent delays are applied to the various channels to align the pulses before summing the channels

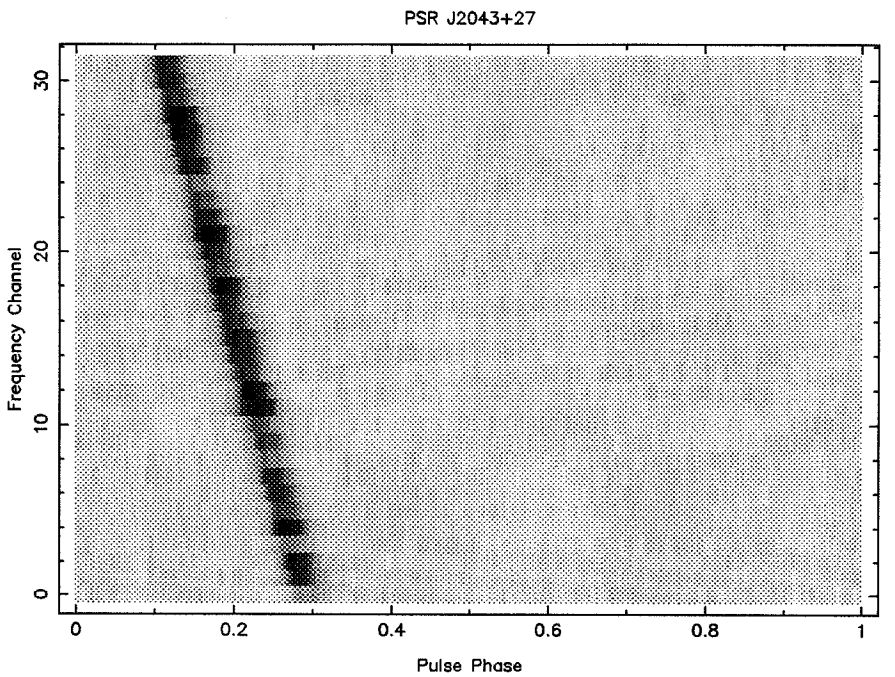

Figure 2.1: A folded pulse profile of PSR J2043+27 in 32 adjacent frequency bands of 0.25 MHz, centered around 430 MHz. Grayscale represents intensity, and the channel number is on the y axis. The delayed arrival of the lower frequency bands is clearly evident for this 96 ms pulsar at a DM of 20.1 pc cm^{-3}.

into the final time series. For searching, a set of trial DMs is used in order to be sensitive to pulsars over a wide range of dispersion measure. These DM trials are spaced such that the difference in total delay across the bandwidth between two trials is small compared to the shortest period pulsar the observation is intended to be sensitive to. Any particular survey is fundamentally limited by the dispersive smearing across a single channel of the filter bank.

Fast Fourier Transforms

The Fast Fourier Transform (FFT) is the primary method of searching for periodic signals in noisy data. The Fourier transform is just the decomposition of a time series onto a basis set of sinusoidal functions, $\cos(\omega t + \phi)$. For a time series of length N, this naively requires the computation of N dot products of length N, or $\mathcal{O}\ (N^2)$ operations. This can

be written (Press *et al.* 1992) as

$$H_n = \sum_{k=0}^{N-1} W^{nk} h_k, \tag{2.4}$$

where

$$W = e^{2\pi i/N}. \tag{2.5}$$

However, Cooley and Tukey (1965) showed that an algorithm existed to calculate a Fourier transform in $\mathcal{O}\ (N \log_2 N)$ operations, called the fast Fourier transform (FFT). The Fourier *power spectrum* of a time series is derived from the magnitude of the complex numbers H_n and quantifies the amount of power present at each frequency.

Harmonic Folding

Since pulsars have typical duty cycles of less than 10%, their Fourier power spectra typically show several (usually 4–32) significant harmonics at multiples of the fundamental frequency. Thus, detection efficiency can be greatly increased by summing harmonics in the power spectrum before searching for significant peaks. It is convenient to store the sums at the highest harmonic since the resolution of a harmonic fold is fractions of a frequency bin at the lowest harmonic. The harmonically-folded power in frequency bin i is given by

$$P_i' = \sum_{h=1}^{N_h} P_{ih/N_h} \tag{2.6}$$

where N_h is the maximum harmonic number. Evaluating P_{ih/N_h} can be done either by getting the power in the nearest bin or by interpolation between bins. Harmonic folds for most of the surveys described here were done for 1, 2, 3, 4, 8, and 16 harmonics.

2.2 Computational Requirements

The first pulsar searches were done by inspecting chart recorder records of the total power received by the antenna. As searches have pushed toward fainter and faster pulsars, the computation involved in searching has also increased. With the fast sampling (100–500 μs) required to be sensitive to millisecond pulsars, even low-sensitivity, large-area surveys require FFTs of 128 kpoints or more. Deep, pointed observations like those used to search for faint pulsars in supernova remnants (Chapter 3) or globular clusters

(Anderson 1993) require transforms of $2^{20} - 2^{30}$ points. These searches require either large-scale supercomputers, or in some cases clusters of fast workstations, to reduce the data in a reasonable time. Here we count the number of floating point operations (FLOPs) that are involved in reducing a typical single pointing.

Many modern CPUs have been optimized to increase the number of "MFLOPs" (million floating point operations per second) that they can perform. This has resulted in heavily pipelined sophisticated floating point units, while sometimes sacrificing integer performance. In the following, I will count some of the more complicated integer manipulations as "FLOPs".

Given a data set of N samples of M frequencies, there are several steps involved in finding candidate pulsar signals in the data.

- The data are usually packed into 2–8 bit integers for data-rate considerations, so these integers must be unpacked into floating point numbers, usually requiring some combination of bit arithmetic and look-up tables. Counting each of these mappings to a floating point number as one FLOP,

$$N_{\text{unpack}} = N \times M. \tag{2.7}$$

- A time series for each trial dispersion measure must be created. Let N_{DM} be the number of trials and each trial involves about M adds for each of the N time series points, thus,

$$N_{\text{dedispersion}} = N_{\text{DM}} \times M \times N. \tag{2.8}$$

- Now each of these time series undergoes a real FFT, using a standard algorithm. An FFT of a real sequence of length N is performed as an FFT of a complex FFT of length $N/2$ followed by an $\mathcal{O}$ (N) unpacking step (Press *et al.* 1992),

$$N_{\text{FFT}} = N_{\text{DM}} \times (\frac{5}{2} N \log_2(N/2) + 8N). \tag{2.9}$$

- A power spectrum is generated by squaring and adding the real and imaginary part of each complex value in the transform,

$$N_{\text{pwr}} = N_{\text{DM}} \times 3N/2. \tag{2.10}$$

TABLE 2.1

Computation budget for two surveys.

Parameter	Large-Area Survey	SNR Survey
$t_{\rm samp}$	250 μs	500 μs
$t_{\rm obs}$	34 s	1800–4200 s
DM range	0–50 pc cm^{-3}	0–1000 pc cm^{-3}
N	2^{17}	2^{22}
$N_{\rm DM}$	50	500
M	64	256
H	16	16
$N_{\rm total}$	830 MFLOP	700 GFLOP
# pointings	4×10^4	50
Complete survey	33 TFLOP	35 TFLOP
Sparc 10	9 MFLOP/s	
Intel Delta	1 GFLOP/s	

- Finally, because pulsar signals typically have many significant harmonics in the power spectrum, a harmonic fold of up to H harmonics is done,

$$N_{\rm harm} = N_{\rm DM} \times NH. \tag{2.11}$$

So, summing and collecting terms, the total operations required is approximately

$$N_{\rm total} = N \log_2(N/2) \left(\frac{5}{2} N_{\rm DM}\right) + N \left[M + (M+H) N_{\rm DM} + \frac{13}{2} N_{\rm DM}\right]. \tag{2.12}$$

The parameters for a typical deep, pointed survey such as in Chapter 3 and a typical large-area survey such as in Chapters 4 and 5 are presented in Table 2.1.

2.3 Pulsar Data Collection

To understand the computational problem, one needs to know the characteristics of the raw data. The chief difficulty in detecting pulsar signals is dispersion. The broad-band pulsar signal travels through the dispersive interstellar medium, in which the group velocity of the signal is a function of the frequency, and therefore the pulse arrives at different times across the bandpass of the receiver system (see §2.1). Some sort of correction for this differential delay must be performed either by the backend electronics or in the data analysis.

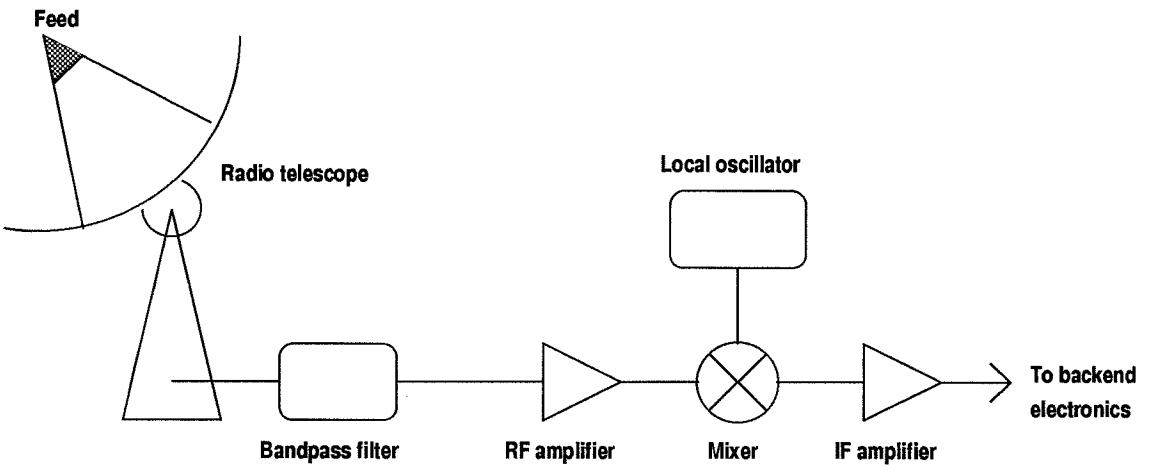

Figure 2.2: Block diagram of pulsar receiver. Everything but the telescope is replicated for the orthogonal linear or circular polarization.

2.3.1 Receiving Pulsar Signals

The broad band radio signal from the pulsar arrives at a radio telescope as plane waves. The telescope dish reflects the waves and focuses them to a point in the case of a parabolic reflector, or a line in the case of a spherical reflector (e.g. Arecibo). The feed is an antenna which converts the incident electric field into an oscillating voltage. This signal is bandpass-filtered to define the frequency range of the observation then amplified by a low-noise radio frequency (RF) amplifier. The RF signal is mixed down to an intermediate frequency (IF) using a local oscillator which is phase-locked to the observatory frequency standard. The IF is amplified and fed to the backend electronics.

2.3.2 Pulsar Signal Processing

The primary role of pulsar signal processing hardware is to compress the data to a manageable rate, while retaining enough information to be able to compensate for dispersion in the later processing.

IF Recorders

The very simplest pulsar backend is the direct digitizing and recording of the IF signal voltage. Until recently, this technique has not been widely used, due to the limited speeds of tape recorders. To retain the full information content of the signal, the sampling must be faster than twice the bandwidth of the IF signal. For typical pulsar observations

the bandpass is from 1 to 100 MHz, which is too high a data rate for most digital tape recorders, even with only 1 or 2-bit sampling.

This method retains all the information in the raw pulsar signal and allows great flexibility in the data analysis methods after the observations are made. Current technology has made very fast tape recorders available; however, the computational and I/O demands of this type of data analysis are just becoming meetable with the most recent parallel supercomputers. This method is the most promising for the future, but as yet has not been used extensively.

Coherent Dedispersers

Coherent dedispersers, which can be implemented in either analog or digital form, remove the frequency-dependent dispersive delay from the received pulsar signal *before* square-law detection (Hankins and Rickett 1975). This is done by convolving the complex voltage signal with the inverse of the transfer function of the interstellar medium. This dedispersed data can then be square-law detected and sampled at any time scale. This method requires knowing the pulsar's DM accurately before the observation is made. To date, coherent dedispersion is primarily used for precise pulsar timing and high time resolution studies of pulse microstructure.

Filterbanks

A common approach used to reduce the data volume is to use a filterbank. This consists of a moderate number (usually 32–128) notch filters, evenly spaced across the IF bandpass. Each filter is sensitive to a narrow frequency band, so smearing from dispersion is limited. The output of each filter is fed to a square-law detector and integrator with a time constant about twice the sampling time. This signal, which is reduced in both time and frequency resolution is digitized and recorded on magnetic tape. For example, the 10 MHz bandpass of the Arecibo 430 MHz line feed has a total information content of about 40 Mbits/s, but when put through the 32×250 kHz filterbank and sampled at 250 μs intervals, the data rate is reduced to less than 131 kbits/s, a factor of ~ 300 reduction.

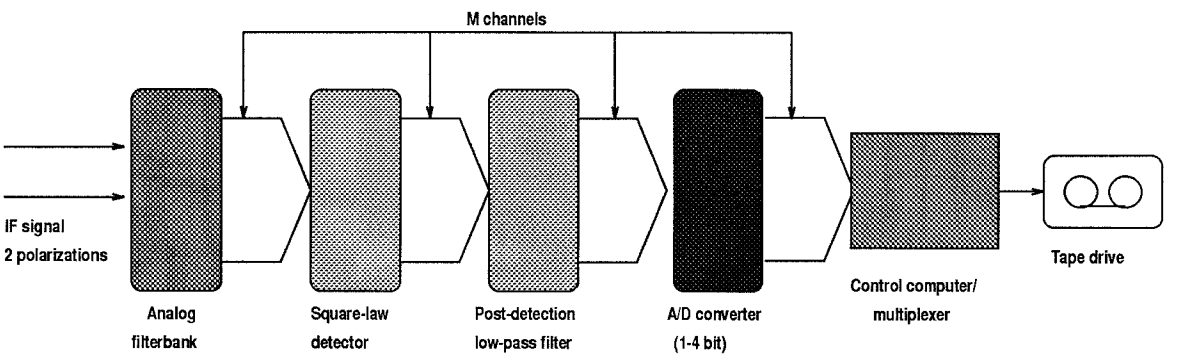

Figure 2.3: Simplified block diagram for a typical pulsar filter bank backend. M varies from 2×32 to 2×128. The post-detection filter time constant is normally set to twice the A/D converter sampling time so that the data is Nyquist sampled.

Autocorrelation Spectrometers

More recently, digital autocorrelation spectrometers have been used to generate the spectrally resolved data that is required by pulsar searches. These digital devices can be simply constructed out of many adders, multipliers, and shift registers and therefore can have many more channels than a standard filter bank. Autocorrelation spectrometers make use of the Wiener-Khinchin theorem which says that autocorrelation functions are related to power spectra by a Fourier transform. Thus, a measurement of the autocorrelation function of a sequence of data points can be Fourier transformed to yield the same information as a filterbank.

2.4 Parallel Computing

Parallel computing involves the application of more than one computational element (processor) to a problem. There are many possible parallel architectures. One that is becoming familiar to many is the multiprocessor, shared memory machine. In this case several processors share one large address space which they can all access equally. Most high-end workstations can have several processors installed. In this case, when more than one process is scheduled to run under a multitasking operating system like Unix, several can run simultaneously on different processors. The operating system takes care to keep each process's address space distinct to prevent conflicts. One step up from that are the machines whose compilers are capable of building programs which run on more than one processor of the shared memory machine. Typically this is done by identifying loops whose iterations are

independent of one another and performing some on each processor. In this case the compiler is responsible for keeping memory integrity. Even traditional vector supercomputers like Crays have now begun to use small numbers (4–8) of processors.

Another architecture that is used for parallel machines is called single instruction, multiple data (SIMD). These machines have many processors which share their code memory and run identical sequences of instructions, but have distinct data memory spaces. Parallelizing a problem for this architecture is somewhat different than for the other architectures and is usually done through the use of special purpose languages (*e.g.* C* or CM Fortran).

Finally, there is the class of multiple instruction, multiple data (MIMD) machines. In this case, each independent processor has its own memory space for both code and data which is not directly available to the other processors. MIMD machines range from being very loosely coupled, such as a network of workstations, to very tightly coupled such as a parallel supercomputer. When one processor needs information that is contained on another processor, a "message" is passed between the two containing the required data. Thus, the bandwidth of the interconnection between the various processors becomes very important for problems that require significant amounts of communication. We will restrict our discussion to MIMD machines used for the data analysis in Chapters 3–6. Some of the MIMD machines we used in this work are: networks of workstations, the Intel Touchstone Delta and Paragon machines, and the nCUBE/2 (Ray 1992).

2.5 Parallel Analysis of Pulsar Data

The reduction of most pulsar data is too demanding for a single conventional workstation, particularly for a large survey. There are several choices of how to decompose the problem onto multiple processors. Conveniently, there are two independent dimensions in a pulsar search: dispersion measure trials and pointings. This provides a convenient means of breaking up the problem. Normally, an observing run at a radio observatory will result in many "pointings[1]," each of which needs to be searched at a large number of trial dispersion measures. Each dispersion trial of each pointing presents a computational problem which can be solved independently[2]. This falls in the "embarrassingly parallel"

[1]Sometimes these pointing are not distinct re-orientations of the telescope, as in a drift survey, but are normally analyzed as if they were.

[2]As long as one is not using the so-called "tree" dedispersion scheme (Taylor 1974)

class of problems, where each sub-problem can be solved on a separate processor (whether it be a workstation or a node of a parallel supercomputer) with little or no communication needed between the processors.

We now consider two cases: coarse-grained parallelism, where one processor is able to perform the complete search of (at least) one DM trial for one pointing, and fine-grained parallelism, where the pointings are sufficiently long that one processor cannot perform the required Fourier transforms.

2.5.1 Coarse-Grained Parallelism

In the coarse-grained case, one is able to perform the full Fourier transform needed in the core memory of one of the processors. This allows the use of canned, generic and highly-optimized FFT routines where available. In general, one needs to pay little attention to the parallel nature of the problem when coding. This approach works equally well on networks of workstations or on nodes of a parallel supercomputer as long as the node memory is sufficient.

The parallel processing of the survey data described in Chapters 4 and 5 was accomplished using a network of workstations, where each reduced a complete pointing. Since the surveys consisted of many thousands of pointings, this allowed the work to be divided among many workstations. This was accomplished by using a manager-worker scheme, where one manager workstation reads a pointing off magnetic tape, and spawns jobs on any free worker machine to reduce the data. The manager machine schedules tasks on the various worker machines according to their availability.

2.5.2 Fine-Grained Parallelism

In the fine-grained case, the FFTs required are too long to be performed in the core memory of one of the processors being used. This was the case for the long pointings toward supernova remnants described in Chapter 3. In this case, the time series must be divided among several (or many) processors. Two parts of the pulsar search algorithm (the FFT and the harmonic fold) require a great deal of communication between processors and thus workstation networks are no longer suitable for this problem.

Chapter 3

A Survey of 18 Supernova Remnants[1]

ABSTRACT

We have performed a pulsar search of 18 known or probable supernova remnants with the Arecibo 305-m radio telescope at 430 and 1420 MHz. The remnants were selected to have angular sizes less than or of order a few telescope beam diameters ($\sim 10'$ at 430 MHz and $\sim 3'$ at 1420 MHz). In some cases, larger remnants with centrally brightened cores of this scale were also included. The observations were sensitive to pulsars with periods $\gtrsim 1$ ms, and flux densities as low as ~ 0.2 mJy. The targets included two probable plerionic objects, and several shell-type remnants with centrally brightened X-ray profiles. No new pulsars were discovered in the survey, and we discuss some of the selection effects which make the interpretation of pulsar surveys of supernova remnants problematic. Effects of high pulsar velocities, uncertain distances, and bright remnant temperatures make it difficult to exclude the presence of a pulsar in most remnants.

3.1 Introduction

In spite of the strong evidence that supernovae produce the neutron stars which then become pulsars, the role of pulsars in the formation and evolution of supernova remnants (SNRs), and conversely, the role of supernova remnants in producing (or obscuring) the observed properties of pulsars are poorly understood. Several known radio and X-ray pulsars are believed to be directly associated with supernova remnants. There is evidence that an additional 15 – 20 SNRs contain a "central engine" which is likely to be either a

[1]This chapter has been submitted to THE ASTROPHYSICAL JOURNAL (Gorham *et al.* 1995)

neutron star or black hole (Seward 1990). Although the list of SNR-pulsar associations is growing, the corresponding growth of the list of SNRs still outpaces it, and at present only $\sim 15\%$ of the known Galactic SNRs show any evidence that a compact object was produced in the supernova event.

Table 3.1 lists several proposed pulsar-supernova remnant associations. Supernova remnants are classified (Weiler and Sramek 1988, for a review) as: plerions (P), which show a filled center flat spectrum nebula presumably powered by a compact object, shell (S) which show basically empty shells of emission, and composite (C) which show a shell in addition to a central plerion. The pulsar velocities are estimated by the distance to the remnant, the angular distance from the geometric center of the remnant, and either the pulsar characteristic age or the estimated remnant age. Because many of these quantities are difficult to estimate and prone to systematic errors, the quoted velocities should be taken as indicative rather than precise measurements. The table also includes pulsar name, associated SNR, pulsar characteristic age ($P/2\dot{P}$), approximate distance to the pulsar as derived from the dispersion measure (DM) and the Galactic electron density model of Taylor and Cordes (1993), pulse period, pulsar flux at 430 and 1400 MHz, DM, and references to the literature.

There are three primary criteria on which associations of pulsars with supernova remnants are judged: positional alignment, distance, and age. Several of the associations do not have very good positional alignment, but this is usually explained by postulating very high birth velocities for pulsars. Some of the associations require extremely high velocities ($\gtrsim 1000$ km/s) to be imparted to the pulsar by the supernova explosion, while most require only a few hundred km/s which is typical of the older pulsar population (Lyne and Lorimer 1994). For most of these pulsars, the velocities are rather uncertain because of the difficulty in measuring distances and ages of supernova remnants. However, the possibility of very high pulsar velocities introduces a clear selection effect into pulsar surveys of supernova remnants.

Observational evidence for pulsar-SNR associations comes from several different sources. First, the Crab and Vela were found in plerionic remnants which obviously required a central engine (Staelin and Reifenstein 1968; Large, Vaughan, and Mills 1968). Then, X-ray data from the *Einstein Observatory* resulted in several more pulsar discoveries in SNRs (Seward and Harnden 1982; Seward, Harnden, and Helfand 1984). Recently, progress has been made with additional radio observations of SNRs near young pulsars that resulted

TABLE 3.1

Known pulsars with proposed supernova remnant associations.

PSR	SNR[a]	SNR Type	τ_c (kyr)	Dist (kpc)	v_{PSR} (km/s)	P (ms)	S_{400} (mJy)	S_{1400} (mJy)	DM (pc cm^{-3})	Ref[c]
B0531+21	Crab	P	1.2	2.0	?	33.3	950	14	57	1
B1509–58	G320.4–1.2	C	1.5	4.4	350	150.2	1.5	1.4	248	6
B0540–69	SNR0540–693	C	1.7	50	?	50.3	< 0.1	< 0.5	146	2,25
B1610–50	Kes 32†	S	7.5	7.3	1600	231.6	...	2.4	586	7
B0833–45	Vela X	C	11.3	0.5	120	89.3	5000	1100	69	4
J1341–6220	G308.8-0.1	C?	12	6.9	$\gtrsim 50$	193.3	...	2	730	5,16
1E2259+586	CTB 109†	S	14[b]	4	?	6978.8	...	...	...	18,19
B1757–24	G5.4–1.2	C?	15.5	4.6	$\gtrsim 1600$	124.9	...	0.7	289	9,22,23
B1800–21	G8.7–0.1†	S?	15.8	3.9	1700	133.6	20	15	234	11
B1706–44	MSH 17–41	S	17.5	1.8	900	102.4	...	8.6	76	8
B1853+01	W44	S	20.3	3.3	200	267.4	...	1.2	97	12
B1930+22	G57.3+1.2†	S?	39.8	9.3	750	144.4	...	1.2	211	13
B2334+61	G114.3+0.3	S	40.9	2.5	125	495.2	9	1.4	58	15,17
B1758–23	W28†	C	58.3	13.5	290	415.7	...	6	1074	10,24
B1951+32	CTB 80	?	107.1	2.5	300	39.5	7	1.0	45	14
B0656+14	Monogem†	S	110.8	0.8	230	384.9	6	4	14	3
B0535+28	G180.0–1.7	S	600	1.5	35	143	3	...	40	21
B0458+46	G160.9+2.6†	S	1813	1.8	$\lesssim 10$	638.6	10	3	41	20

[a]Associations marked with † are uncertain. [b]Remnant age, not pulsar characteristic age

[c]References: [1] Staelin and Reifenstein (1968), [2] Seward, Harnden, and Helfand (1984), [3] Cordova *et al.* (1989), [4] Large, Vaughan, and Mills (1968), [5] Caswell *et al.* (1992), [6] Seward and Harnden (1982), [7] Caraveo (1993), [8] McAdam, Osborne, and Parkinson (1993), [9] Manchester, D'Amico, and Tuohy (1985), [10] Frail, Kulkarni, and Vasisht (1993), [11] Kassim and Weiler (1990), [12] Wolszczan, Cordes, and Dewey (1991), [13] Routledge and Vaneldik (1988), [14] Kulkarni *et al.* (1988), [15] Kulkarni *et al.* (1993), [16] Kaspi *et al.* (1992), [17] Fürst, Reich, and Seiradakis (1993), [18] Gregory and Fahlman (1980), [19] Fahlman and Gregory (1981), [20] Leahy and Roger (1991), [21] Anderson *et al.* (1994), [22] Frail and Kulkarni (1991), [23] Manchester *et al.* (1991), [24] Kaspi *et al.* (1993), [25] Manchester *et al.* (1994).

in new remnants being discovered, or older remnants found to be larger than originally suspected which made some associations more plausible (Caswell *et al.* 1992; McAdam, Osborne, and Parkinson 1993; Routledge and Vaneldik 1988). And, continued directed and un-directed searches have resulted in the discovery of several other pulsars associated with SNRs (Wolszczan, Cordes, and Dewey 1991; Anderson *et al.* 1994, for example).

We have performed a pulsar search of 18 known or probable supernova remnants with the Arecibo 305-m radio telescope at 430 and 1420 MHz. To our knowledge, the only previous published search of comparable scope and sensitivity for radio pulsars associated with supernova remnants is that of Manchester, D'Amico, and Tuohy (1985), which used the Parkes 64 m telescope, covering mainly sources in the southern sky. A recent, unpublished search using the Arecibo telescope yielded a pulsar, PSR B1853+01, in the SNR W44, reported by Wolszczan, Cordes, and Dewey (1991).

3.1.1 Rationale for Sensitive Pulsar Searches Toward SNRs

Until recently it was believed that shell type remnants could not contain young, fast pulsars (Narayan and Schaudt 1988). However, the discovery of pulsars like PSR B1853+01 in W44, and PSR B2334+61 in G114.3+0.3 shows the importance of continued pulsar searches in shell-type remnants. Several of these recent associations with shell type remnants have fluxes $\lesssim 2$ mJy at 1400 MHz. This strongly suggests that success in finding more pulsars in SNRs requires very sensitive searches, e.g. searches with large telescopes (such as Arecibo) and long integration times.

Most early associations were in plerionic or composite SNRs, but the current list of associations has a majority of shell-type remnants (see Table 3.1). Narayan and Schaudt (1988) argue that pulsars with reasonably fast rotation rates (such as those expected, and found in SNRs) may have beaming factors close to unity. The detection of pulsars with short initial periods in MSH 17–41, G180.0–1.7, W44, and others implies that shell SNRs may contain pulsars likely to be beamed toward Earth. Thus if adequate sensitivity can be achieved and if other selection effects (discussed below) can be minimized then, in principle, one should be able to detect pulsars in many SNRs.

Branch (1990) describes which types of supernova events, from among Type II (having hydrogen), Type Ia (lacking hydrogen and helium), and Type Ib (having helium but not hydrogen), are likely to leave neutron stars in their remnants. However, it is difficult

to be certain which type of supernova event a particular SNR came from. Thus, we have not used this as a selection criteria.

3.1.2 Searches and Selection Effects

Several pulsar search selection effects in SNR surveys are competing, so that efforts to minimize one selection effect may exacerbate another. For example, SNRs of angular scale larger than the beam of a single dish telescope must be observed by mosaic techniques; thus the observing time required to cover the area of the SNR increases as the square of the ratio of the remnant diameter to the beam diameter. An alternative is to observe at a lower frequency where the beam is larger; however, this reduces the sensitivity at higher dispersion measures due to both instrumental pulse broadening and scattering effects. On the other hand, steep spectrum pulsars may produce much more signal in a lower frequency observation, in spite of the increased system noise due to the SNR thermal background. For a typical SNR, the spectral index is ~ -0.6 (see Green 1993), compared to a range of values of –0.5 to –2.0 for pulsars. However, the break-even spectral index depends both on the brightness temperature of the SNR and its shape, making it difficult to judge the optimal observation frequency *a priori*.

Recent work (Lyne and Lorimer 1994) has demonstrated that pulsars are born with mean birth velocity of 450 km/s, much higher than was previously believed. For remnants whose age is $\gtrsim 10^5$ yr, or younger for pulsars with very high birth velocities, the proper motion of a high velocity pulsar may have moved it close to or beyond the expanding shell of the remnant. Cases have been made for associations that require pulsar velocities of up to 1600 km/s (Johnston *et al.* 1995; Caraveo 1993). These high-velocity pulsars move quickly out of their remnants and within a few million years have moved out of range of most surveys and populate an extended Galactic halo.

A published pulsar survey of SNRs is that performed by Manchester, D'Amico, and Tuohy (1985) using the 64-m Parkes telescope at a frequency of 1400 MHz. This survey was sensitive to pulsars with periods greater than 10 ms and had a minimum detectable flux density of typically ~ 1 mJy for periods above ~ 300 ms and DM $\leq 1600\,\mathrm{pc\,cm^{-3}}$. Since the minimum detectable flux density (MDF) depends linearly on the sky temperature (see §3.3.1), a bright supernova remnant will increase the MDF significantly, reducing the survey sensitivity. For typical SNR flux densities, this increase in the MDF may be a factor of 5

or more above the nominal cold-sky MDF. This explains the fact that the Parkes survey did not detect the W44 pulsar (1.2 mJy at 1400 MHz) in two different observations. Given the $\sim$ 200 Jy flux density of the remnant at this frequency, the sky temperature observed was at least a factor of two greater than the receiver temperature. The pulsar, which is $\sim$ 7 arcmin below the remnant centroid, was also near the half-power point of the telescope beam. This example indicates that determination of the completeness of any SNR survey is complicated because selection effects associated with beam size and the SNR background can introduce wide variations in the MDF.

Manchester, D'Amico, and Tuohy (1985) observed 53 SNRs and 59 other objects, many of which are accessible only from southern hemisphere sites. Four pulsars, one of which was already known as an X-ray pulsar, were discovered among the observed SNRs. For the remaining three pulsars, the association of each with the SNR was judged by Manchester *et al.* to be most likely a chance alignment, based on discrepancies between the positions of the pulsars relative to the remnants, and the derived distances from the observed dispersion measures, relative to those estimated independently for the remnants (usually from HI absorption). Based on further measurements, all three of these pulsars have turned out to be young, and all three now have proposed supernova remnant associations, though one (PSR B1758-23) is quite controversial.

3.2 Search Strategy, Observations, and Analysis

3.2.1 Search Strategy

The present search was performed on a selected set of SNRs observable from Arecibo (i.e., $-2^\circ < \delta < 39^\circ$) which could be covered fairly completely with a small number of beams, either at 430 or 1420 MHz. By using long observations (20 minutes – 2 hours) with rapid sampling (0.5 – 1 ms) we achieved high sensitivity ($\lesssim$ 0.5 mJy) down to several millisecond periods. The sample of SNRs included at least two plerionic SNRs, a number of SNRs from the 2.7 GHz Effelsberg Galactic plane survey (Reich *et al.* 1984), and several previously known SNRs with associated X-ray emission, filled center X-ray or radio morphologies, or associated compact radio sources. Table 3.2 provides a source list, with nominal centroid positions, spectral index, extrapolated flux densities, approximate sizes, and distances from Green (1993) or Reich *et al.* (1984).

TABLE 3.2

Supernova remnants included in the search

Source	Name	RA(1950) hh mm ss	Dec(1950) dd mm	Size (arcmin)	Type	Spect. Index	1 GHz F_ν (Jy)	Dist kpc
30.7+1.0	...	18 42 10	–01 35	24 × 18	S?	–0.4	6	...
31.9+0.0	3C391	18 46 50	–00 59	5	S	–0.55	24	8.5
33.6+0.1	Kes 79	18 50 15	+00 37	10	S	–0.5	22	10
36.6–0.7	...	18 58 05	+02 52	25?	S?	–0.5	0.7	...
39.2–0.3	3C396	19 01 40	+05 23	8 × 6	S	–0.6	18	$\gtrsim 7.7$
39.5+0.6	...	18 59 41	+06 02	12	C	–0.15	3	...
41.1–0.3	3C397	19 05 08	+07 03	4.5 × 2.5	S	–0.48	22	$\gtrsim 7.5$
41.4+0.4	...	19 03 13	+07 40	12?	?	–0.3	6	...
43.3–0.2	W49B	19 08 44	+09 01	4 × 3	S	–0.5	38	10
45.7–0.4	...	19 14 05	+11 04	22	S	–0.3	4	...
49.2–0.7	W51	19 21 30	+14 00	25?	S?	–0.3?	160	4.5
53.6–2.2	3C400.2	19 36 30	+17 08	28	S	–0.6	8	6.7
54.1+0.3	...	19 28 28	+18 46	1.5	P?	–0.13	0.5	...
65.2+5.7	...	19 31 00	+31 05	310 × 240	S?	–0.6	52?	0.8
65.7+1.2	DA 495	19 50 10	+29 18	18	C?	–0.6	5	...
73.9+0.9	...	20 12 20	+36 03	22?	S?	–0.3	9?	...
74.0–8.5	Cyg loop	20 49 00	+30 30	230 × 160	S	varies	210	0.77
74.9+1.2	CTB 87	20 14 10	+37 03	8 × 6	P	–0.24	9	12

3.2.2 Observations

The observations were made 1988 December 24–28, 1989 July 6–15, 1989 September 11–20, and 1991 March 28–April 1 using the 305-m transit dish at Arecibo, Puerto Rico. The data were recorded in a manner identical to that described by Anderson *et al.* (1990), except that in some instances a sample integration time of 1 ms, rather than 0.5 ms, was used. The duration of the observations varied from $\sim$ 20 min to $\sim$ 2 hrs per source transit, and several of the sources were observed more than once. The objects were usually observed at 430 MHz if the conditions allowed; however, severe radio interference problems often made 430 MHz observations impractical, and in these cases 1420 MHz observations were done instead. Certain interference bands appear in power spectra for almost all the data; for example, a moderately broad-band noise signal at the first 3–4 harmonics of 0.32–0.35 Hz effectively eliminates any sensitivity at these frequencies. Also, most of the observations show power at 60 Hz and its harmonics.

Table 3.3 gives a log of the observations. The repeated entries for the same source in column (1) are either repeated observations, or observations at a different beam position

within the same remnant if the size of the remnant was larger than the telescope beam. The position of the beam center is given in columns (6) and (7). Column (11) gives an approximate value of the mean zenith angle of the source during the observation, and is relevant to estimates of the telescope sensitivity.

The gain of the telescope at the zenith was 18 K Jy^{-1}at 430 MHz, and 8 K Jy^{-1} at 1420 MHz (NAIC 1989). The system temperatures were 60–70 K at 430 MHz for the two polarization channels, and 40 K at 1420 MHz. At large zenith angles ($\sim 20°$) the gain at both frequencies decreases by about 40%, and the system temperatures increase by about a factor of 2, due both to the decrease in effective aperture, and illumination of the warm ground.

3.2.3 Data Analysis

The pulse search used standard power spectral analysis. A time series is formed by converting the correlator output into 128 individual frequency channels and combining these into a single time series assuming a dispersive time delay across the band due to a trial value of the dispersion measure (see Anderson 1993). The time series used varied from $2^{20} - 2^{24}$ samples in length, depending on the duration of the observation and the sampling interval used. The power spectra were computed and searched using the concurrent supercomputers of the Caltech Concurrent Supercomputing Facility (CCSF) and the Concurrent Supercomputing Consortium (CSCC). The initial data analysis was done on the CCSF nCUBE/10, and later analysis was done on the CSCC Intel Touchstone Delta and the CCSF nCUBE/2.

Standard spectral analysis techniques for pulsar searches, such as the normalizing the power spectra using the local mean value from a boxcar average, and summing of harmonically related portions of the spectrum, were employed to maximize the sensitivity to short duty cycle pulses.

Dispersion measure values up to 1500 pc cm^{-3} were used for the 430 MHz data. At this DM, the pulse broadening is equal to $\sim$ 12 ms per channel in the correlator, and the DM value corresponds to distances well outside the galaxy for the mean Galactic electron density (Taylor and Cordes 1993). Higher values toward an individual source are possible if there is significant HII column density; however, interstellar scattering strongly reduces the sensitivity for 430 MHz observations at DM values higher than this (Sutton

TABLE 3.3

SNR observation log

Source	Ref Pos	Day GMT	Year	T min	RA 1950.0 hh mm ss.d	DEC 1950.0 dd mm ss	ν MHz	B MHz	t ms	$\langle ZA \rangle$ °
(1)	(2)	(3)	(4)	(5)	(6)	(7)	(8)	(9)	(10)	(11)
30.7+1.0	A	189	89	45	18 41 12.9	-01 32 38	1418	40	0.5	20
30.7+1.0	B	193	89	45	18 40 46.2	-01 34 20	1418	40	0.5	20
30.7+1.0	C	90	91	46	18 41 17.5	-01 37 20	1411	40	0.5	20
31.9+0.0	...	91	91	70	18 46 53.0	-00 59 45	1411	40	0.5	20
33.6+0.1	...	262	89	22	18 50 04.0	00 35 21	1408	40	1.0	19
36.6–0.7	...	254	89	45	18 57 53.4	02 58 41	430	10	0.5	16
39.2–0.3	...	88	91	70	19 01 33.6	05 22 35	1411	40	0.5	14
39.5+0.6	...	195	89	70	18 59 08.7	06 00 58	430	10	0.5	13
41.1–0.3	...	88	91	70	19 05 10.1	07 04 00	1411	40	0.5	12
41.1–0.3	...	194	89	70	19 05 10.0	07 03 45	1418	40	0.5	13
41.4+0.4	A	191	89	75	19 03 13.0	07 39 54	430	10	0.5	11
41.4+0.4	B	192	89	75	19 03 34.0	07 43 29	430	10	0.5	11
41.4+0.4	C	196	89	70	19 03 24.0	07 41 42	430	10	0.5	11
43.3–0.2	...	187	89	70	19 08 44.3	09 01 10	430	10	0.5	11
45.7–0.4	A	258	89	35	19 14 21.8	11 02 10	430	10	1.0	14
45.7–0.4	B	259	89	24	19 13 32.3	11 08 04	1408	40	1.0	11
45.7–0.4	C	258	89	28	19 14 00.3	11 14 36	1408	40	1.0	16
49.2–0.7	A	87	91	45	19 20 49.0	14 08 10	430	10	0.5	15
49.2–0.7	B	87	91	70	19 21 11.2	14 00 00	430	10	0.5	6
49.2–0.7	B	91	91	70	19 21 11.2	14 00 00	1411	40	0.5	8
53.6–2.2	...	90	91	45	19 35 48.8	17 11 26	430	10	0.5	4
54.1+0.3	...	361	88	45	19 28 17.5	18 45 42	430	10	0.5	3
54.1+0.3	...	188	89	148	19 28 17.5	18 45 42	430	10	0.5	6
54.1+0.3	...	260	89	30	19 28 17.0	18 45 50	1408	40	1.0	3
65.3+5.7	...	262	89	30	19 33 36.0	30 02 00	1408	40	1.0	12
65.7+1.2	...	193	89	90	19 50 10.7	29 18 15	430	10	0.5	12
73.9+0.9	A	187	89	45	20 11 42.5	36 05 25	430	10	0.5	18
73.9+0.9	B	257	89	20	20 11 45.6	35 59 41	430	10	0.5	18
73.9+0.9	BC	191	89	45	20 12 03.0	35 58 46	430	10	0.5	18
73.9+0.9	BC	192	89	45	20 12 03.0	35 58 46	430	10	0.5	18
73.9+0.9	C	196	89	45	20 12 20.4	35 57 51	1418	40	0.5	18
73.9+0.9	D	195	89	70	20 12 59.1	35 52 09	430	10	0.5	18
73.9+0.9	D	258	89	30	20 12 59.1	35 52 10	430	10	0.5	18
74.0–8.5	...	89	91	50	20 49 33.9	30 51 37	430	10	0.5	19
74.9+1.2	...	363	88	45	20 14 11.8	37 02 50	430	10	0.5	18
74.9+1.2	...	190	89	45	20 14 14.0	37 04 00	430	10	0.5	18
74.9+1.2	...	254	89	45	20 14 14.0	37 04 00	431	10	0.5	18

1971). At 1420 MHz, scattering effects are usually not important for DM values below a few $\times 10^3\,\mathrm{pc\,cm^{-3}}$, although this varies with the line of sight.

The step size used for the DM trials for each observing frequency was chosen to retain uniform sensitivity to pulsars up to the Nyquist frequency of the sampling. In the 430 MHz data sets the pulse broadening across one of the 128 frequency channels becomes larger than 2 ms for DM values above about $200\,\mathrm{pc\,cm^{-3}}$. Therefore, the time series for large DM values were resampled to 2 ms sampling time. While significantly reducing the computational time, this resampling does not affect the sensitivity to pulsars with period longer than about 8 ms. Shorter period pulsar signals are strongly degraded by dispersion and scattering and could not have been detected anyway.

During the sequence of observations in this program, a search for globular cluster pulsars was also conducted using identical data reduction and analysis software. The globular cluster search was successful, yielding a total of 4 binary systems and 7 isolated pulsars in the clusters M13, M15, M53 and NGC6760 (Anderson *et al.* 1990; Anderson 1993; Kulkarni *et al.* 1991; Prince *et al.* 1991). These results provided a cross-calibration on the SNR search sensitivity, and allowed us to assess the effective detection threshold in the analysis.

3.3 Results

3.3.1 Minimum Detectable Flux Density

The minimum detectable flux density (MDF) for a radio pulsar search depends directly on sky and receiver temperature, inversely on the square root of the duration of the observation, and directly on the square root of the observed pulse duty cycle. The pulse duty cycle is not known *a priori*. The *observed* pulse duty cycle may also be broadened by dispersion or other effects; thus the MDF also increases with increasing DM. A general expression for the MDF is given by Stokes *et al.* (1986) and in a slightly different form by Biggs and Lyne (1992):

$$S_{\mathrm{min}} = K \left[\frac{T_{\mathrm{rec}} + T_{\mathrm{sky}}(l,b) + T_{\mathrm{sp}}(ZA)}{G\,(N_p B t)^{1/2}}\right] \left(\frac{w_{\mathrm{eff}}}{P - w_{\mathrm{eff}}}\right)^{1/2}, \tag{3.1}$$

where the factor $K \sim 12$ is empirically determined from detection of known pulsars and expresses the analysis detection threshold ($\sim 8\sigma$). T_{rec}, $T_{\mathrm{sky}}(l,b)$, and $T_{\mathrm{sp}}(ZA)$ are the

receiver temperature, sky temperature (depending on Galactic longitude and latitude), and effective spillover temperature (depending on zenith angle), respectively. Here G is the telescope gain in units of $\mathrm{K\,Jy^{-1}}$, N_p the number of polarization senses received, B the total bandwidth in MHz, and t the total duration of the observation in seconds. The rightmost term in Eqn. 3.1 gives the dependence on pulse duty cycle, with P the pulse period, and w_{eff} the effective pulse width:

$$w_{\mathrm{eff}} = \left[w^2 + \beta^2 \tau^2 + \left(\frac{\tau\, DM}{DM_0} \right)^2 \right]^{1/2}, \tag{3.2}$$

where w is the intrinsic pulse width, τ is the sampling interval in seconds, $\beta \simeq 2$ is related to the time constant of the post-detection smoothing filter, and $\mathrm{DM_0}$ is the dispersion measure value at which the pulse delay across the bandpass of a single narrow frequency channel equals the sampling interval. This value is approximately

$$\mathrm{DM_0} = 1.2 \times 10^{-4} \frac{\tau \nu^3}{\Delta\nu}\ \mathrm{pc\,cm^{-3}}, \tag{3.3}$$

where ν and $\Delta\nu$ are the observing frequency and channel bandwidth, respectively, both in MHz.

Figure 3.1 plots S_{min} for a range of parameters encountered in this survey. Unless otherwise indicated, each of the plots use the following parameters: DM= $300\,\mathrm{pc\,cm^{-3}}$; pulse duty cycle (fraction of the pulse period when the pulse is "on") $\delta = 0.10$; sampling interval $\tau = 0.5\,\mathrm{ms}$; duration of observation $t = 2800\,\mathrm{s}$; mean zenith angle $\langle ZA \rangle = 15°$. For the effective sky temperature due to the SNR, a spectral index of -0.6 was assumed, with a 430 MHz flux density of 15 Jy. This implies $T_{\mathrm{sky}} = 300\,\mathrm{K}$ (430 MHz) and 150 K (1400 MHz) where a beam filling factor of unity is assumed. This flux density is meant to represent the typical SNR included in the search. It should be noted that there is a great deal of variability in the sky temperature from remnant to remnant, and from pointing to pointing within a particular remnant. In each case the solid curves correspond to the 430 MHz results, and the dashed curve to the 1400 MHz results.

Figure 3.1(a) shows the sensitivity variations for the three different sampling intervals used. Figure 3.1(b) shows variation for different average zenith angle of the observations. The effect is caused by two factors: the spillover effects increase with increasing zenith angle, and the system gain decreases with increasing zenith angle as the effective aperture is truncated. Figure 3.1(c) shows the variation for three different values of the DM, and Figure 3.1(d) shows the change for differing values of the pulse duty cycle.

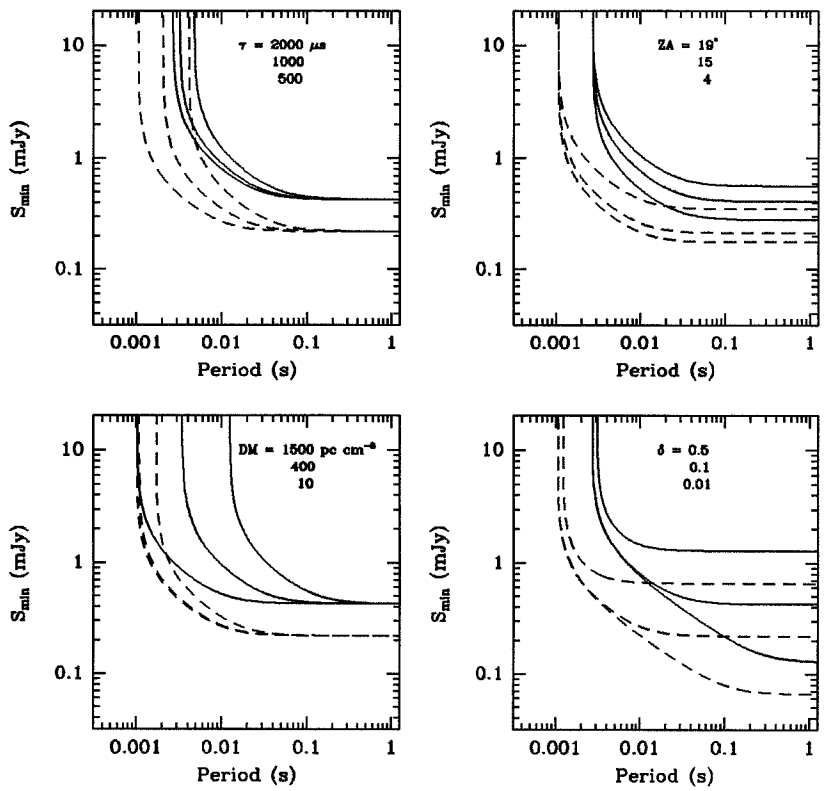

Figure 3.1: Minimum detectable flux density $S_{\min}$ as a function of pulsar period, for a range of parameters used in this survey, computed from Eqn. 3.1 in the text. Unless otherwise indicated by the notes in the upper right of each panel, the plots use the following parameters: DM = 300 pc cm^{-3}; pulse duty cycle $\delta = 0.10$; sampling interval $\tau = 0.5$ ms; duration of observation $t = 2800$ s; mean zenith angle $\langle ZA \rangle = 15°$. For the effective sky temperature due to the SNR, a spectral index of -0.6 was assumed, with a 430 MHz flux density of 15 Jy. This implies $T_{\rm sky} = 300$ K (430 MHz) and 150 K (1400 MHz) where a beam filling factor of unity is assumed. (a) Variation of $S_{\min}$ with sampling interval. (b) Variation of $S_{\min}$ with mean source zenith angle during the observation. (c) Variation of $S_{\min}$ with dispersion measure. (d) Variation of $S_{\min}$ with pulse duty cycle. In each case the solid curves correspond to the 430 MHz results, and the dashed curve the 1400 MHz results, and the order of the curves follows that of the indicated parameters in each panel.

During observations of G39.5+0.6, a signal was detected at a pulse period of 746 ms, from the known pulsar PSR B1900+05, which was about 19′ to the Galactic south of the 430 MHz beam center. The position corresponded to a sidelobe of the beam with a gain of -12 dB relative to the beam center, at a zenith angle of $\sim 13°$, thus giving about 5% of the zenith gain at beam center. PSR B1900+05 has a 400 MHz flux density of 20 mJy

in the sidelobe, giving an equivalent beam-center flux of ~ 1 mJy. The pulsar was detected in its first 18 harmonics with an average of ~ 8 times the noise power in each harmonic, at a DM of 176 pc cm^{-3}. The pulse width for this pulsar is 26 ms, giving a duty cycle of 0.03. Taking into account the position of PSR B1900+05 relative to the beam center, and using Eqns. 3.1 & 3.2, we obtain a sensitivity estimate of 0.7 mJy at the beam center, providing some independent validation of the results in Figure 3.1.

3.3.2 Flux Density Limits

Table 3.4 gives limits for average pulsar flux density, using the minimum detectable flux densities estimated from Eqn. 3.1 and the known properties of the remnants. No attempt was made to correct for the inhomogeneity of the sky temperature of the objects, although some corrections were made when the beam filling factors were obviously small and the background sky temperature much lower than that of the remnant.

The observations at different frequencies and at different positions within the remnant are each given distinct limits in Table 3.4, and the fraction of the remnant solid angle that was covered by the observation is also indicated. The values for pulsar parameters used in determining the limits are: $P = 30$ ms; DM= 300 pc cm^{-3}; duty cycle $\delta = 0.1$. Limits for values other than the nominal values may be obtained from Figure 3.1 or by scaling with Eqn. 3.1. Limits for distinct observations of the same beam position have not been combined in Table 3.4, but are quoted separately.

3.4 Discussion

Flux limits for surveys of supernova remnants are rather hard to interpret in terms of making a definite statement that a pulsar was not born in the supernova. Distances to supernova remnants are difficult to constrain and their ages are similarly uncertain. This significantly affects both luminosity and velocity estimates. Pulsar distances are believed to be somewhat better, but there is not a simple, empirical law for predicting pulsar radio luminosities. So, it is hard to place a luminosity limit for a particular remnant, and it is not clear what luminosity a pulsar of the remnant age would be expected to have. For remnants that are not very young, a high velocity pulsar might be outside the remnant radio shell.

The median luminosity of the pulsars in Table 3.1 is about 80 mJy kpc^2 using the DM-derived distances and estimates of the 400 MHz flux densities. They range from

TABLE 3.4

SNR pulse search limits

Source	Ref Pos	430 MHz limit (mJy)	% of area covered (430 MHz)	1400 MHz limit (mJy)	% of area covered (1400 MHz)
(1)	(2)	(3)	(4)	(5)	(6)
30.7+1.0	A	...	...	0.3	3
30.7+1.0	B	...	...	0.3	3
30.7+1.0	C	...	...	0.3	3
31.9+0.0	...	...	...	0.8	45
33.6+0.1	A	...	...	0.7	10
36.6–0.7	...	0.2	15	...	...
39.2–0.3	...	...	...	0.3	23
39.5+0.6	...	0.2	70	...	...
41.1–0.3	...	...	...	0.35	80
41.1–0.3	...	...	...	0.35	80
41.4+0.4	A	0.3	70	...	...
41.4+0.4	B	0.3	70	...	...
41.4+0.4	C	0.3	70	...	...
43.3–0.2	...	1.2	100	...	...
45.7–0.4	A	0.4	20	...	...
45.7–0.4	B	...	...	0.3	3
45.7–0.4	C	...	...	0.3	3
49.2–0.7	A	1.0	15	...	...
49.2–0.7	B	0.6	15	0.5	2
53.6–2.2	...	0.2	13	...	...
54.1+0.3	...	0.5	100	...	...
54.1+0.3	...	0.3	100	0.3	100
65.3+5.7	...	...	...	0.1	< 1
65.7+1.2	...	0.3	30	...	...
73.9+0.9	A	0.3	20	...	...
73.9+0.9	B	0.5	20	...	...
73.9+0.9	BC	0.3	20	...	...
73.9+0.9	BC	0.3	20	...	...
73.9+0.9	C	...	...	0.3	3
73.9+0.9	D	0.2	20	...	...
73.9+0.9	D	0.4	20	...	...
74.0–8.5	...	0.3	< 1	...	...
74.9+1.2	...	0.5	100	...	...
74.9+1.2	...	0.4	100	...	...
74.9+1.2	...	0.4	100	...	...

$\sim 5\,\mathrm{mJy\,kpc^2}$ for PSR B0656+14 and PSR B0535+28 to $3800\,\mathrm{mJy\,kpc^2}$ for the Crab pulsar. The obvious selection effect in this sample implies that the median luminosity for the whole population of pulsars in SNRs is considerably lower. For a typical flux limit of 0.3 mJy at 430 MHz as seen in Table 3.4 and a distance from 7–10 kpc this survey places pulsar luminosity limits from 15 to $30\,\mathrm{mJy\,kpc^2}$. The limit is much better for the few closer remnants, and 8 of the remnants don't have good distance estimates, thus preventing luminosity limits.

The mean of the distance estimates for those whose diameters fall within one telescope beam in this survey is ~ 10 kpc (Green 1993). At this distance the 267 ms pulsar in W44 would appear at a flux density of 0.15 mJy at 1400 MHz, and W44 itself would have a 1 GHz flux density of about 25 Jy and a diameter of $5'$. These values for the size and diameter are very similar to those actually observed for a number of the SNRs surveyed here, such as G31.9+0.0, G41.1-0.3, and G43.3-0.2, all of which also have centrally brightened X-ray emission similar to W44. At 1400 MHz, the effective sky temperature due to these remnants is ~ 150 K. From Eqn. 3.1, using the 55 K system temperature for the 1420 MHz feed at Arecibo (zenith angle 15°) and a 70 min observation, the W44 pulsar would be detectable as long as the pulse duty cycle were less than 0.06, corresponding to a pulse width of 16 ms at 267 ms pulse period. The majority of observed pulsars have duty cycles within the range between 0.02 – 0.10, which will also be increased by interstellar scattering at the high DMs expected for most of the remnants included in this search, and such variation will introduce a clear selection effect on detectability.

The effective sky temperature at 430 MHz for these remnants is ~ 300 K. In this case, the effective sky temperature dominates the sensitivity in Eqn. 3.1. For a 70 min observation, and a duty cycle of 0.1, $S_{\mathrm{min}} \geq 0.5$ mJy. Thus a spectral index of ~ -1.0 or steeper is required for a pulsar like the pulsar in W44 to be detectable at 430 MHz when placed at a distance of 10 kpc. Such a spectral index is not unusual for pulsars as a whole, and the spectral index of the W44 pulsar is -1.7.

If we accept the results of Narayan and Schaudt (1988), that beaming effects are not important for SNR pulsars, then the limits obtained here for G74.9+1.2 (CTB 87), which is classified as a plerion, give some indication of the aging of the pulsed intensity of such a pulsar. Using a distance of 12 kpc for CTB 87, and 2 kpc for the Crab nebula, a Crab-like pulsar in CTB 87 would have ~ 40 times less flux density, or ≤ 20 mJy at 430 MHz. The age of CTB 87 is probably at least 10 times that of the Crab, or about 10 kyr. Our limit (≤ 0.5 mJy for $P \geq 100$ ms and DM ≤ 400 pc cm^{-3}) implies that any

pulsar in CTB 87 must be a factor of at least 40 less luminous in pulsations than the Crab pulsar at 430 MHz. This limit allows for a somewhat brighter pulsar in CTB 87 than in W44 but still consistent with the apparent remnant age.

One other remnant in our survey has been suggested to be plerionic in nature: G54.1+0.3 (Velusamy and Becker 1988). G54.1+0.3 has a centrally brightened radio core with a high degree of linear polarization and is an X-ray source. Imaging the central portion of this SNR has been limited in resolution due to its compact size and faintness. The distance to G54.1+0.3 has been estimated with large uncertainty to be 17 kpc. At this distance the Crab pulsar would have a flux density of about 10 mJy at 430 MHz, and the DM would be ~ 400 pc cm^{-3} (Taylor and Cordes 1993), giving a pulse smearing of about 5 ms. The Crab pulsar would thus be about a factor of 20 above the minimum detectable flux density for this SNR, and the possibility of a relatively bright pulsar in this remnant is not excluded by our limit if the distance is actually this large. Thus further searches on this object should attempt to minimize the dispersion effects if possible.

Another remnant included in our search is SNR G33.6+0.1 which shows a compact radio peak with a coincident linear polarization maximum, and a suggestion of a flattening of the spectral index in the central region of the remnant. Our observations of G33.6+0.1, made without the benefit of the high resolution maps of Velusamy, Becker, and Seward (1991), did not point directly at the radio maximum, but $1.0 - 1.4'$ to the southeast. The radio maximum is still within the 3 dB beamwidth of $3.3'$ of the 1408 MHz Arecibo feed, but there is a $\sim 30 - 40\%$ reduction in gain relative to the beam center. This effect, combined with the increased apparent sky temperature on this SNR and the large zenith angle necessary to observe it from Arecibo, increase the limiting detectable flux density for this object to ~ 0.3 mJy for a 10% duty cycle pulse. This is probably insufficient to detect a W44-type pulsar in G33.6+0.1 unless the SNR is at the lower limit of its estimated range of distance (~ 7 kpc).

3.5 Conclusions

We conclude that the most prominent selection effects in detecting pulsars in supernova remnants are the severe sensitivity limits imposed by the large distances and intrinsic brightness temperatures of the majority of known objects or the Galactic plane in which they lie, and high birth velocities of radio pulsars causing many pulsars associated

with SNRs to be off-center or even outside the remnant. It is evident that any theoretical estimates regarding the presence of pulsars in supernova remnants must consider carefully the loss of sensitivity that occurs in pulsar searches of SNRs compared to the more numerous sky surveys.

Future searches will require significant improvements in sensitivity in order to constrain the pulsar population in more distant remnants, as well as searching a larger solid angle to account for high pulsar velocities. A reduced system temperature from the newly installed ground screen at Arecibo, as well as improvements in correlator bandwidth and spectral sampling, along with requisite computing power to reduce the increased volume of data, will be necessary since constraints on observing time will probably continue to limit the maximum attainable duration of time series in similar survey projects. It appears that observations of Galactic plane SNRs should concentrate on higher frequencies than 430 MHz , since the effects of the high temperature of the Galactic plane, and possible pulse smearing from scattering probably offset the improvement in sampling given by the larger beam diameter.

This work would not have been possible without the use of the Caltech nCUBE/10 operated by the Caltech Concurrent Supercomputing Facility. This research was performed in part using the Intel Touchstone Delta System operated by Caltech on behalf of the Concurrent Supercomputing Consortium. Access to this facility was provided by Caltech.

We thank the staff of Arecibo Observatory for help in performing the observations. The Arecibo Observatory is part of the National Astronomy and Ionosphere Center, which is operated by Cornell University under cooperative agreement with the National Science Foundation.

Chapter 4

Large-Area Surveys For Radio Pulsars From Arecibo[1]

4.1 Introduction

For the reasons described in §1.4, we undertook a survey for fast pulsars in the Galactic anticenter. Spurred by the success of Wolszczan (1991) in discovering two high-latitude millisecond pulsars, the anticenter survey was enlarged, and several groups began an effort to survey the entire Arecibo sky for millisecond pulsars. The two pulsars discovered by Wolszczan, using 32 s integrations, had flux densities much higher than his survey limit. This motivated us to undertake a survey with a much shorter integration time, 8.2 seconds per beam in order to cover sky faster.

We report on several major pulsar searches carried out at the Arecibo Observatory from 1988 to 1993. All surveys covered large areas of sky that had not been previously searched with comparable sensitivity or sampling rates required to detect millisecond pulsars.

In §4.2 we describe the hardware, observation strategy, and pulsar detections for each of the surveys. In §4.3 we describe the data analysis techniques. In §4.4 we discuss the sensitivity of the surveys and implications for the Galactic population of millisecond pulsars, and the low-luminosity cutoff of the normal pulsar population.

[1]This chapter has been adapted from a paper accepted for publication in THE ASTROPHYSICAL JOURNAL (Ray *et al.* 1995a)

TABLE 4.1

Summary of surveys included in this chapter.

Telescope Diameter (m)		305		
Number of Polarizations		2		
Receiver Gain (K Jy^{-1})		18		
Noise Temperature (K)		90		
Survey	AC	SHL	DHL	CBHL
Backend	Autocorrelator	Filterbank	Filterbank	Filterbank
Sample Interval (μs)	506.625	250	250	180
Integration Time (s)	67, 32	8	32	47, 23
Observing Frequency (MHz)	430	430	430	428.5
Total Bandwidth (MHz)	10	8	8	8
Channel Bandwidth (kHz)	78.125	250	250	250
RFI-free Area (sq. deg.)	100†	285	63	68
RA Range	04^h– 09^h	01^h– 04^h	01^h– 04^h	08^h– 13^h
Dec. Range	+11°– +25°	+22°– +35°	+19.5°– +22°	+13°– +18°
l Range	170°– 210°	125°– 170°	126°– 170°	205°– 319°
b Range	-30°– +30°	-13°– -40°	-22°– -43°	+21°– +75°

†Approximate

4.2 The Surveys

All surveys used the same telescope, radio frequency, receivers, and analysis software. The survey parameters are summarized in Table 4.1. They differed in sky coverage, pointing strategy, integration time, and spectrometer.

All surveys employed the 430 MHz line feed at the Arecibo 305-m radio telescope. The feed received two circular polarizations using cryogenically cooled receivers in the carriage house. The feed/receiver system has an inherent half-power bandpass of 10.2 MHz (NAIC 1989) and a forward gain at zenith of 18 K Jy^{-1}. Typically, the center frequency of the observation was set to 428.5 MHz, near the peak sensitivity of the receiver system, but sometimes values of up to 430 MHz were used. The half-power beam width of the 430 MHz observing system is 10′.

Observations at high Galactic latitudes employed a $2 \times 32 \times 0.25$ MHz filterbank, covering a total of 8 MHz in bandwidth for each polarization. The signal in each channel was square-law detected and smoothed with a time constant of 330 μs. The two polarizations were then summed and the result digitized with 3-bit precision. Sample times for the digitizer were between 180 and 250 μs. Because of the relatively wide channel bandwidths,

the filter bank induces significant loss of sensitivity to 1.0 ms pulsars at a dispersion measure (DM) of $\sim 20\,\mathrm{pc\,cm^{-3}}$ (the dispersion-induced smearing across one filter bank channel is $260\,\mu\mathrm{s} \times \mathrm{DM}/10\,\mathrm{pc\,cm^{-3}}$).

The anticenter (AC) survey (§4.2.3) used the Arecibo autocorrelation spectrometer (NAIC 1989), which can only sample as fast as $\sim 500\,\mu$s, but which has a 10 MHz bandwidth and much narrower channels (78.125 kHz as compared to 250 kHz), allowing searches at DMs up to $60\,\mathrm{pc\,cm^{-3}}$ with negligible loss of sensitivity from dispersion smearing. The autocorrelation spectrometer divides the band into four 2.5 MHz banks, each of which is fed into a 32-lag autocorrelator. Each correlator integrated for $500\,\mu$s and then was inactive for $6\,\mu$s while it dumped its data to the control computer. There was an additional dead time of $40\,\mu$s when each block of 64 samples was dumped, resulting in an average time between samples of $506.625\,\mu$s. These autocorrelation functions for each polarization along with additional 12-bit total power counters were blocked into records and written to magnetic tape by the Harris H800 control computer.

4.2.1 The Slewing and Drifting High Latitude Surveys (SHL & DHL)

In this survey, observations were made while slewing the telescope, hence the designation as the Slewing High-Latitude (or SHL) survey. Sky coverage was between Galactic latitudes -15° and -40°. At these high latitudes, the expected maximum DM is only $\sim 30\,\mathrm{pc\,cm^{-3}}$ (Taylor and Cordes 1993), which yields a smearing of $750\,\mu$s across one of the 250 kHz channels. Thus, the benefits of faster sampling and somewhat simpler data reduction made the filter bank appropriate for this project.

The Arecibo telescope can only point within 20° of the zenith, and the sensitivity decreases and system temperature increases as the pointing moves away from the zenith. Therefore, maximum sensitivity is obtained when objects are observed at transit. For this reason, observations began at zenith and the telescope was driven at 1 hour of right ascension (RA) per hour of time. To achieve faster sky coverage, the telescope was driven north at $70°30'\,\mathrm{h^{-1}}$ for 4 minutes and then reversed for 4 minutes; this cycle was repeated throughout the observation. This pointing scheme traced a zig-zag pattern on the sky. For the next observation, the entire pattern was shifted in RA by a beam width. If this is completed for all starting positions, then a strip of sky of height 04°42′ is covered twice (once by a northward-slewing scan and once by a southward-slewing scan). Although the

survey proceeds only twice as fast as a traditional drift survey, the double coverage is advantageous because both radio-frequency interference (RFI) and pulsar scintillation can cause an otherwise detectable pulsar to be missed on the first pass.

The RFI-free sky coverage of this survey is included in Figure 4.1. The survey covers the region $01^h < \alpha < 04^h$, $22° < \delta < 35°$ with a filling factor of $\sim 50\%$, for a total of 285 square degrees. About 105 square degrees of this region were covered more than once by interference-free observations. There are no known pulsars in the survey region. These data were taken during two observing sessions: 1991 September 8–18 and 1991 October 13–November 3. This survey has a minimum detectable flux twice that of a normal drift survey for fast pulsars, but the limit is somewhat worse for slow pulsars. This is predominantly due to a very large red-noise component in the power spectra generated by sky background changes as the telescope beam slewed across the sky. For drift surveys, the variation is slow and is removed by AC coupling the post-detection signal with a time constant of ~ 12 s. This time constant was too long for the slewing survey, and it produced power spectra that were difficult to search for slow pulsars. The sensitivity of this survey is discussed further in §4.4.

No pulsars were detected in the 1991 September–October data. At that time, other surveys (Nice 1992; Camilo, Nice, and Taylor 1993; Foster, Wolszczan, and Camilo 1993) were successfully discovering millisecond pulsars which were much nearer the detection limit of drift surveys. Since similar pulsars might have been missed by the fast slewing survey, the Drifting High Latitude (DHL) survey in 1993 February 1–14 used the drift survey mode, with 32-second integrations. No pulsars were detected in these data. The sky coverage was $01^h < \alpha < 04^h$ and $19°40' < \delta < 21°50'$. The RFI-free sky coverage, which totals about 63 square degrees, is shown on Figure 4.1.

4.2.2 The Caltech-Berkeley High Latitude Survey (CBHL)

This survey used the filter bank. The data were acquired between 1991 September and 1993 May, in the region $08^h < \alpha < 13^h$ and $12° < \delta < 18°$. The sky coverage that was unaffected by RFI totaled 68 square degrees. Of this total, 27 square degrees were surveyed as the sky drifted past the telescope beam at the sidereal rate, giving an effective integration time of about ~ 42 s per point. The resulting search sensitivity as a function of pulsar period and dispersion measure is identical to Figure 2 of Thorsett et al. (1993). The

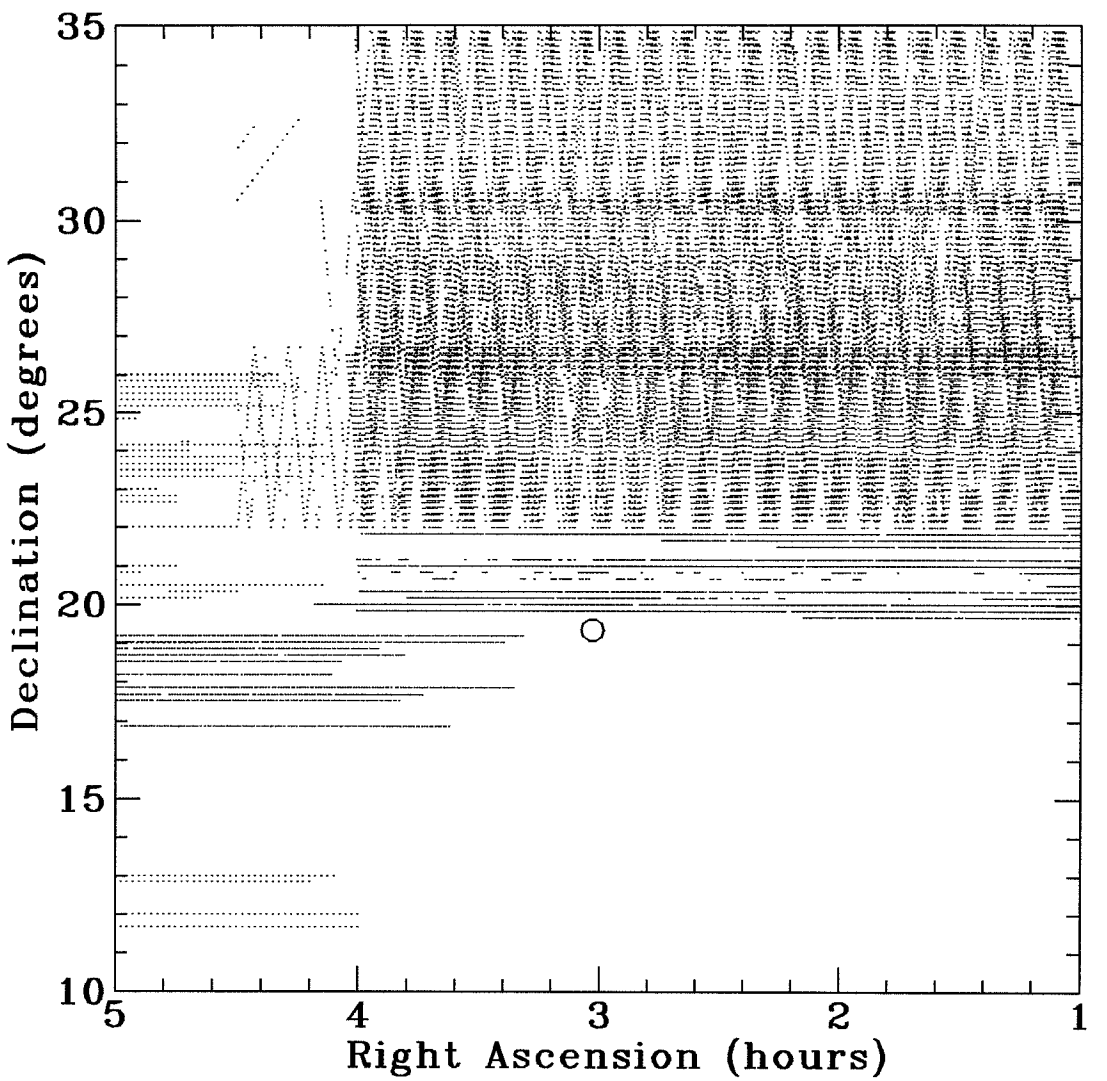

Figure 4.1: RFI-free sky coverage (B1950) of these surveys from 1^h to 5^h right ascension. The drift scans are separated in declination by 10′. Gaps in the scans are from sporadic RFI or observing problems. Filled circles represent known pulsars detected in these surveys, while unfilled circles are other known pulsars.

remaining 41 square degrees were searched with the telescope slewing east at the sidereal rate along lines of constant declination, giving an effective integration time per point of 21 s. The sensitivity in this part of the sky was a factor $\sqrt{2}$ worse than that in the first region.

Because of a scheduling error, a large fraction of this survey was directed at regions of the sky already surveyed by Wolszczan (1990). Thus, it is not surprising that no

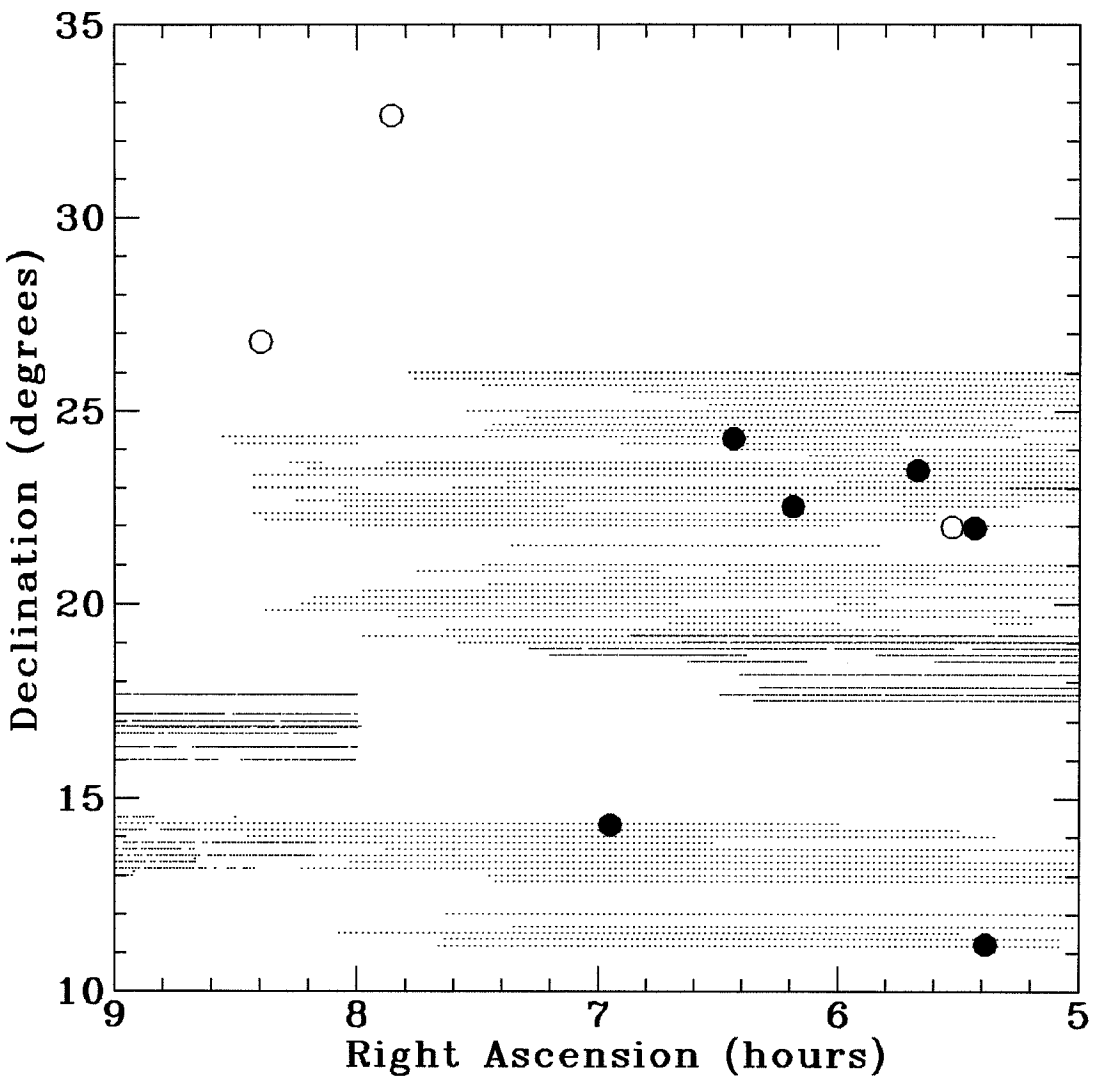

Figure 4.2: RFI-free sky coverage (B1950) of these surveys from 5^h to 9^h right ascension. The drift scans are separated in declination by 10′. Gaps in the scans are from sporadic RFI or observing problems. Filled circles represent known pulsars detected in these surveys, while unfilled circles are other known pulsars.

new pulsars were found, though both known pulsars in the search region were detected, including the millisecond pulsar PSR B1257+12. The sky coverage of this survey is shown on Figure 4.2 and Figure 4.3.

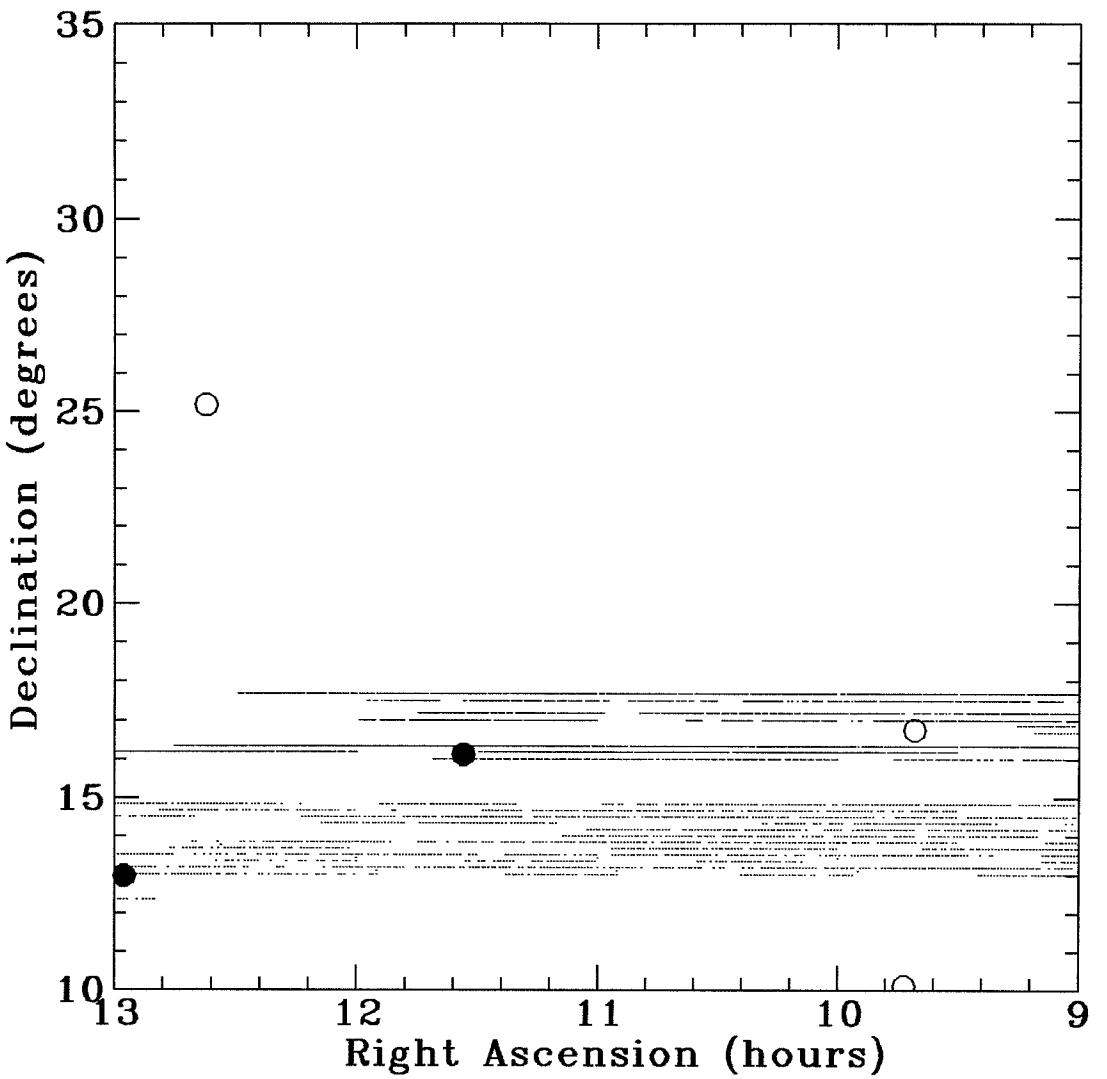

Figure 4.3: RFI-free sky coverage (B1950) of these surveys from 9^h to 13^h right ascension. The drift scans are separated in declination by 10′. Gaps in the scans are from sporadic RFI or observing problems. Filled circles represent known pulsars detected in these surveys, while unfilled circles are other known pulsars.

4.2.3 The Galactic Anticenter (AC) Survey

This survey consisted of three observing sessions: 1988 November–1989 January, 1989 November–December, 1991 January–February. The first two sessions used 67-second pointings on a grid with 22.5′ spacing, while the final session used the drift scan method. A total of $\sim$ 100 square degrees of RFI-free sky were searched and analyzed (see Figure 4.1

and Figure 4.2). The survey was primarily in the region with $170° < l < 210°$, and with $|b| < 20°$. All six known pulsars within the survey region were detected.

In the anticenter direction, the expected DM at 2 kpc is 55 pc cm^{-3} and at 10 kpc is 155 pc cm^{-3} (Taylor and Cordes 1993). The correlator was used because these DMs result in an unacceptable loss in sensitivity to fast pulsars due to pulse smearing within one of the filter bank channels. The survey data was searched up to DM$\sim$ 300 pc cm^{-3}.

4.3 Data Analysis

The data analysis for the non-pointed surveys (all but the AC survey) was performed with groups of up to 12 Sun, IBM, and HP workstations. The suite of programs used for the analysis (PSRPACK) is described by Deich (1994). The 8-mm tape containing each data segment was mounted on the manager workstation, which ran a script that sequentially read blocks of raw data off the tape (32, 128 or 256 kilopoints, depending on sampling rate and telescope slew rate). The manager workstation dynamically maximized the work load on the analysis machines by providing each with a new pointing to reduce as soon as it had completed the previous one. To maintain a consistent sensitivity limit along the drift scans, each tape was run through the system twice, offset by one-half of a beam size.

The data reduction script first reads the raw filter bank data, dedisperses it at typically 50 trial DMs, and writes the dedispersed data to a temporary file. The zero-DM trial is searched for sections of the time series that are substantially different from the mean. The anomalous sections, which are usually due to sporadic radar, lightning, or other interference, are replaced by the local median. This file is then subjected to the standard pulsar search scheme of Fourier transforming, generating a power spectrum, and normalizing the power spectrum to its local mean value. Frequencies that correspond to common RFI peaks are then excised from the power spectrum. This spectrum is searched both for individual peaks and for harmonic sums of 2, 3, 4, 8 and 16 frequencies. Candidates are ranked and the best from each of several DM ranges is used to produce a light curve from the dedispersed data file. The candidate list and light curves are then copied to a storage directory for manual sorting later.

The reduced data are later sorted into clean and RFI-polluted categories. Data are deemed RFI-polluted if the non-zero DM trials cannot be cleaned of spurious signals

TABLE 4.2

Previously known pulsars detected in these surveys.

Name	RA (J2000.0)	DEC (J2000.0)	Period (s)	DM ($pc\,cm^{-3}$)	S_{400} (mJy)	w/P (%)
B0523+11	$05^h25^m56.4^s$	$+11°15'19''$	0.35443	79	19	4.5
B0525+21	$05^h28^m52.3^s$	$+22°00'01''$	3.74552	51	60	4.8
B0540+23	$05^h43^m09.6^s$	$+23°29'06''$	0.24596	78	30	2.4
B0611+22	$06^h14^m17.1^s$	$+22°29'58''$	0.33492	97	30	1.9
B0626+24	$06^h29^m05.7^s$	$+24°15'42''$	0.47662	84	30	2.5
B0656+14	$06^h59^m48.1^s$	$+14°14'22''$	0.38487	14	6	3.9
B1133+16	$11^h36^m03.0^s$	$+15°51'18''$	1.18791	5	300	2.3
B1257+12	$13^h00^m02.7^s$	$+12°40'59''$	0.00622	10	20	9.3

by both time and frequency domain RFI removal techniques. The files of clean data are used to produce maps of RFI-free coverage and to determine positions and parameters of candidates for follow-up. All known pulsars that are in the surveyed area were detected with very high signal-to-noise ratios by these searches; their positions, periods, DMs, fluxes (S_{400}) and duty cycles (w/P) are reported in Table 4.2.

The analysis of the AC survey data proceeded similarly using supercomputers at the Cornell Supercomputing Center, the San Diego Supercomputer Center, and the Jet Propulsion Laboratory. An additional step required in analyzing the data from the correlator is to perform a Fourier transform on the autocorrelation functions to produce power spectra. This step requires four 32-point Fourier transforms per sample.

4.4 Discussion

The minimum detectable flux in a pulsar survey (Dewey 1984; Biggs and Lyne 1992; Stokes *et al.* 1986) is:

$$S_{\rm min} = K \left[\frac{T_{\rm rec} + T_{\rm sky}(l,b) + T_{\rm sp}({\rm ZA})}{G\,(N_p B t)^{1/2}}\right] \left(\frac{w_{\rm eff}}{P - w_{\rm eff}}\right)^{1/2}, \qquad (4.1)$$

where the factor $K \sim 12$ is empirically determined from detection of known pulsars and expresses the analysis detection threshold ($\sim 8\sigma$). $T_{\rm rec}$, $T_{\rm sky}(l,b)$, and $T_{\rm sp}({\rm ZA})$ are the receiver temperature, sky temperature (depending on Galactic longitude and latitude), and effective spillover temperature (depending on zenith angle), respectively. Here, G is the

telescope gain in units of $\mathrm{K\,Jy^{-1}}$, N_p is the number of polarizations received, B is the total bandwidth in MHz, and t is the duration of the observation in seconds. The rightmost factor in equation (4.1) gives the dependence on the pulse duty cycle, where P is the pulse period, and w_{eff} is the effective pulse width:

$$w_{\mathrm{eff}} = \left[w^2 + \beta^2 \tau^2 + \left(\frac{\tau\ \mathrm{DM}}{\mathrm{DM_0}} \right)^2 \right]^{1/2}. \tag{4.2}$$

Here, w is the intrinsic pulse width, τ is the sampling interval in seconds, $\beta \simeq 2$ is related to the time constant of the post-detection smoothing filter, and $\mathrm{DM_0}$ is the dispersion measure at which the pulse delay across the bandpass of a single narrow frequency channel equals the sampling interval. This latter value is

$$\mathrm{DM_0} = 1.2 \times 10^{-4} \frac{\tau \nu^3}{\Delta\nu}\ \mathrm{pc\ cm^{-3}}, \tag{4.3}$$

where ν and $\Delta\nu$ are the observing frequency and channel bandwidth in MHz, respectively.

Figure 4.4 shows the flux limit as a function of period for a typical drift survey at Arecibo (e.g. DHL, CBHL) that employs the filter bank. Figure 4.5 provides the same information for the autocorrelator. Pulsars detected in the surveys are plotted with their cataloged flux densities. The drift surveys have a typical sensitivity of about 0.7 mJy for slow pulsars, but this degrades somewhat for observations far from $\delta = 18°$ because of the zenith angle dependence of the gain and system temperature. The shorter integration times used in the SHL and double-speed portion of the CBHL surveys result in sensitivities of 1.5 and 1.0 mJy, respectively.

The AC, SHL, DHL, and CBHL surveys cover 4% of the total sky available at Arecibo, and they significantly increase the area of Arecibo sky which has been surveyed with sensitivity to millisecond pulsars. Table 4.3 summarizes other high-latitude surveys at Arecibo, all of which have sensitivity comparable to the surveys described here. In about 2700 square degrees, 9 recycled pulsars and 33 normal pulsars were discovered.

The non-detection of millisecond pulsars in the surveys reported in this paper is consistent with the results of other surveys. The previous drift surveys at Arecibo, with 1 mJy sensitivity for slow pulsars (see Table 4.3), have found millisecond pulsars at an average rate of one per 250 square degrees. The Parkes southern sky survey, with 3 mJy sensitivity to slow pulsars, has discovered millisecond pulsars at a rate of one per 1500 square degrees thus far (Bailes *et al.* 1994). These rates are consistent with an isotropic

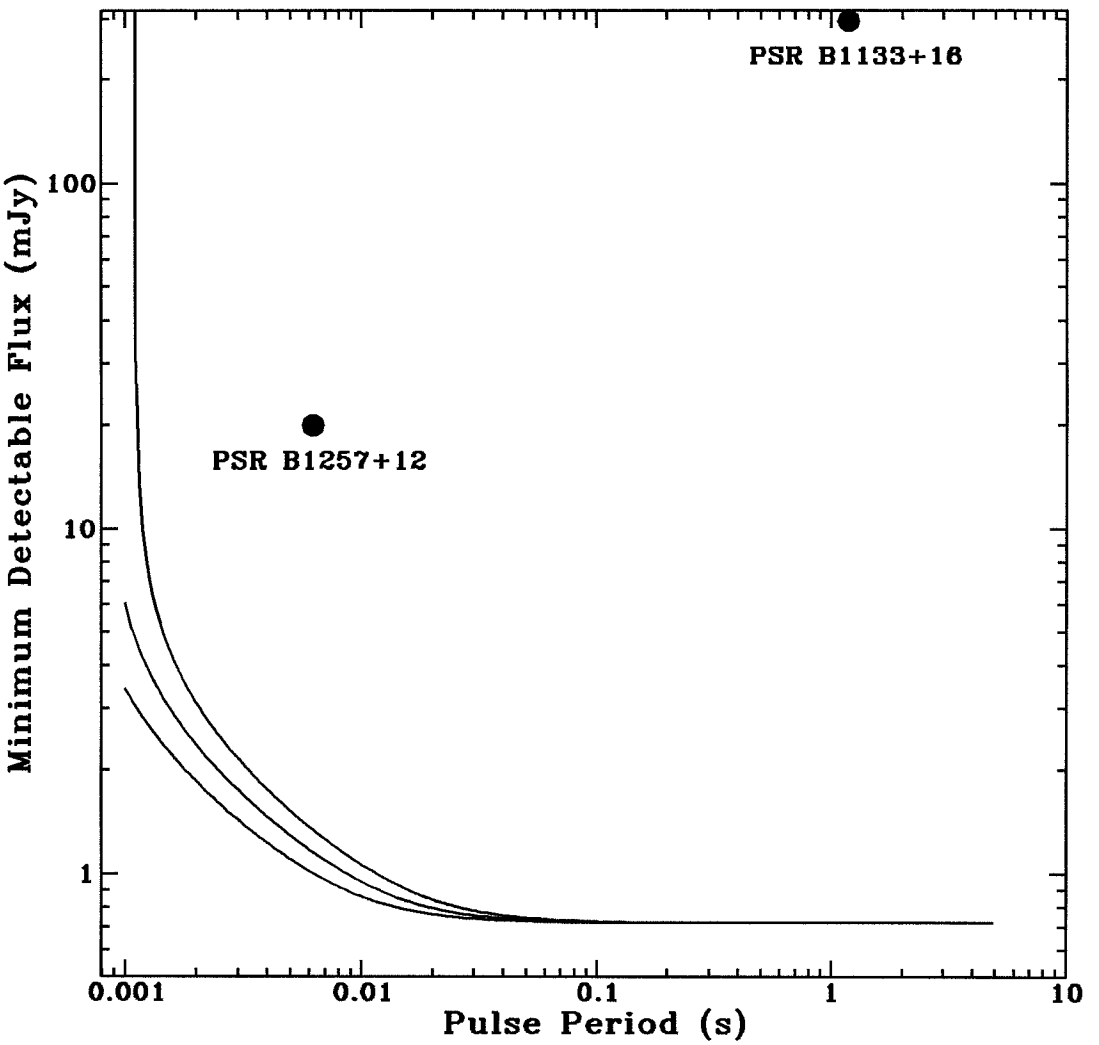

Figure 4.4: The flux limit as a function of period for a typical drift survey from Arecibo using the 2×32 channel filter bank, with a sample time of $250\,\mu$s and an integration time of 32 s. The curves from bottom to top are for DMs of 10, 20, and 30 pc cm^{-3}. An intrinsic duty cycle of 6% is assumed. For other surveys using the filter bank, the sensitivity scales as the square root of the integration time.

distribution of millisecond pulsars, as pointed out by Camilo (1994b). Most of the area covered by surveys in this paper was accounted for by the SHL survey with sensitivity of about 2 mJy. Based on area covered and flux limits of these surveys, the expected number of millisecond pulsars in the 515 square degrees is between 1 and 2, whereas we report no

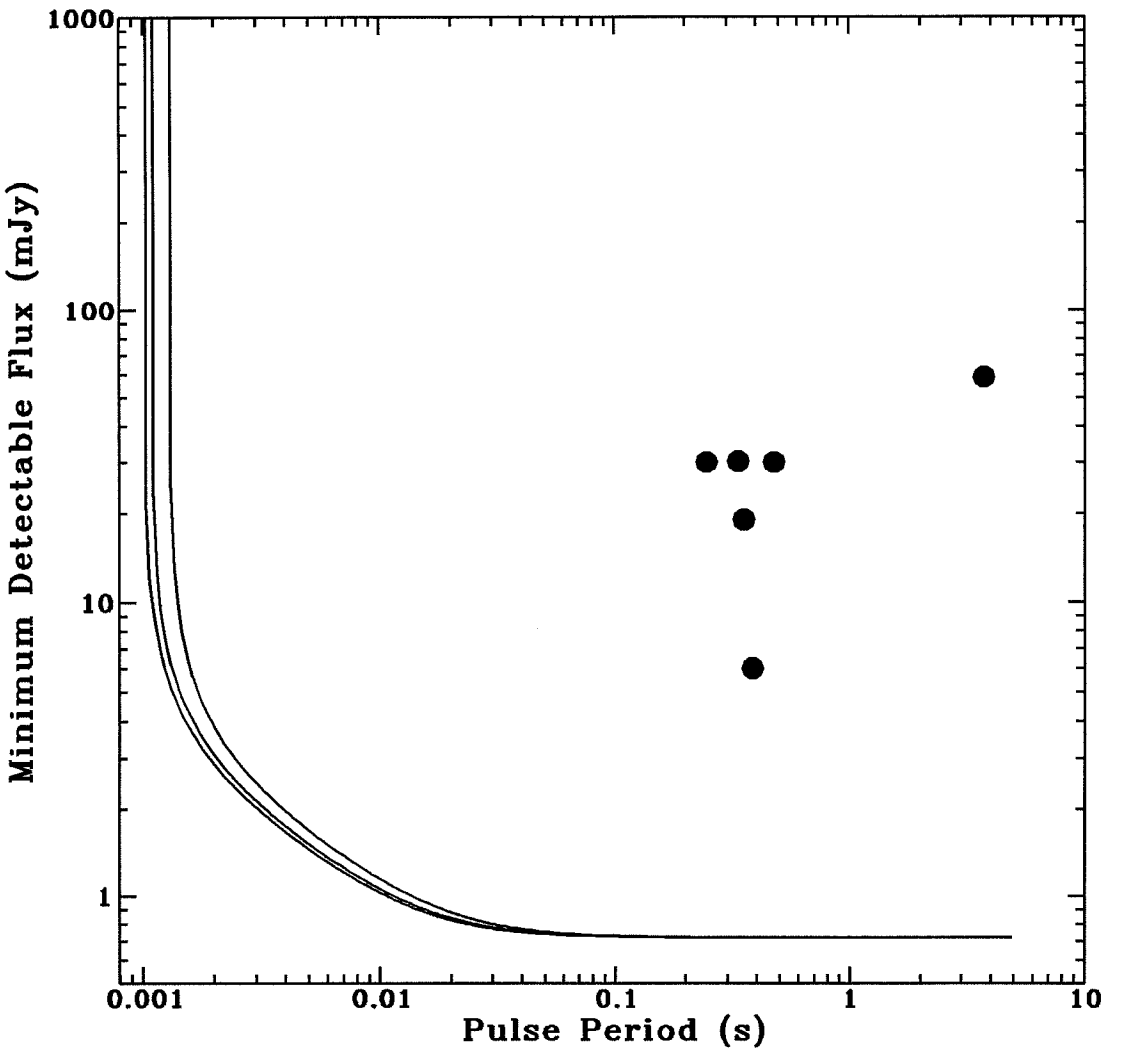

Figure 4.5: The flux limit as a function of period for a typical drift survey from Arecibo using the 2×128 channel autocorrelator, with a sample time of 506.625 μs and an integration time of 32 s. The curves from bottom to top are for DMs of 10, 50 and 100 pc cm^{-3}. An intrinsic duty cycle of 6% is assumed. For other surveys using the autocorrelator, the sensitivity scales as the square root of the integration time. The known pulsar detected in the AC survey are plotted with their cataloged flux densities.

TABLE 4.3

Recent high-latitude surveys at Arecibo

Area (sq. deg.)	Type	$N_{\rm recycled}$ New	$N_{\rm recycled}$ Total	$N_{\rm normal}$ New	$N_{\rm normal}$ Total	Reference
170	Drift	1	1	3	4	[1]
292	Drift	3	3	4	4	[2,3]
150	Drift	2	2	0	0	[4,5]
678	Drift	2	2	13	16	[6]
~ 900	Drift	1	2	13	21	[7,8]
515	Various	0	1	0	7	this work

References: [1] (Nice, Taylor, and Fruchter 1993); [2] (Camilo, Nice, and Taylor 1993); [3] (Camilo 1994a); [4] (Wolszczan and Frail 1992); [5] (Wolszczan 1991); [6] (Foster, Wolszczan, and Cadwell 1994); [7] (Ray *et al.* 1995b); [8] (Thorsett *et al.* 1993).

new discoveries, and one re-detection of PSR B1257+12.

These surveys achieve a nearly constant sensitivity of $\lesssim 1$ mJy over the entire period range of normal pulsars. With their large sky coverage, they place limits on the population of low-luminosity pulsars. The pulsar luminosity distribution is a power-law with slope -1 over most of its range, but appears to flatten at about 10 mJy kpc^2 (Lyne, Manchester, and Taylor 1985); however, it still diverges unless a low-luminosity cutoff is imposed. Observationally, the luminosity distribution is very poorly determined below 1 mJy kpc^2 (Dewey *et al.* 1985). The surveys reported in this paper were sensitive to pulsars of luminosity 0.5 mJy kpc^2 in a volume of $\sim 2 \times 10^7$ pc^3, but none were discovered. This implies that the luminosity distribution ($\Phi(L)$) as described in Lyne, Manchester, and Taylor (1985) at least remains flat and possibly begins to turn down by 0.5 mJy kpc^2. A detailed statistical analysis combining the surveys presented in Table 4.3 and current surveys at Arecibo, Parkes and Jodrell Bank will determine the low end of the pulsar luminosity function and will allow the total number of normal pulsars in the Galaxy and their birth rate to be determined accurately.

We would like to thank José Navarro as well as the staff of Arecibo Observatory for help in performing the observations. The Arecibo Observatory is part of the National Astronomy and Ionosphere Center, which is operated by Cornell University under cooperative agreement with the National Science Foundation.

Chapter 5

Discovery of Fourteen Pulsars in Drift Surveys From Arecibo[1]

5.1 Introduction

The Arecibo telescope is undergoing a major upgrade during which its pointing capabilities are limited and there are no high-frequency feeds available. During this upgrade, five groups are performing drift surveys using the 430 MHz feed at Arecibo, with the goal of surveying the entire sky accessible to Arecibo with excellent, and consistent sensitivity to millisecond pulsars.

This chapter reports on the completion of a survey described by Thorsett *et al.* (1993) (the THL survey) as well as the first 600 square degrees of a very large survey being performed during the upgrade of the Arecibo telescope (the UHL survey). The UHL survey is still in progress and this chapter presents the current status and preliminary results. The most interesting result of the survey so far is the discovery of a binary, millisecond pulsar which is described in Chapter 6. The pulsar discoveries in this chapter are presented primarily for completeness. Analysis of the completed survey when combined with the other current large scale surveys will be a powerful probe of the pulsar population. In Section 5.2 we describe the observations and data analysis. In Section 5.3 we describe the characteristics of the fourteen new pulsars, and in Section 5.4 we discuss the implications of this work and the future of large area searches.

[1]The results of this chapter will be submitted to THE ASTROPHYSICAL JOURNAL (Ray *et al.* 1995b).

5.2 Data Collection and Analysis

All of these surveys used a center frequency of 430 MHz, and the $2 \times 32 \times 0.25$ MHz filter bank. The half power beam width is $10'$.

The first survey we report is the completion of the survey described by Thorsett *et al.* (1993) (hereafter TDK). Further observations were made on 1993 May 25–June 8 from 08^h to 13^h right ascension and 18° to 26° declination. The survey coverage is shown in Figure 5.1. The positions of the four new pulsars discovered in this survey are marked with filled triangles (including the two pulsars reported by TDK). The one previously known pulsar in the region was re-detected by this survey, and is denoted by a filled circle. The declination strips are separated by $10'$ in declination and are lines of constant B1950.0 declination. The total sky coverage was ~ 360 square degrees.

The observations and analysis of these data were described in TDK. In summary, the 8 MHz bandpass was divided into 32 channels and sampled with 3 bit resolution every 180 μs. Overlapping blocks of 47.2 s were analyzed. A more detailed description of the observing and analysis can be found in Ray *et al.* (1995a).

The second survey reported here is the beginning of a large search during the Arecibo upgrade. Because telescope motion is often restricted during the upgrade, this survey is performed with the telescope at a fixed azimuth and zenith angle, drifting in strips of current (1994.10–1994.25) declination. The entire sky has been divided into 1° declination strips and parceled out to several groups doing surveys during the upgrade. We report here on the 7°, 12°, 17°, 27°, and 32° declination strips. We have divided each strip into 6 tracks separated in declination by $9'.2$ beginning at $7'$ north of the stated declination lines. The sample time used for this survey was 250 μs, and the data were analyzed in overlapping blocks of 32.8 s. The completed sky coverage, excluding that which was corrupted by radio frequency interference, is shown in Figures 5.2, 5.3, and 5.4.

5.3 Pulsars Discovered

In a total of ~ 960 square degrees reported by this chapter and TDK, fifteen young pulsars were discovered. The parameters of these new pulsars are summarized in Table 5.1, and their profiles are shown in Figures 5.5 and 5.6.

Most of the new pulsars are typical members of the young pulsar population with

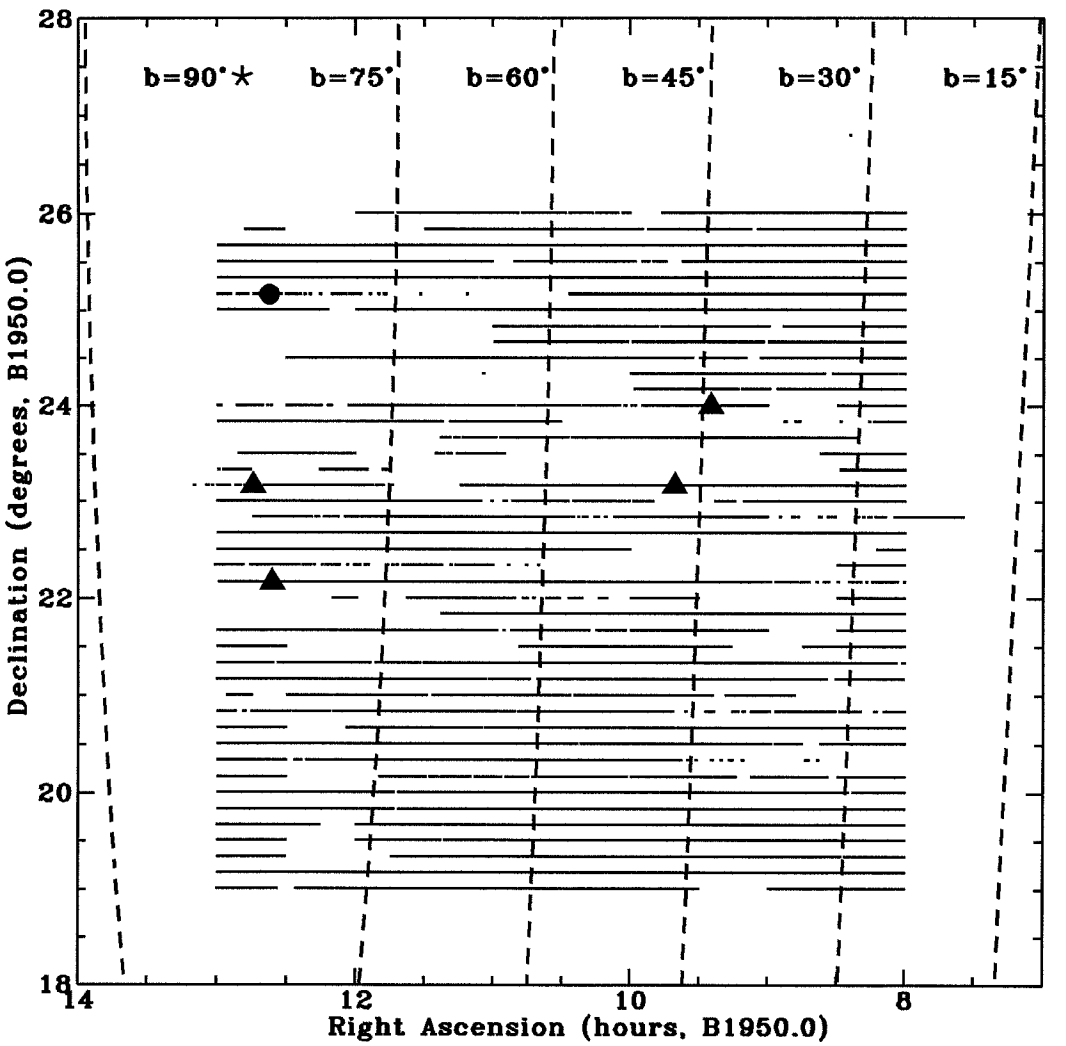

Figure 5.1: RFI-free sky coverage of the complete THL survey, including that reported by Thorsett *et al.* (1993). The declination strips are in B1950.0 coordinates and are spaced by 10′. Note that the horizontal axis of the plot covers 105° while the vertical axis is only 10°. Newly discovered pulsars are marked with filled triangles and the previously known pulsar which was re-detected is marked with a filled circle. The north Galactic pole is marked with a star.

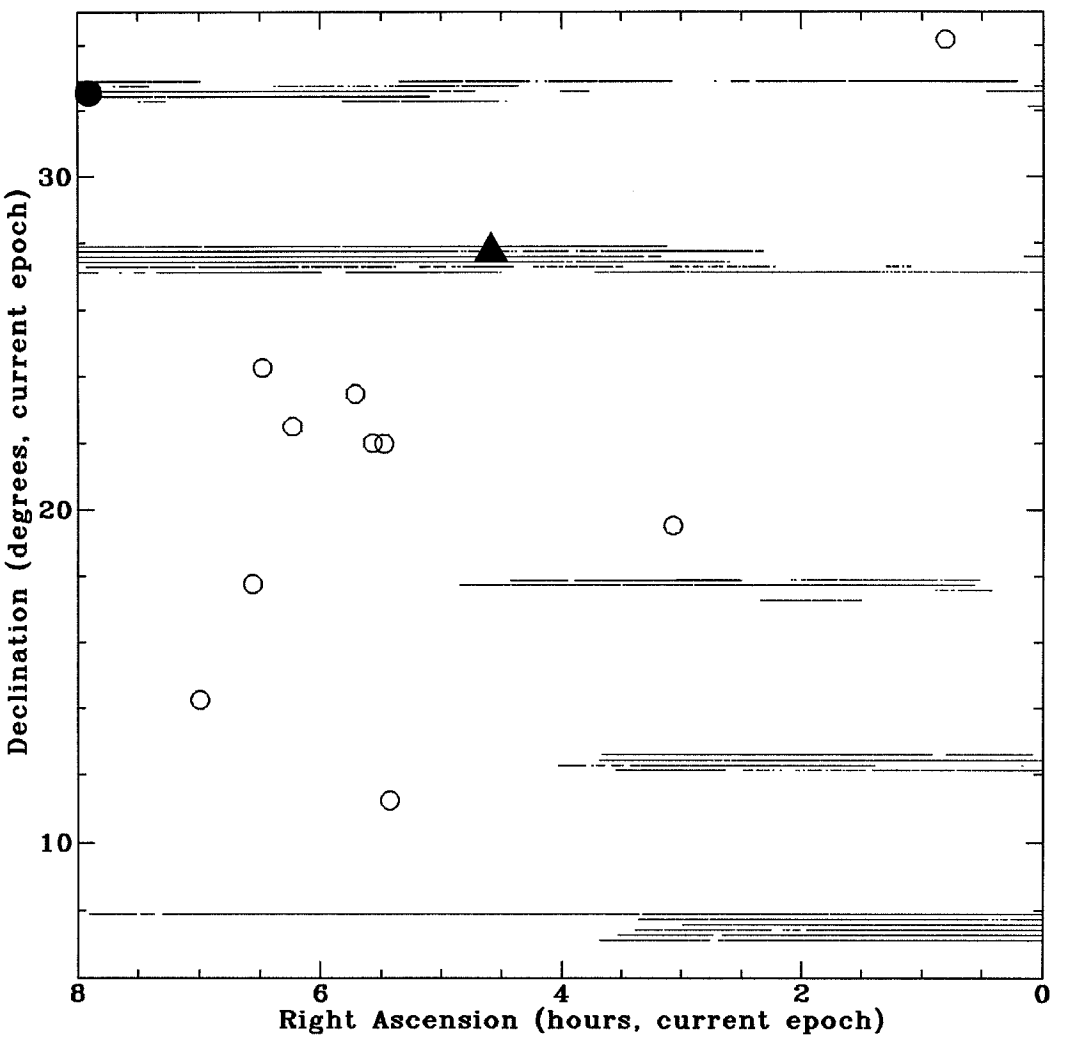

Figure 5.2: RFI-free sky coverage of the UHL survey between 00^h and 08^h. New pulsars are marked with filled triangles, known pulsars that were re-discovered with filled circles, and known pulsars that have not been detected in this survey with open circles. Adjacent declination strips are separated by 9.2 arcmin.

two exceptions: PSR J2033+17, a 5.9 ms pulsar in a binary system (described in Chapter 6), and PSR J2043+2740, one of the fastest non-recycled pulsars for which an association with the Cygnus Loop supernova remnant cannot be ruled out.

During the survey, nine previously known pulsars, including the 4.57 ms pulsar PSR J1713+0747, were detected (see Table 5.2).

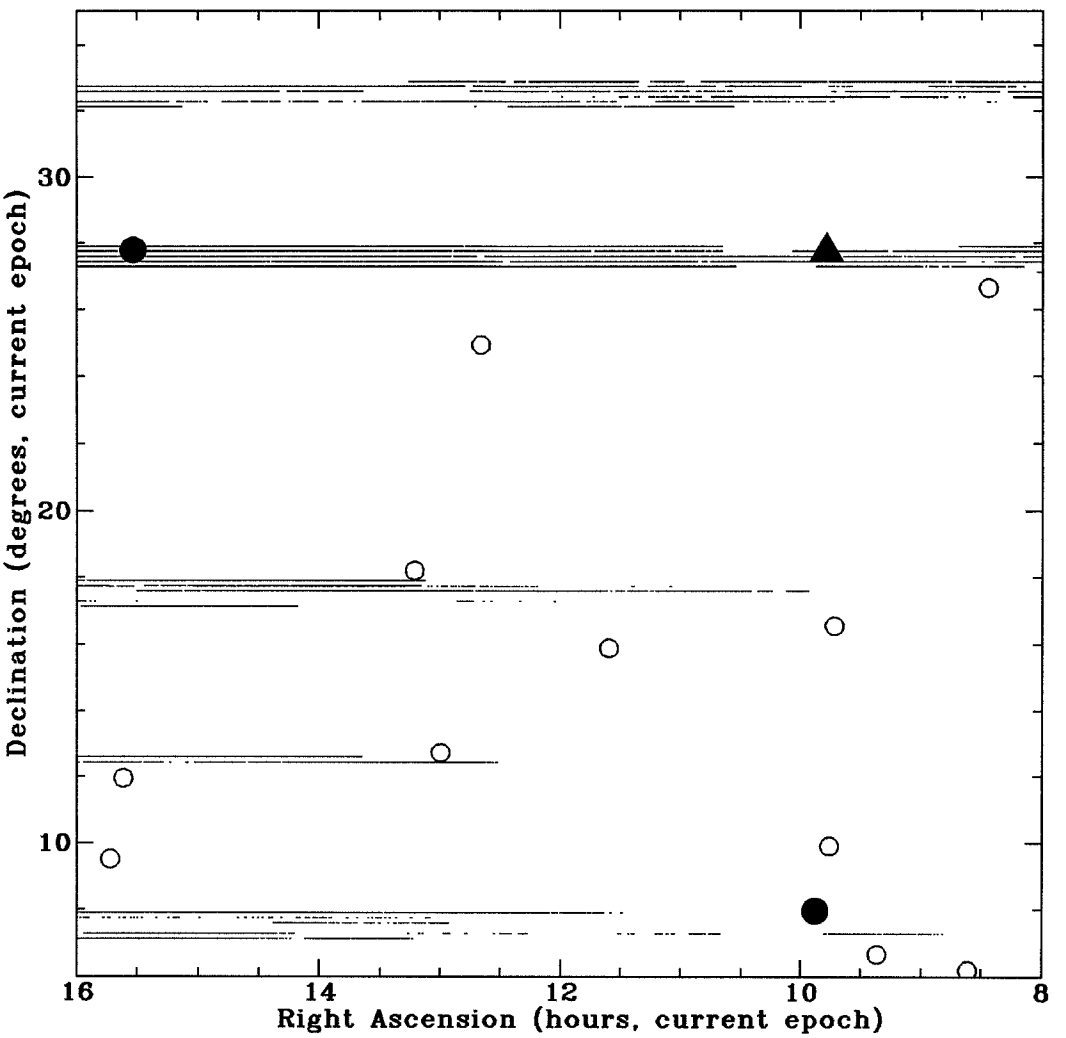

Figure 5.3: RFI-free sky coverage of the UHL survey between 08^h and 16^h.

The flux limits for this survey are the same as those shown in Figure 4.4. The flux limit for slow pulsars is ~ 0.7 mJy, increasing to 1–3 mJy for millisecond pulsars due to the effects of dispersion smearing and harmonic content beyond the Nyquist frequency of the sampling.

TABLE 5.1

New pulsars detected in this survey.

Name	RA[1] (J2000.0)	DEC[1] (J2000.0)	Period[2] (s)	DM ($pc\,cm^{-3}$)	d (kpc)
J0435+27	$04^h35^m34^s$	27:44	0.3262793(9)	53	3.4
J0927+23	$09^h27^m37^s$	23:47	0.761886(3)	23	> 2.5
J0943+22†	$09^h43^m25^s$	22:56	0.532913(12)	25.1	> 2.4
J0947+27	$09^h47^m22^s$	27:42	0.85105(2)	29	> 2.3
J1238+21	$12^h38^m21^s$	21:54	1.11836(4)	20	> 1.8
J1246+22†	$12^h46^m38^s$	22:53	0.473830(4)	17.9	> 1.8
J1742+27	$17^h42^m02^s$	27:53	1.360744(8)	36	3.7
J1807+07	$18^h07^m42^s$	07:53	0.46430(2)	89	> 7.7
J1821+17	$18^h21^m31^s$	17:17	1.3662(2)	79	> 7.1
J1915+07	$19^h15^m01^s$	07:53	2.0588(2)	118	3.7
J1916+07	$19^h16^m54^s$	07:53	0.54218(4)	305	8.2
J1933+07	$19^h33^m20^s$	07:53	0.437446(5?)	170	8.9
J2033+17	$20^h33^m21^s$	17:36	0.0059490	25.2	1.4
J2043+2740	$20^h43^m43.5^s$	27:40:56	0.0961305	21	1.1
J2053+17*	$20^h53^m55^s$	17:17	0.11926	25	1.4
J2113+27	$21^h13^m54^s$	27:54	0.601422(5)	30	1.7

[1] The positions for all pulsars except for J2043+2740 are uncertain by $\pm 5'$ in each coordinate. [2] The periods are barycentric periods and were all measured in 1993 or 1994. Distances are derived from the Galactic free electron model of Taylor and Cordes (1993).

* Not yet confirmed with a followup observation.

† Previously reported by Thorsett *et al.* (1993)

TABLE 5.2

Previously known pulsars detected in this survey. Parameters are from Taylor, Manchester, and Lyne (1993)

Name	RA (J2000.0)	DEC (J2000.0)	Period (s)	DM (pc/cm^3)	S_{400} (mJy)	W50 (ms)
B0751+32	07:54:40.6	+32:31:58	1.44234	39.4	6	10
B0950+08	09:53:09.3	+07:55:36	0.25306	3.0	400	11
B1237+25	12:39:40.5	+24:53:49	1.38244	9.3	110	5
B1530+27	15:32:10.0	+27:45:47	1.12483	14.6	12	26
B1612+07	16:14:41.0	+07:37:31	1.20680	21.3	10	12
B1921+17	19:23:21	+17:06	0.54721	135	2	25
B1944+17	19:46:53.0	+18:05:41	0.44062	16.3	35	18
B2110+27	21:13:04.3	+27:54:00	1.20285	24.7	14	13
J1713+0747	17:13:49.5	+07:47:38	0.00457	16.0	36	0.25

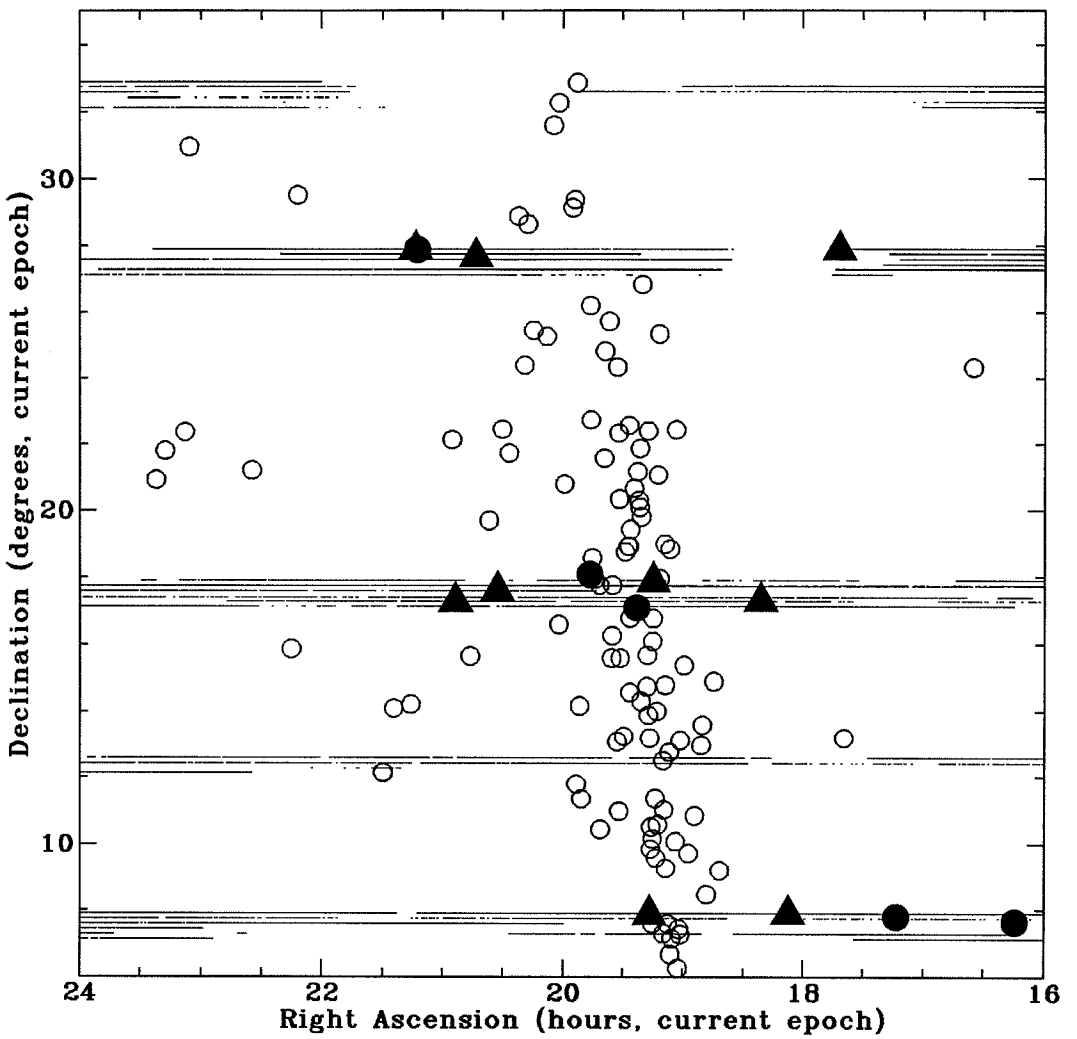

Figure 5.4: RFI-free sky coverage of the UHL survey between 16^h and 24^h.

5.3.1 PSR J2043+2740

In survey observations taken on 23 May 1994, a pulsar was discovered with a period of 96.1 ms and a DM of 21 $\mathrm{pc\,cm^{-3}}$ (Thorsett *et al.* 1994, and Appendix A). What is particularly notable about this pulsar is that all but one (PSR B1830-08) previously known pulsars with period shorter than 96 ms are either recycled pulsars or are associated with a supernova remnant. In addition, an association of this pulsar with the Cygnus Loop supernova remnant cannot be ruled out, although this does require that the pulsar's

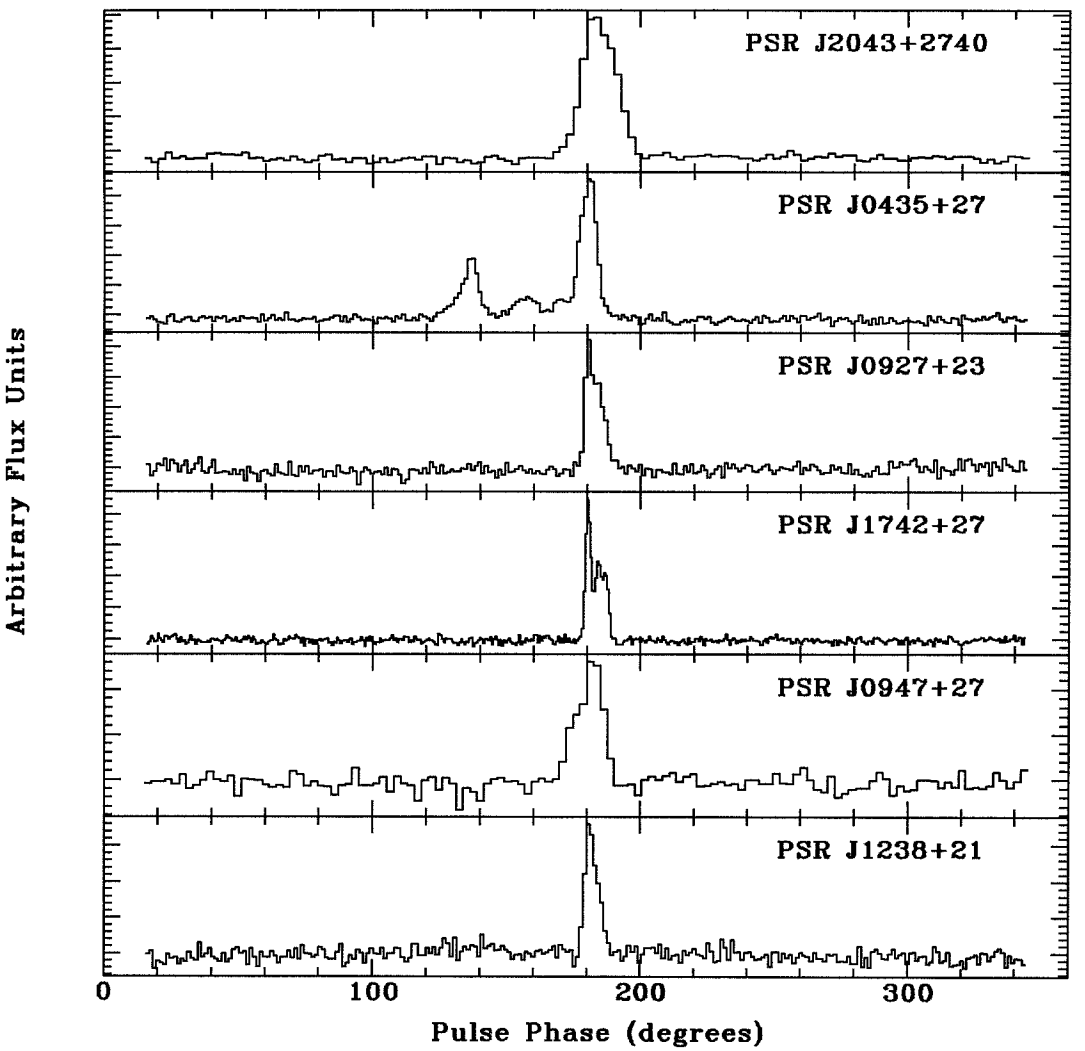

Figure 5.5: The profiles of 6 new pulsars reported in this chapter. The vertical scale is arbitrary, and the highest point in the profile has been shifted to line up at phase 180°.

true age be rather different than its characteristic age, and that it was born with a very high velocity. This pulsar lies approximately 1° outside the boundary of the Cygnus Loop supernova remnant. The DM-derived distance for the pulsar ($\sim$ 1.1 kpc) is consistent with the estimated distance to the remnant (600 pc with 1 σ limits of 300 and 1200 pc) (Shull Jr. and Hippelein 1991). In addition, the period of the pulsar is similar to that of PSR B0833-45 in the Vela supernova remnant, approximately the period expected for a pulsar which is

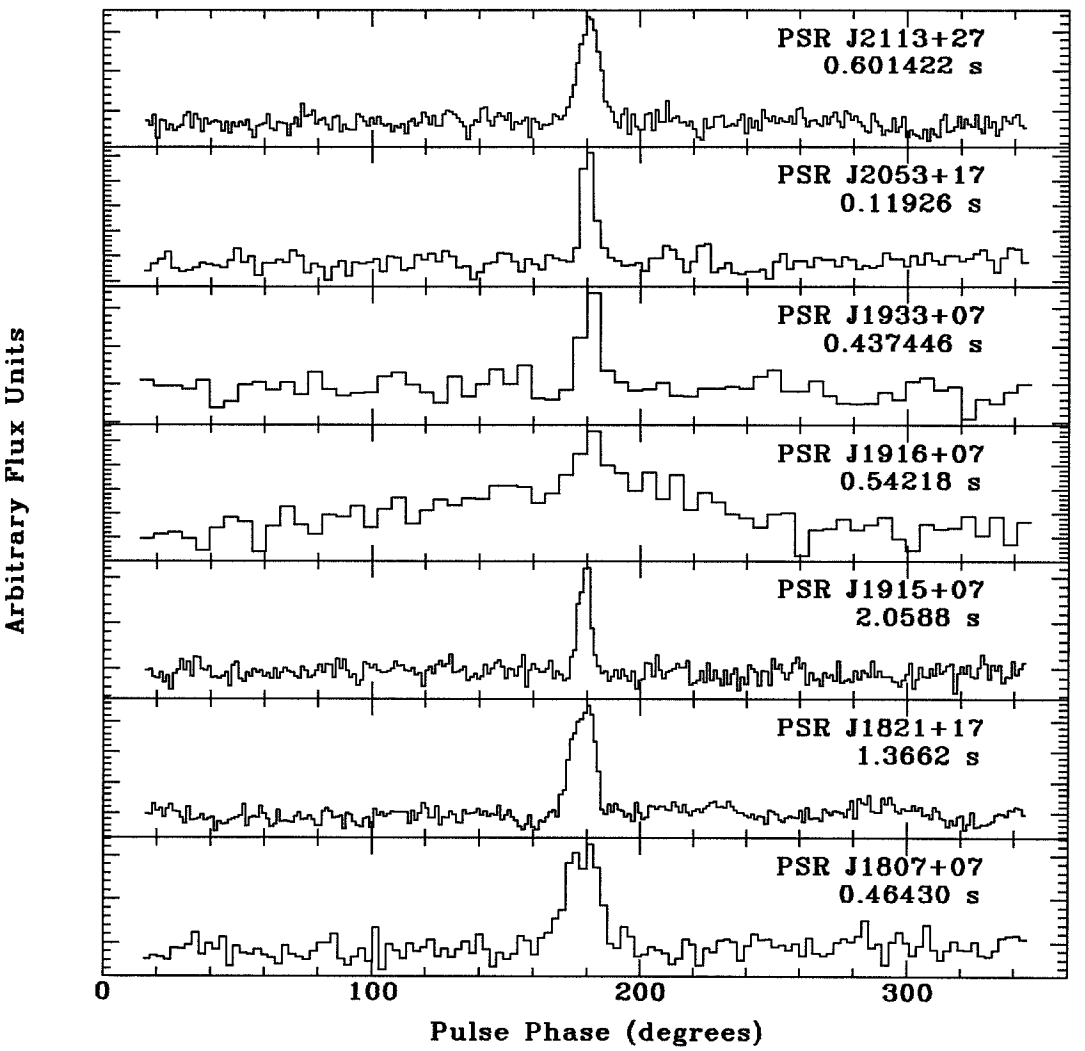

Figure 5.6: The profiles of another 7 new pulsars reported in this chapter. The vertical scale is arbitrary, and the highest point in the profile has been shifted to line up at phase 180°.

$\sim 2 \times 10^4$ years old—the estimated age of the remnant (Ku *et al.* 1984).

The pulsar birth velocity required for association with the Cygnus Loop is uncertain, as neither the age, nor the distance to the remnant is accurately known, however it could be as high as 1500 km/s. This is not impossible, and is comparable to velocities inferred from several other currently proposed pulsar-SNR associations (see Chapter 3). There has also been speculation that the supernova that formed the Cygnus Loop did not

occur in the geometric center of the remnant, but rather in the so-called "southern break-out" region of the remnant. This would reduce the required velocity by at least a factor of two.

We have performed timing observations at Green Bank and Arecibo in order to measure the characteristic age of the pulsar. Data were taken at the Green Bank 140-ft telescope on 1994 July 7–11 and September 8–11, and data were taken at the Green Bank 85-ft telescope almost daily from 1994 July 16–December 2.

The observing system at the 85-ft receives two linear polarizations using a 20 × 1 MHz filter bank with a 70 μs post-detection time constant. Four filter bank channels are contaminated by RFI from UHF TV stations and are excised from the data. The remaining 16 channels are sampled with a Princeton Mark III pulsar timing system (Stinebring *et al.* 1992), which digitizes the inputs and synchronously folds the data at the predicted topocentric pulsar period into pulse profiles with 256 bins. Each integration is $4^{\rm m}40^{\rm s}$. The observing system at the 140-ft uses center frequencies of 575 MHz, 800 MHz, and 1.4 GHz. These IFs are fed into the Spectral Processor, an FFT spectrometer which provides 512 channel spectra across a 40 MHz bandwidth. These spectra are integrated into a pulse profile of 128 bins spanning the topocentric pulse period of the pulsar. The integrations are 2–3 minutes in duration. The individual channels are combined into a single, dedispersed profile by summing them with delays chosen to correct for the interstellar dispersion. The resulting profiles are then cross correlated with a standard template to generate pulse times-of-arrival.

During the first several months of timing a pulsar, the residuals from position error, which are a sine wave with a 1-year period, and residuals from a period derivative, which are a parabola, are highly covariant. So, to aid in making a measurement of the period derivative quickly, an interferometric position was measured at the Very Large Array (VLA). Two 5 minute snapshots were taken on 1994 July 15 and 16. Two bright sources are evident in the synthesized map from the July 15 data. One is apparently a double or slightly extended source with position (accurate to about 1″) $20^{\rm h}43^{\rm m}50.1^{\rm s}$ $+27°40'45''$ (J2000.0) and a flux of 120 mJy at 1.66 GHz. We identify this source with the cataloged radio source 87GB 204141.8+272952. The other prominent source in the field was at the position $20^{\rm h}43^{\rm m}43.50^{\rm s}$ $+27°40'56.3''$ (J2000.0) with a 1.66 GHz flux of 7 mJy. In the next day's observation, the bright source was still present, but the other source was not seen. We identify the second source with the pulsar; the non-detection the second day being consistent with pulsar scintillation. We note that the absolute fluxes are not carefully calibrated and

TABLE 5.3

Parameters of PSR J2043+2740 as of MJD 49688

Interferometric Parameters	
Right Ascension (J2000.0)	$20^h43^m43.5(2)^s$
Declination (J2000.0)	$+27°40'56(2)''$
Flux at 1.66 GHz (mJy)	7(3)
Timing Parameters	
Right Ascension (J2000.0)	$20^h43^m43.65(4)^s$
Declination (J2000.0)	$+27°40'54(2)''$
Period (s)	0.09613053755(2)
Period Epoch (MJD)	49540.5
Period Derivative	$1.258(5) \times 10^{-15}$
Dispersion Measure ($pc\,cm^{-3}$)	21.01(2)
Derived Parameters	
Characteristic Age (yr)	$1.21(1) \times 10^6$
Surface Magnetic Field (G)	3.5×10^{11}
Spin-down Luminosity (erg/s)	5.6×10^{34}
Distance (kpc)	1.1

are uncertain by about 50%.

This timing analysis yields a period derivative of $1.258(5) \times 10^{-15}$. The characteristic age of the pulsar is 1.21(1) Myr, which, if the pulsar's true age is near its characteristic age, is inconsistent with being formed in the Cygnus Loop birth event. However, it is possible that the pulsar was born with a period close to its current period and is not as old as 1.2 Myr. A measurement of the proper motion could definitively confirm or rule out an association with the remnant birth event.

The results of the pulse timing analysis of this pulsar and some of the derived parameters are presented in Table 5.3. In addition to the parameters shown, instrumental offsets were fit between the data sets from Arecibo, the Green Bank 140-ft system and the Green Bank 85-ft system. A total of 543 times of arrival spanning the range 1994 May 23 to 1994 October 17 were included in the fit, which was done using the standard program TEMPO. A plot of the post-fit timing residuals is shown in Figure 5.7. The data from Arecibo has a RMS post-fit residual of 135 μs , and the Green Bank 140-ft and 85-ft data has RMS residuals of 120 μs, and 780 μs, respectively. A moderately large covariance remains between the timing measurements of declination and period derivative.

Based on the fact that the association with the Cygnus Loop requires both a rather

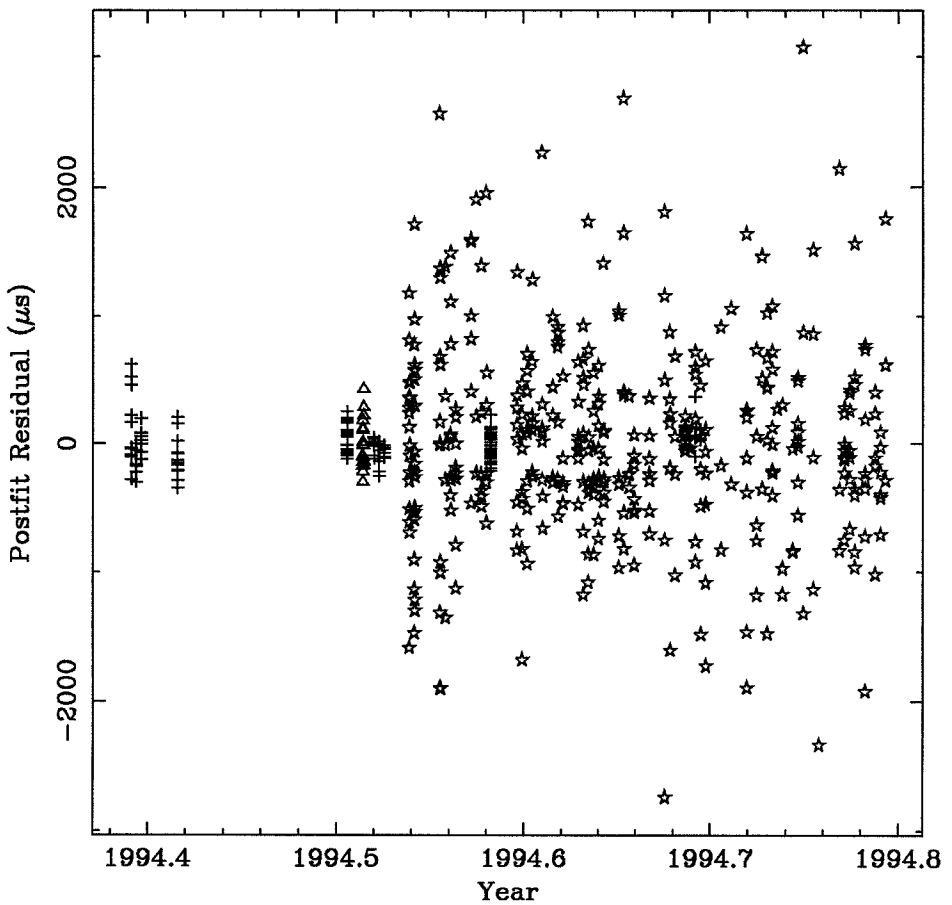

Figure 5.7: Post-fit timing residuals for PSR J2043+2740. Plus signs are TOAs taken at 430 MHz or 575 MHz, triangles are TOAs taken at 1400 MHz, and stars are TOAs taken at 610 MHz or 800 MHz.

high birth velocity and a true age very different from the characteristic age, we conclude that PSR J2043+2740 was not formed in the supernova that resulted in the Cygnus Loop. Thus, the pulsar was either born with the low magnetic field of 3×10^{11} G or is a mildly recycled pulsar which had is magnetic field reduced through a short episode of accretion from a companion which has been lost.

5.4 Discussion

In over 900 square degrees of sky, the surveys in this chapter combined with TDK detected 23 young pulsars (15 new), and 2 millisecond binary pulsars (1 new). In Chapter 4,

one (previously known) millisecond pulsar was detected in about 225 square degrees surveyed at the same sensitivity[2]. The combined surveys imply a surface density of millisecond pulsars above 1 mJy of 1 per 375 square degrees. This is somewhat, but not significantly, lower than the rate found in the Penn State-NRL survey and the Princeton surveys with identical observational hardware (see Table 4.3).

Using a recent model of the Galactic free-electron distribution (Taylor and Cordes 1993), the distances to the new pulsars can be estimated. These distance estimates are shown in Table 5.1. Seven of these are only lower limits, since the integral along the line of sight of the free-electron density model never reaches the measured DM for the pulsar. The model underpredicts the maximum DM in the direction of these pulsars up to 25%. These pulsars will be useful for making the next generation of free-electron distribution models and provide information about the thickness of the electron layer in our Galaxy.

The current estimate of pulsar birth velocities is very large ($\sim 450\,\mathrm{km/s}$). However, the average velocity of observed older ($\gtrsim 10^7\,\mathrm{yr}$) pulsars is considerably lower ($\sim 100\,\mathrm{km/s}$) (Lyne and Lorimer 1994) because fast, old pulsars have moved far from the Galactic plane, where they are difficult to detect. Current, sensitive high latitude surveys may start to reveal this population; some of the pulsars discovered in this survey at large distances from the Galactic plane may be members of this "fleeing" pulsar population. Proper motion velocities for these pulsars will be interesting, if measurable. Scintillation velocities for these pulsars may be particularly unreliable because of systematic errors due to the unknown distance to the "scattering screen" (Nicastro and Johnston 1995).

Most of the data has been analyzed only out to DMs of $\sim 70\,\mathrm{pc\,cm^{-3}}$. This is primarily because only a small fraction of the data is taken at Galactic latitudes small enough that DMs greater than $70\,\mathrm{pc\,cm^{-3}}$ are expected, and sensitivity to millisecond pulsars which were the primary target of this survey is greatly reduced at high DM due to smearing across the 250 kHz filter bank channels.

Inspection of the pulse profiles in Figures 5.5 and 5.6 reveals several things. At the current signal to noise level, eleven of the thirteen pulsars appear to have single component profiles. The majority of the pulsar population have single component profiles. Without the benefit of polarized intensity profiles and multi-frequency observations, we cannot distinguish between the core-single profiles and the conal-single profiles as defined by Rankin

[2]We exclude the slewing survey due to its higher flux limit.

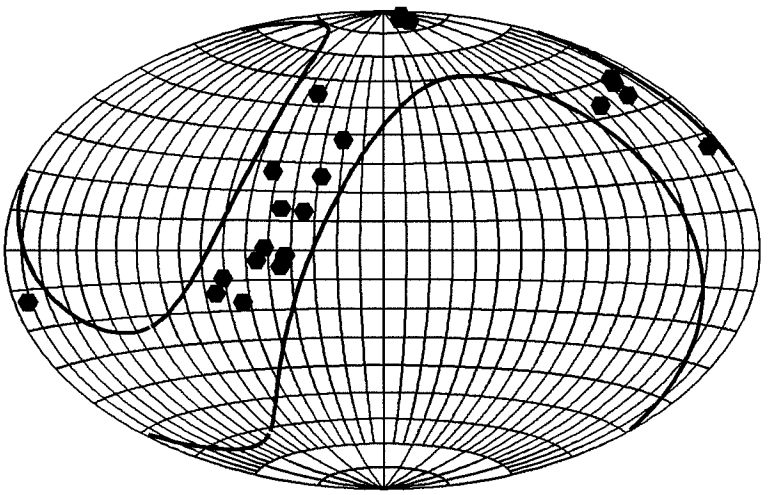

Figure 5.8: Map of the detected pulsars in Galactic coordinates.

(1983). Two of the pulsars display clear multiple component profiles. PSR J1742+27 shows a standard triple profile with a total extent of $\lesssim 10°$ of pulse longitude. This is a representative of a fairly large class of pulsar profiles. PSR J0435+27 has a rather unusual profile that shows at least three and possibly four components with a total separation of about 45° of longitude. The profile is rather similar to PSR B1541+09 which also shows a rather wide multi-component profile and Rankin (1990) classifies as a triple. PSR J0435+27 deserves of further study to establish its classification and see if it exhibits drifting subpulses or mode changing as seen in several triples by Hankins and Wolszczan (1987).

5.5 Conclusion

The survey during the Arecibo upgrade is incomplete and will continue throughout 1995. At the current rate, we expect the discover of ~ 2 more recycled pulsars as well as a dozen or so young pulsars. The completed survey will be particularly useful for population studies when combined with the rest of the Arecibo surveys, the Parkes southern sky survey and the Jodrell Bank northern sky survey. Their consistent flux limits, and minimal selection effects due to short periods, will allow the recycled pulsar population to be characterized far better than previously possible. They will also help constrain the local population of low-luminosity young pulsars which is important for estimating the pulsar birth rate.

Chapter 6

Discovery of a 5.9-ms Pulsar[1]

6.1 Introduction

The surveys described in Chapters 4 and 5 were designed to have excellent sensitivity to millisecond pulsars. Understanding the formation and evolution of millisecond pulsars requires a large sample of pulsars from which statistical inferences can be drawn. Our surveys, and the surveys of several other groups, were designed to vastly increase the number of known millisecond pulsars. Before 1990, there were only four known millisecond pulsars outside of the globular cluster system. There are now about 30 known pulsars with period $\lesssim 16$ ms in the Galaxy, and this number is increasing rapidly. As large portions of the sky have not yet been surveyed at high sensitivity, the continuation of large surveys at Arecibo and Parkes promise to keep up the pace of discoveries for the next couple of years.

In the course of our large-area surveys, a 5.9-ms pulsar was discovered. The initial parameters of the system are presented here along with prospects for more interesting measurements with continued timing.

6.2 Observations

The pulsar PSR J2033+17 was discovered using the 32×0.25 MHz filterbank, sampled at 250 μs as described in Chapter 5. The discovery data were taken on 1994 July 17. The pulsar was confirmed with the same instrument on 1994 August 18, and reobserved on 1994 September 9 and 1994 October 19. These data are sufficient to measure barycentric

[1]The results of this Chapter will be submitted to THE ASTROPHYSICAL JOURNAL, LETTERS (Ray, Thorsett, and Prince 1995), after a phase-connected timing solution is established.

TABLE 6.1

Parameters of PSR J2033+17 (as of 1994 November)

Right ascension (J2000.0)	$20^h33^m21^s(20)$
Declination (J2000.0)	17°36′(5)
Galactic longitude (l)	60.9°
Galactic latitude (b)	−13.1°
Dispersion measure (pc cm^{-3})	25.2(3)
Pulse period (s)	0.0059489575(2)
Orbital period (d)	56.2(1)
Semi-major axis (lt-s)	20.07(8)
Epoch of ascending node (MJD)	49584.32(12)
Eccentricity	< 0.05
Mass function	0.00275(3) $M_\odot$
Minimum companion mass	0.2 $M_\odot$
Companion mass at $i = 60°$	0.22 $M_\odot$
Inferred Distance	1.4 kpc

periods for the pulsar, and establish that it is in a binary system (see the first four points in Figure 6.2). However, the orbital period is not well constrained with these data, and precise timing of the pulsar is not possible due to apparent "slips" in the data of multiples of the 250 μs sample time.

Consequently, we performed observations of the pulsar from 1994 November 2-6 using the Arecibo 128 × 78.125 kHz autocorrelator, which has been used for extensive millisecond pulsar timing (Anderson 1993). For each of these data sets, the observation was subdivided into short intervals, and average pulse profiles were computed by folding the data modulo the best period determined from a Fourier transform of the day's data. Topocentric arrival times were computed for each profile by cross correlating with a high signal to noise template. These daily sets of TOAs were fitted using the program TEMPO (Taylor and Weisberg 1989) to determine a barycentric period for the pulsar each day.

The observed periods were fitted to a circular orbit model (see Eqn. 1.6), which describes the data well with only a limit on the eccentricity of $\lesssim 0.05$. All known millisecond pulsars which are in binary systems (LMBPs) have eccentricities much less than 10^{-3}, and therefore more data is required in order to set useful constraints on this parameter. The observed barycentric periods and best-fit model are shown in Figure 6.2. The best-fit orbital model parameters, are presented in Table 6.1.

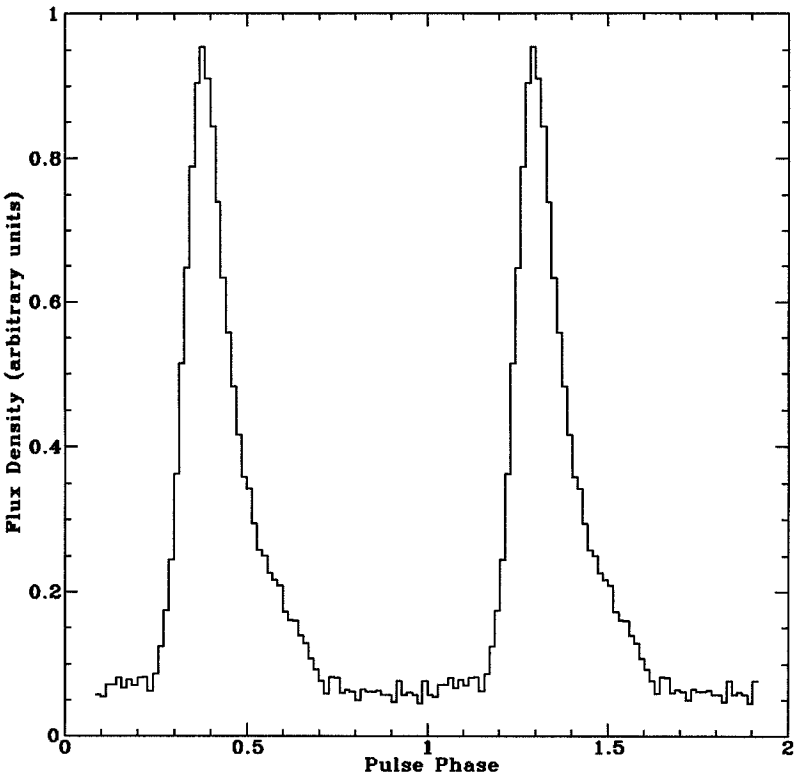

Figure 6.1: Pulse profile of PSR J2033+17. This profile was taken with the Arecibo 32 × 0.25 MHz filterbank at a center frequency of 430 MHz. The dispersive smearing across one channel of the filter bank is $\sim 650\,\mu$s or 0.11 pulse periods.

6.3 Discussion

A pulsar with an orbit whose Keplerian parameters are determined from Doppler shifts in the pulse period is akin to a single-line spectroscopic binary in which the orbit is determined by measuring Doppler shifts of spectral lines in one of the members. In such a system, a useful quantity is the mass function ($f(m_1, m_2, i)$) which relates the mass of the members of the system to the measured orbital period (P_b) and projected semi-major axis ($a_1 \sin i$). The mass function is defined as

$$f(m_1, m_2, i) = \frac{(m_2 \sin i)^3}{(m_1 + m_2)^2} = \frac{4\pi^2 (a_1 \sin i)^3}{P_b^2 G}, \tag{6.1}$$

where m_1 is the pulsar mass, m_2 is the companion mass, a_1 is the semi-major axis of the pulsar's orbit, $\sin i$ is the orbital inclination, and G is Newton's gravitational constant. The

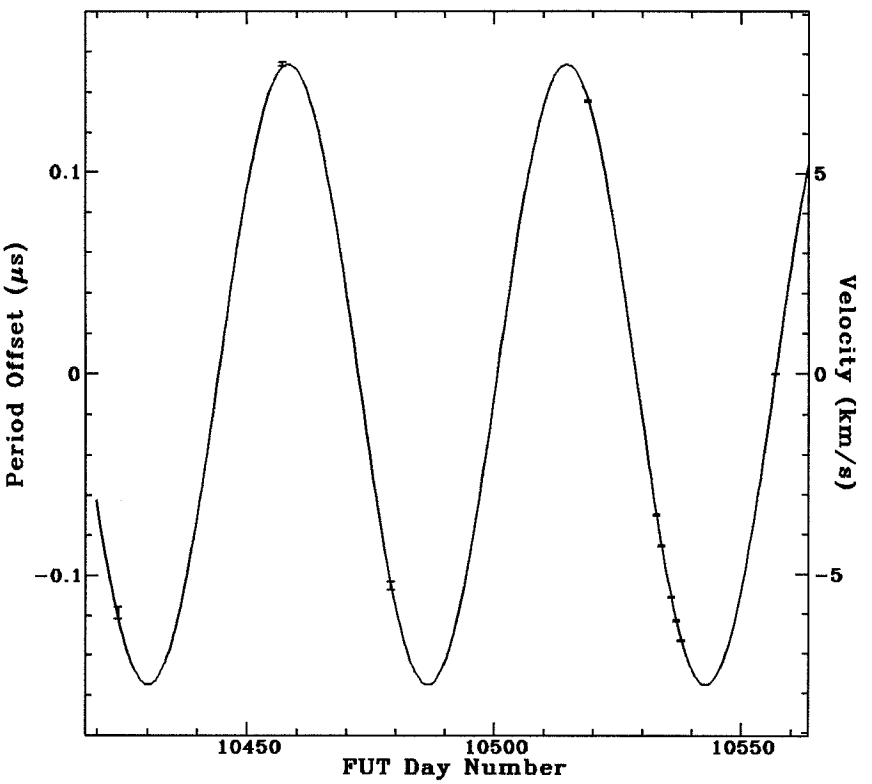

Figure 6.2: Observed barycentric period offsets relative to 5.9489582 ms for PSR J2033+17, and the best fit circular orbit model. The errors on the first two points are considerably larger than the later points due to short integration times (30 s and 10 min). The projected orbital velocity is shown on the right axis.

mass function for the PSR J2033+17 system is 0.00275(3) $M_\odot$. This implies a minimum companion mass for an edge-on orbit of 0.2 $M_\odot$, and a most probable companion mass ($i = 60°, m_{\rm NS} = 1.4\ M_\odot$) of 0.22 $M_\odot$.

In the preceding analysis, the mass of the pulsar is assumed to be 1.4 $M_\odot$, since all measured neutron star masses are close to 1.4 $M_\odot$. However, most of the well-measured neutron star masses are from double neutron star systems (*i.e.* HMBP systems), such as PSR B1913+16, PSR B1534+12, and PSR B2127+11C. These systems likely did not undergo the long period of mass accretion needed to spin them up to millisecond pulsars (see §1.2.4). So, it is particularly important to make mass measurements of some neutron stars that are not in double neutron star systems.

The parameters in double neutron star systems which allow precise determinations

of the mass are the relativistic precession of periastron ($\dot{\omega}$) and the combined effect of time dilation and transverse Doppler shift (γ) (Taylor and Weisberg 1989). These effects are extremely difficult to measure in a nearly circular, wide binary like J2033+17. Mass measurements of millisecond pulsars are particularly interesting as they are believed to have undergone an extended period of mass accretion to spin them up to millisecond periods. For the case of completely conservative mass transfer, where all the mass that provides angular momentum to the star ends up being accreted by the star, the mass may be as high as 2.0 $M_\odot$. Therefore, a good mass measurement will help constrain evolutionary theories and yield a lower limit on the duration of the accretion phase which is identified with LMXBs in the standard model.

High-quality timing measurements may eventually lead to a direct mass determination. Measurement of the Shapiro delay, a general relativistic delay in pulse arrival time due to the gravitational potential of the companion can be used to measure or constrain the system masses. Three systems have had masses determined or constrained by Shapiro delay measurements. If the orbital plane is relatively close to edge-on, then the pulses emitted near superior conjunction have to travel close to the companion star on their path to Earth. These pulses will be delayed by traveling through a deep potential well. This effect has been observed in two low mass binary pulsars, PSR B1855+09 (Ryba and Taylor 1991; Kaspi, Taylor, and Ryba 1994) and PSR J1713+0747 (Camilo, Foster, and Wolszczan 1994) and in the high-mass binary pulsar PSR 1534+12. Simulated timing delays as a function of orbital phase for Shapiro delay in the J2033+17 system are shown in Figure 6.3. Two parameters are used to fit the Shapiro delay, the range (r), and the shape (s) (Damour and Deruelle 1986; Shapiro 1964). For a circular orbit, the Shapiro delay reduces to

$$\Delta_s = -2r \log(1 - s \cos\theta), \tag{6.2}$$

where $s \equiv \sin i$, θ is the orbital position angle measured from the superior conjunction, r is the "range" parameter. If general relativity is the correct theory of gravity, then the range parameter becomes

$$r = \frac{Gm_2}{c^3} = 4.9254 \frac{m_2}{M_\odot} \mu\text{s}. \tag{6.3}$$

It has been pointed out by Refsdal and Weigert (1971) that in systems where mass transfer comes from a low mass ($\lesssim 2\ M_\odot$) star filling its Roche lobe, there should be a relation between the final core mass (the mass of the white dwarf) and the orbital period.

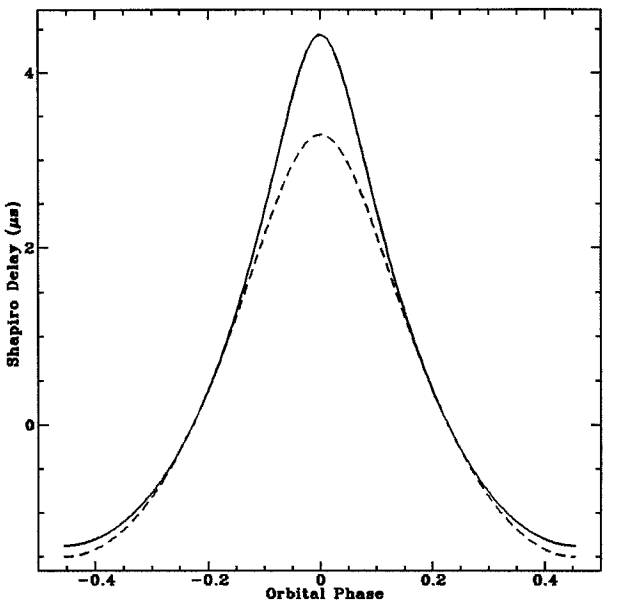

Figure 6.3: Plot of Shapiro delay versus orbital phase for two possible companion masses and inclinations of the PSR J2033+17 system. The orbital phase is 0 at superior conjunction. The solid line is for $i = 60°$, the median value of i for random orientations, and the dashed line is for $i = 43°$, the orientation implied if the white dwarf mass is 0.295 $M_\odot$ as predicted by the core-mass period relation. In each case, the companion mass is calculated assuming that the pulsar mass is 1.4 $M_\odot$.

This relation is roughly (Phinney and Kulkarni 1994)

$$P_b \simeq 1.3(m_c/0.16\ M_\odot)^7\ \mathrm{d}, \tag{6.4}$$

yielding a mass of $\sim 0.27\ M_\odot$. The predicted companion mass for PSR J2033+17 from a more accurate model (Phinney and Kulkarni 1994) is 0.295 $M_\odot$ implying an inclination of 43°. There is considerable uncertainty in the prediction due to the unknown metallicity of the white dwarf progenitor, but it provides an indication of a likely mass for the white dwarf companion of PSR J2033+17.

Phinney (1992) applied the fluctuation dissipation theorem to the randomly induced multipole moments in a convective red giant star, and showed that one expects a relation between the orbital period of such a system and its eccentricity. During the mass transfer phase of the evolution, the eccentricity is damped by tidal dissipation, and pumped by fluctuating multipole moments of the giant star. The predicted orbital eccentricity for PSR J2033+17 is between 4×10^{-5} and 4×10^{-4} with a most likely value of 2×10^{-4}. The ob-

served eccentricities of pulsars with white dwarf companions are in good agreement with this theory (Phinney and Kulkarni 1994). A measurement of the eccentricity of PSR J2033+17 will be possible with a few months of precision timing, if it is of the order of magnitude predicted by Phinney.

This pulsar is very similar in pulse period, orbital period, and distance to PSR J1713+0747. During the first 22 months of timing this pulsar, Camilo, Foster, and Wolszczan (1994) were able to measure its annual parallax, proper motion, and Shapiro delay as well as the usual period, period derivative, and position.

Camilo (1994b) notes that when the orbital periods of all known millisecond pulsars in circular orbits about low mass companions are considered, there appears to be a deficit of pulsars with orbital periods between 12 and 67 days. The 56.2 d orbital period of PSR J2033+17 reduces the size of this gap somewhat.

The Shklovskii effect (Shklovskii 1970) is a contribution to the measured period derivative of a pulsar due to its transverse velocity. Camilo, Thorsett, and Kulkarni (1994) point out the importance of considering the Shklovskii effect when calculating the characteristic ages and magnetic fields of millisecond pulsars. Its magnitude is

$$\frac{\dot{P}_s}{P} = 1.1 \times 10^{-18} v_{100}^2 D_{\rm kpc}^{-1}\ {\rm s}^{-1}, \tag{6.5}$$

where v_{100} is the transverse velocity of the pulsar in units of 100 km/s and $D_{\rm kpc}$ is the distance to the pulsar in kpc. For an assumed velocity of 100 km/s, the contribution to $\dot{P}$ for PSR J2033+17 is 4.7×10^{-21}. This is small, but not negligible when compared to the measured period derivatives of millisecond pulsars. If PSR J2033+17 has a magnetic field of 3×10^8 G then the Shklovskii effect will contribute $\sim 25\%$ of the measured period derivative. This will be correctly compensated for only after proper motion measurements are available for this pulsar.

6.4 Conclusion

We will continue to monitor PSR J2033+17 whenever time is available at Arecibo and possibly at the Green Bank 140ft telescope. We hope to have a phase-connected timing solution in the near future, and obtain measurements of the position, period derivative, orbital eccentricity and possibly the Shapiro delay within a year. Also, proper motion and possibly parallax may be measurable, and it will be interesting to test the stability

of this pulsar as a clock for the millisecond pulsar timing array. At a distance of 1.4 kpc and reasonably far out of the crowded Galactic plane, this system might be attractive for searching for optical emission from the cooling white dwarf companion. Only a few white dwarf companions have been identified for millisecond pulsars, but the cooling age of the white dwarf has important implications for the initial periods of millisecond pulsars (Camilo, Thorsett, and Kulkarni 1994). This project would likely require the Keck telescope.

Appendix A

IAU Circular

(Thorsett *et al.* 1994, IAU Circular 6012)

PSR J2043+27

S. E. Thorsett, P. S. Ray, S. R. Kulkarni, and T. A. Prince, California Institute of Technology, report: "We have discovered a 96.13-ms pulsar in data taken on May 23 UT with the 305-m Arecibo telescope. The position is R.A. = 20h43m.7, Decl. = +27o40' (equinox 2000.0; uncertainty of 5' in radius). The flux density at 430 MHz is roughly 25 mJy. This could either be a young pulsar or a mildly recycled pulsar. We note that the pulsar is within a degree of the boundary of the southern blowout region of the Cygnus Loop supernova remnant, and the dispersion measure of 21 +/- 1 pc cmE-3 implies a distance of about 1 kpc, consistent with the distance to the remnant. If the pulsar were born at the remnant center 40 kyr ago, its implied transverse velocity would be about 1500 km/s."

Bibliography

Abramovici, A. *et al.* 1992, *Science*, **256**, 325–333.

Anderson, S. B. 1993. Ph.D. thesis, California Institute of Technology.

Anderson, S. B., Cadwell, B. J., Wolszczan, A., and Foster, R. S. 1994. IAU circular 6012.

Anderson, S. B., Gorham, P. W., Kulkarni, S. R., Prince, T. A., and Wolszczan, A. 1990, *Nature*, **346**, 42.

Backer, D. C. and Hellings, R. W. 1986, *ARA&A*, **24**, 537–575.

Bailes, M. 1989, *ApJ*, **342**, 917.

Bailes, M. *et al.* 1994, *ApJ*, **425**, L41.

Bhattacharya, D. and van den Heuvel, E. P. J. 1991, *Phys. Rep.*, **203**, 1.

Biggs, J. D. and Lyne, A. G. 1992, *MNRAS*, **254**, 257.

Branch, D. 1990, in *Neutron Stars and Their Birth Events*, ed. W. Kundt, Kluwer Academic Publishers, 281.

Camilo, F. 1994a, personal communication.

Camilo, F. 1994b, in *The Lives of the Neutron Stars (NATO ASI Series)*, ed. A. Alpar, Ü Kiziloğlu, and J. van Paradis, (Dordrecht: Kluwer), 243.

Camilo, F., Foster, R. S., and Wolszczan, A. 1994, *ApJ*, **437**, L39.

Camilo, F., Nice, D. J., and Taylor, J. H. 1993, *ApJ*, **412**, L37.

Camilo, F., Thorsett, S. E., and Kulkarni, S. R. 1994, *ApJ*, **421**, L15.

Caraveo, P. A. 1993, *ApJ*, **415**, L111.

Caswell, J. L., Kesteven, M. J., Stewart, R. T., Milne, D. K., and Hanes, R. F. 1992, *ApJ*, **399**, L151.

Chen, K. and Ruderman, M. 1993, *ApJ*, **402**, 264.

Clifton, T. R., Lyne, A. G., Jones, A. W., McKenna, J., and Ashworth, M. 1992, *MNRAS*, **254**, 177.

Cooley, J. W. and Tukey, J. W. 1965, *Mathematics of Computation*, **19**, 297.

Cordova, F. A., Hjellming, R. M., Mason, K. O., and Middleditch, J. M. 1989, *ApJ*, **345**, 451.

Coté, J. and Pylyser, E. 1989, *A&A*, **218**, 131.

Damashek, M., Taylor, J. H., and Hulse, R. A. 1978, *ApJ*, **225**, L31.

D'Amico, N., Manchester, R. N., Durdin, J. M., Stokes, G. H., Stinebring, D. R., Taylor, J. H., and Brissenden, R. J. V. 1988, *MNRAS*, **234**, 437–443.

Damour, T. and Deruelle, N. 1986, *Ann. Inst. H. Poincaré (Physique Théorique)*, **44**, 263.

Damour, T., Gibbons, G., and Taylor, J. H. 1988, *Phys. Rev. Lett*, **61**, 1151.

Damour, T. and Taylor, J. H. 1992, *Phys. Rev. D*, **45**(6), 1840.

Davies, J. G., Lyne, A. G., and Seiradakis, J. H. 1977, *MNRAS*, **179**, 635–650.

Deich, W. T. S. 1994. Ph.D. thesis, California Institute of Technology.

Dewey, R. J. 1984. Ph.D. thesis, Princeton University.

Dewey, R. J. and Cordes, J. M. 1987, *ApJ*, **321**, 780.

Dewey, R. J., Taylor, J. H., Weisberg, J. M., and Stokes, G. H. 1985, *ApJ*, **294**, L25.

Fahlman, G. G. and Gregory, P. C. 1981, *Nature*, **293**, 202.

Foster, R. S., Wolszczan, A., and Cadwell, B. J. 1994, in *Millisecond Pulsars: A Decade of Surprise*, ed. A. Fruchter, M. Tavani, and D. Backer, ASP Conference Series, preprint.

Foster, R. S., Wolszczan, A., and Camilo, F. 1993, *ApJ*, **410**, L91.

Frail, D. A. and Kulkarni, S. R. 1991, *Nature*, **352**, 785.

Frail, D. A., Kulkarni, S. R., and Vasisht, G. 1993, *Nature*, **365**, 136.

Fruchter, A. S. 1989. Ph.D. thesis, Princeton University.

Fruchter, A. S. *et al.* 1990, *ApJ*, **351**, 642–650.

Fürst, E., Reich, W., and Seiradakis, J. H. 1993, *A&A*, **276**, 470.

Ghosh, P. and Lamb, F. K. 1992, in *X-Ray Binaries and the Formation of Binary and Millisecond Radio Pulsars*, ed. E. P. J. van den Heuvel and S. Rappaport, (Dordrecht: Kluwer).

Goldreich, P. and Julian, W. H. 1969, *ApJ*, **157**, 869–880.

Gorham, P. W., Ray, P. S., Anderson, S. B., Kulkarni, S. R., and Prince, T. A. 1995, ApJ, to be submitted.

Green, D. A. 1993, in *Supernovae and Supernova Remnants: IAU Colloquium 145*, ed. R. McCray and Z. Wang, Cambridge University Press.

Gregory, P. C. and Fahlman, G. G. 1980, *Nature*, **287**, 805.

Hankins, T. H. and Rickett, B. J. 1975, *Meth. Comp. Phys.*, **14**, 55.

Hankins, T. H. and Wolszczan, A. 1987, *ApJ*, **318**, 410.

Hulse, R. A. and Taylor, J. H. 1974, *ApJ*, **191**, L59.

Hulse, R. A. and Taylor, J. H. 1975, *ApJ*, **201**, L55.

Johnston, S. and Bailes, M. 1991, *MNRAS*, **252**, 277.

Johnston, S., Lyne, A. G., Manchester, R. N., Kniffen, D. A., D'Amico, N., Lim, J., and Ashworth, M. 1992, *MNRAS*, **255**, 401.

Johnston, S., Manchester, R. N., Lyne, A. G., Kaspi, V. M., and D'Amico, N. 1995, *A&A*. preprint.

Kaspi, V. M. 1994a, in *IAU Meeting on Astrometry*, in press.

Kaspi, V. M. 1994b, in *Millisecond Pulsars: A Decade of Surprise*, ed. A. Fruchter, M. Tavani, and D. Backer, ASP Conference Series, preprint.

Kaspi, V. M., Lyne, A. G., Manchester, R. N., Johnston, S., D'Amico, N., and Shemar, S. L. 1993, *ApJ*, **409**, L57.

Kaspi, V. M., Manchester, R. N., Johnston, S., Lyne, A. G., and D'Amico, N. 1992, *ApJ*, **399**, L155.

Kaspi, V. M., Taylor, J. H., and Ryba, M. F. 1994, *ApJ*, **428**, 713.

Kassim, N. E. and Weiler, K. W. 1990, *Nature*, **343**, 146.

Kluźniak, W., Ruderman, M., Shaham, J., and Tavani, M. 1989, in *Timing Neutron Stars, (NATO ASI series)*, ed. H. Ögelman and E. P. J. van den Heuvel, (Dordrecht: Kluwer), 641.

Ku, W. H. M., Kahn, S. M., Pisarski, R. P., and Long, K. S. 1984, *ApJ*, **278**, 615.

Kulkarni, S. R., Anderson, S. B., Prince, T. A., and Wolszczan, A. 1991, *Nature*, **349**, 47.

Kulkarni, S. R., Clifton, T. C., Backer, D. C., Foster, R. S., Fruchter, A. S., and Taylor, J. H. 1988, *Nature*, **331**, 50.

Kulkarni, S. R. and Narayan, R. 1988, *ApJ*, **335**, 755.

Kulkarni, S. R., Predehl, P., Hasinger, G., and Aschenbach, B. 1993, *Nature*, **362**, 135.

Large, M. I. and Vaughan, A. E. 1971, *MNRAS*, **151**, 277.

Large, M. I., Vaughan, A. E., and Mills, B. Y. 1968, *Nature*, **220**, 340–341.

Leahy, D. A. and Roger, R. S. 1991, *AJ*, **101**(3), 1033.

Lorimer, D. R., Bailes, M., Dewey, R. J., and Harrison, P. A. 1993, *MNRAS*, **263**, 403.

Lorimer, D. R. *et al.* 1995, *ApJ.* preprint.

Lyne, A. G. and Lorimer, D. R. 1994, *Nature*, **369**, 127.

Lyne, A. G., Manchester, R. N., and Taylor, J. H. 1985, *MNRAS*, **213**, 613.

Lyne, A. G. and Smith, F. G. 1990, *Pulsar Astronomy*, (Cambridge: Cambridge University Press).

Manchester, R. N. 1994, in *Millisecond Pulsars: A Decade of Surprise*, ed. A. Fruchter, M. Tavani, and D. Backer, ASP Conference Series, preprint.

Manchester, R. N., D'Amico, N., and Tuohy, I. R. 1985, *MNRAS*, **212**, 975.

Manchester, R. N., Kaspi, V. M., Johnston, S., Lyne, A. G., and D'Amico, N. 1991, *MNRAS*, **253**, 7P.

Manchester, R. N., Lyne, A. G., Taylor, J. H., Durdin, J. M., Large, M. I., and Little, A. G. 1978, *MNRAS*, **185**, 409.

Manchester, R. N., Mar, D. P., Lyne, A. G., Kaspi, V. M., and Johnston, S. 1994, *ApJ*, **403**, L29.

Manchester, R. N. and Taylor, J. H. 1977, *Pulsars*, (San Francisco: Freeman).

McAdam, W. B., Osborne, J. L., and Parkinson, M. L. 1993, *Nature*, **361**, 516.

Michel, F. C. 1991, *Theory of Neutron Star Magnetospheres*, (Chicago: The University of Chicago Press).

National Astronomy and Ionosphere Center, Cornell University. *Arecibo Observatory User's Manual* 1989.

Narayan, R. and Schaudt, K. J. 1988, *ApJ*, **325**, L43.

Nicastro, L. and Johnston, S. 1995, *MNRAS*. preprint.

Nice, D. J. 1992. Ph.D. thesis, Princeton University.

Nice, D. J., Taylor, J. H., and Fruchter, A. S. 1993, *ApJ*, **402**, L49.

Nordtvedt, K. 1990, *Phys. Rev. Lett*, **65**, 953.

Phinney, E. S. 1992, *Phil. Trans. R. Soc. Lond. A*, **341**, 39–75.

Phinney, E. S. and Kulkarni, S. R. 1994, *ARA&A*, **32**.

Press, W. H., Teukolsky, S. A., Vetterling, W. T., and Flannery, B. P. 1992, *Numerical Recipes in C: The Art of Scientific Computing*, (Cambridge: Cambridge University Press), 2nd edition.

Prince, T. A., Anderson, S. B., Kulkarni, S. R., and Wolszczan, A. 1991, *ApJ*, **374**, L41.

Rankin, J. M. 1983, *ApJ*, **274**, 333.

Rankin, J. M. 1990, *ApJ*, **352**, 247.

Ray, P. S. 1992, in *Proc. of the First Intel Delta Applications Workshop*, ed. T. Mihaly and P. Messina, (CCSF-14-92).

Ray, P. S. *et al.* 1995a, *ApJ.* in press.

Ray, P. S., Thorsett, S. E., Jenet, F. A., van Kerkwijk, M. H., Kulkarni, S. R., and Prince, T. A. 1995b, in preparation.

Ray, P. S., Thorsett, S. E., and Prince, T. A. 1995, in preparation.

Refsdal, S. and Weigert, A. 1971, *A&A*, **13**, 367.

Reich, W., Furst, E., Steffen, P., Reif, K., and Haslam, C. G. T. 1984, *A&AS*, **58**, 197.

Routledge, D. and Vaneldik, J. F. 1988, *ApJ*, **326**, 751.

Ryba, M. F. and Taylor, J. H. 1991, *ApJ*, **371**, 739.

Seward, F. D. 1990, *ApJS*, **73**, 781.

Seward, F. D. and Harnden, F. R. 1982, *ApJ*, **256**, L45.

Seward, F. D., Harnden, F. R., and Helfand, D. J. 1984, *ApJ*, **287**, L19.

Shapiro, I. I. 1964, *Phys. Rev. Lett*, **13**, 789.

Shapiro, S. L. and Teukolsky, S. A. 1983, *Black Holes, White Dwarfs and Neutron Stars. The Physics of Compact Objects*, (New York: Wiley–Interscience).

Shklovskii, I. S. 1970, *Soviet Ast.*, **13**, 562.

Shull Jr., P. and Hippelein, H. 1991, *ApJ*, **383**, 714.

Srinivasan, G. and Bhattacharya, D. 1989, *Curr. Sci.*, **58**, 953.

Staelin, D. H. and Reifenstein, III, E. C. 1968, *Science*, **162**, 1481–1483.

Stinebring, D. R., Kaspi, V. M., Nice, D. J., Ryba, M. F., Taylor, J. H., Thorsett, S. E., and Hankins, T. H. 1992, *Rev. Sci. Inst.*, **63**, 3551.

Stokes, G. H., Segelstein, D. J., Taylor, J. H., and Dewey, R. J. 1986, *ApJ*, **311**, 694.

Sutton, J. M. 1971, *MNRAS*, **155**, 51.

Taylor, J. H. 1974, *A&AS*, **15**, 367.

Taylor, J. H. 1992, *Phil. Trans. R. Soc. Lond. A*, **341**, 117.

Taylor, J. H. and Cordes, J. M. 1993, *ApJ*, **411**, 674.

Taylor, J. H., Manchester, R. N., and Lyne, A. G. 1993, *ApJS*, **88**, 529–568.

Taylor, J. H. and Weisberg, J. M. 1989, *ApJ*, **345**, 434.

Thorsett, S. E. 1991. Ph.D. thesis, Princeton University.

Thorsett, S. E., Deich, W. T. S., Kulkarni, S. R., Navarro, J. N., and Vasisht, G. 1993, *ApJ*, **416**, 182.

Thorsett, S. E., Ray, P. S., Kulkarni, S. R., and Prince, T. A. 1994. IAU circular 6012.

Velusamy, T. and Becker, R. H. 1988, *AJ*, **95**, 1162.

Velusamy, T., Becker, R. H., and Seward, F. D. 1991, *AJ*, **102**, 676.

Weiler, K. W. and Sramek, R. A. 1988, *ARA&A*, **26**, 295.

Wolszczan, A. 1991, *Nature*, **350**, 688.

Wolszczan, A., Cordes, J. M., and Dewey, R. J. 1991, *ApJ*, **372**, L99.

Wolszczan, A. and Frail, D. A. 1992, *Nature*, **355**, 145.

Colophon

This thesis was produced using the LaTeX document preparation system version 2.09 and TeX version 3.141. The Postscript output was generated by dvips version 5.523.

The overall style of the document is due to the srlthesis style file which was adapted by Stuart Anderson from the ucthesis style and the AASTeX macros. It is due to his efforts that this document conforms to the Caltech guidelines for thesis style.

Many of the figures were created using SM version 2.2.1B by Robert Lupton and Patricia Monger.